Ph.D. DISSERTATION

EFFICIENT PARAMETER ESTIMATION METHODS FOR AUTOMOTIVE RADAR SYSTEMS

차량용 레이더 시스템을 위한
효율적인 파라미터 추정 기법 연구

By
HAN-BYUL LEE

FEBRUARY 2016

DEPARTMENT OF ELECTRICAL AND COMPUTER ENGINEERING
COLLEGE OF ENGINEERING
SEOUL NATIONAL UNIVERSITY

Abstract

EFFICIENT PARAMETER ESTIMATION METHODS FOR AUTOMOTIVE RADAR SYSTEMS

Han-Byul Lee
Department of Electrical and Computer Engineering
The Graduate School
Seoul National University

As the demand for safety and convenience in the automotive-technology field increased, many applications of advanced driving assistance systems were developed. To provide driving information, among the sensors, such as cameras sensor, light detection and ranging sensor, radar sensor, and ultrasonic sensor, a radar sensor is known to exhibit excellent performance in terms of visibility for different weather conditions. Especially

with the legislation of the adaptive cruise control system and autonomous emergency braking system in a global environment, the market of the automotive radar sensor is expected to grow explosively. At present, the development of cost-effective radar offering high performance with small size is required. In addition, the radar system should be enforced to have a simultaneous functionality for both long and short ranges. Thus, challenging issues still remain with respect to radar signal processing including high-resolution parameter estimation, multi-target detection, clutter suppression, and interference mitigation.

For high-resolution parameter estimation, direction-of-arrival (DOA) estimation method has been investigated to identify the target object under complex unban environment. To separate closely spaced target having similar range and distance, high-resolution techniques, such as multiple signal classification (MUSIC), the estimation of signal parameters via rotational invariance techniques (ESPRIT), and maximum likelihood (ML) algorithm, are applied for automotive radars. In general, cycle time for radar system, which is the processing time for one snapshot, is very short, thus to establish a high-resolution estimation algorithm with computational efficiency is additional issue.

On the other hands, multi-target detection scheme is required to identify many targets in the field of view. Multi-target detection is regarded as target pairing solution, whose task is to associate frequency components obtained from multiple targets. Under certain conditions, the association may fail and real target may be combined to ghost components. Thus, reliable paring or association method is essential for automotive radar systems.

The clutter denotes undesired echoes due to reflected wave from background environment, which includes guardrail, traffic signs, and stationary structures around the

load. To minimize the effect of clutter, conventional radar systems use high pass filter based on the assumption that the clutter is stationary with energy concentrated in the low frequency domain. However, the clutter is presented with various energy and frequency under automotive radar environment. Especially, under the specific environment with iron materials, target component is not detected due to clutter with large power.

Mutual interference is a crucial issue that must be resolved for improved safety functions. Given the increasing number of automotive radar sensors operating at the same instant, the probability that radar sensors may receive signals from other radar sensors gradually increases. In such a situation, the system may fail to detect the correct target given the serious interference. Effective countermeasures, therefore, have to be considered.

In this dissertation, we propose efficient parameter estimation methods for automotive radar system. The proposed methods include the radar signal processing issues as above described, respectively. First, the high-resolution DOA estimation method is proposed by using frequency domain analysis. The scheme is based on the MUSIC algorithm, which use distinct beat frequency of the target. The target beat frequency also gives distance and velocity. Thus, the proposed algorithm provides either high-resolution angle information of target or natural target pairing solution. Secondly, we propose the clutter suppression method under iron-tunnel conditions. The clutter in iron-tunnel environments is known to severely degrade the target detection performance because of the signal reflection from iron structures. The suppression scheme is based on cepstral analysis of received signal. By using periodical characteristic of the iron-tunnel clutter, the suppressed frequency response

is obtained. Finally, the interference mitigation scheme is studied. Mutual interference between frequency modulated continuous waveform (FMCW) radars appears in the form of increased noise levels in the frequency domain and results in a failure to separate the target object from interferer. Thus, we propose a high-resolution frequency estimation technique for use in interference environments.

Keywords : Automotive radar, FMCW, Direction-of-arrival, Interference, Mitigation, Clutter, Suppression, High-resolution, Signal processing

Student Number : 2009 - 30928

Contents

List of Tables

List of Figures

Chapter 1

Introduction

1.1 Background

Three major topics in the field of automotive technology are green, convenience, and safety. Among these issues, the goal of research on safety and convenience is to prevent accidents in a variety of dangerous situations commonly encountered by drivers. To provide safety and driving comfort, advanced driving assistance systems (ADAS) are emerging as very active issues [1]-[2]. The sensors have played a vital role in the development of ADAS and enhancement of vehicle safety. Sensor technology provides artificial sensing of the environment, which enables decision making by in-car computers [3]. These sensor enabled systems help in providing warning to drivers and regulating vehicle control to mitigate collisions that can lead to material damage as well as human injury. ADAS includes blind spot detection, adaptive cruise control (ACC), autonomous emergency braking (AEB), obstacle detection, collision avoidance systems, rear view cameras, parking assistance (PA), and lane departure warning as showing in Figure 1.1 [4]-[5]. Key sensor technologies being used in these systems are camera sensor, infrared sensors, radar, light detection and ranging, and ultrasonic sensors.

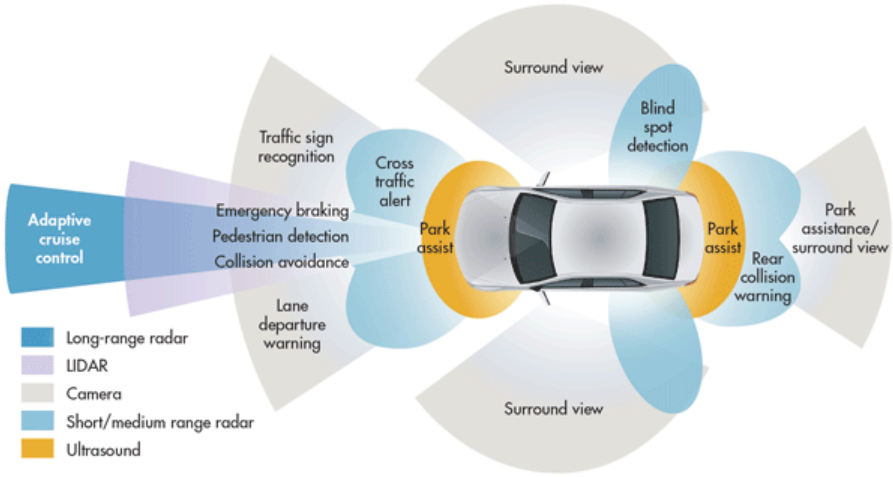

Figure 1.1 ADAS applications

1.2 ADAS Applications for Automotive Radars

ACC ensures that the automobile remains at a predefined distance away from the car ahead, reducing the speed to zero if necessary [6]. For ACC, radar sensors emit and receive radio waves and thus determine the distance of vehicles in front of the user's vehicle. ACC with stop and go facility allows the vehicle to come to a standstill if the preceding vehicle comes to a halt. The system again takes over as the preceding vehicle stars and by controlling acceleration, the predefined cruise speed is again achieved.

The blind spot detection helps the driver while attempting to pass other vehicles [7]. Sensors continuously monitor the presence, direction, and speed of vehicles in the lanes beside the ego-vehicle. If a vehicle moves into the blind spot, warning based on visual or audio signals can be generated to alert the driver of potential danger of collision. Radar sensors mounted on the real bumper or on the side rear view mirrors monitor vehicles behind or on adjacent lanes.

Forward collision warning systems are in-vehicle electronic systems that monitoring the roadway in front of the host vehicle and warn the driver when a potential collision risk exists. The system provides an audible alert when it senses a reduction in traffic speed in vehicles ahead. When the danger of a collision is detected, it provides a red warning light that flashes on the windshield. The forward collision warning is extended as an AEB recently. The system takes sudden braking in an emergency situation.

PA systems consist of visual aids, using real view cameras and side view cameras, Ultrasonic sensors provide distance information which allows the vehicle to be safety guided into the parking space without crashing into any other parked vehicle. Radar is

applied as a form of sensor fusion with camera sensors and ultrasonic techniques. Parking assistance systems will gradually make way for automatic parking systems.

1.3 Motivation and Organization

The development of automotive radar focuses on two types; short-range radar (SRR) using ultra-wide band (UWB) system at the 24 GHz and 77 GHz bands, and long-range radar (LRR) using frequency modulated continuous waveform (FMCW) systems at the 77GHz band [8]-[9]. The 77GHz band is known to be the most appropriate frequency band in global automotive radar environments, as the 24GHz band is shared with other communications systems. Furthermore, multi-mode radar sensors including the function of both SRR and LRR are obliged to miniaturize its size [10]. Considering the size of multi-mode radar sensors, 77GHz FMCW radar is a good candidate for a new automotive radar solution [11]. FMCW radar uses the waveforms of linearly increasing or decreasing frequencies, which increases reliability of radar system by providing the distance and velocity information of the target simultaneously. Moreover, the easy implementation of these radar sensors is the most significant factor making the most popular commercial system at present [12]–[13].

There remain several problems, however, related to the signal processing of automotive FMCW radar, including high-resolution parameter estimation, multi-target detection, clutter elimination and mutual interference elimination [14]–[16]. For high-resolution parameter estimation, direction-of-arrival (DOA) estimation method has been investigated to identify the target object under complex unban environment. To separate closely spaced target having similar range and distance, high-resolution techniques, such as multiple signal classification (MUSIC) [17], the estimation of signal parameters via rotational invariance techniques (ESPRIT) [18], and maximum likelihood (ML) algorithm [19], are applied for automotive radars. In general, cycle time for radar system, which is the processing time for one snapshot, is very short, thus

to establish a high-resolution estimation algorithm with computational efficiency is additional issue. On the other hands, multi-target detection scheme is required to identify many targets in the field of view. Multi-target detection is regarded as target pairing solution, whose task is to associate frequency components obtained from multiple targets. Under certain conditions, the association may fail and real target may be combined to ghost components [20]. Thus, reliable paring or association method is essential for automotive radar systems. The clutter denotes undesired echoes due to reflected wave from background environment, which includes guardrail, traffic signs, and stationary structures around the load. To minimize the effect of clutter, conventional radar systems use high pass filter based on the assumption that the clutter is stationary with energy concentrated in the low frequency domain [21]. However, the clutter is presented with various energy and frequency under automotive radar environment. Especially, under the specific environment with iron materials, target component is not detected due to clutter with large power [22]. Mutual interference is a crucial issue that must be resolved for improved safety functions. Given the increasing number of automotive radar sensors operating at the same instant, the probability that radar sensors may receive signals from other radar sensors gradually increases. In such a situation, the system may fail to detect the correct target given the serious interference [23]. Effective countermeasures, therefore, have to be considered.

This thesis has a focus on efficient parameter estimation for automotive radar signal processing. In chapter 2, high-resolution DOA estimation with having pairing function for automotive FMCW radar is presented. In the section 2 of chapter 2, the MUSIC in the time-domain and frequency-domain is analyzed, and the simulated results are presented in section 3 of chapter 2. In Chapter 3, the clutter suppression scheme for iron tunnels is presented. Radar signal model of iron tunnel,

characterization of iron tunnel, and clutter suppression scheme are presented in in section 2 of chapter 3. Experimental result is analyzed in in section 3 of chapter 3. In chapter 4, interference mitigation method is described. Qualitative analysis of interference is presented in section 2 of chapter 4. In section 3 of chapter 4, high-resolution frequency estimation scheme is presented. Experimental result is analyzed in section 4 of chapter 4. Finally, conclusion is presented in chapter 5.

Chapter 2

High-Resolution Direction of Arrival Estimation with Pairing function for Automotive Radar Systems

2.1 Introduction

Automotive radar sensors are employed for various ADAS applications such as ACC, FCW, and AEB. Conventional FMCW radar provides only range and velocity of targets which exist on field of view. The increasing demand for safety and convenience leads to efforts improving the DOA estimation to allow resolution of targets even in the similar distance-velocity information. In an urban environment, for example, DOA is essential to separate targets with having same distance and velocity. The DOA resolution using conventional beam-former is poor since automotive radars have typically a low antenna aperture due to size restriction [24]. High-resolution methods for DOA estimation such as MUSIC [17] enable radar sensors to resolve very closely spaced targets. These algorithms are well known as subspace based algorithm,

which is applied wide research area to estimate specific parameters. MUSIC is based on exploiting the eigen-structure of input covariance matrix. MUSIC makes assumption that the noise in each channel is uncorrelated making correlation matrix diagonal.

On the other hand, Target pairing is an essential for multi-target detection. FMCW radar uses increasing chirp (which is a up chirp) and decreasing chirp (which is a down chirp) signal to obtain paired beat frequency of target [25]. From these frequency pair, distance and velocity of targets are calculated. However, additional technique is required to combine estimated DOA and distance and velocity.

In this chapter, high-resolution DOA estimation algorithm in frequency domain process is proposed. The proposed method is not significantly different from the conventional MUSIC, whereas it resolves pairing issue naturally by using only beat frequency of target. To analyze detection performance of proposed method, simulation results are presented based on a 77 GHz FMCW radar system. From the simulation, proposed frequency domain approach shows RMSE performance similar to time domain approach.

2.2 High-Resolution DOA Estimation for Automotive Radars

In order to provide DOA information, an array concept with multiple antennas is employed. With a far-field assumption, which means radius of propagation is much larger than array spacing, the propagation delay with respect to array element results in linear phase shift. Array signal processing can largely be classified into spectral approach and the parametric approach. The former uses spectral peak component of estimator, including beamforming techniques and subspace based methods [24]. The latter directly computes the DOA from signal model of estimator, such as maximum likelihood (ML) [19]. In this section, we employed MUSIC algorithm for DOA estimation, well known as subspace based method.

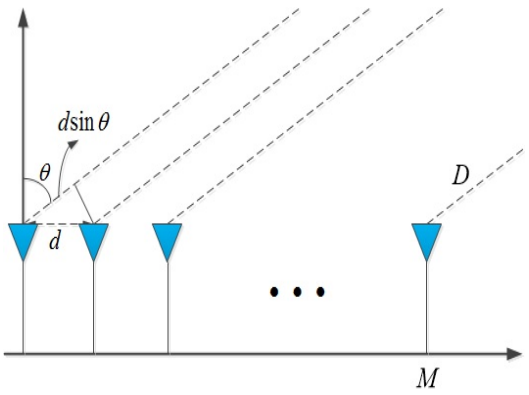

Figure 2.1 ULA structure for DOA estimation

2.2.1 DOA Estimation in the Time-domain Processing

Let us consider uniform linear array (ULA) with M antenna element, uniform spacing of d as shown in Figure 2.1. Plane wave reflected from each D target incidents on a different angle depending on the location of target. Each received signal $x_m(n)$, for $m = 0,1,\ldots,M$, includes additive zero mean, Gaussian noise. Time is represented by the n-th time sample. Thus, Array output $\mathbf{x}[n]$ is expressed as follows,

$$\mathbf{x}[n] = \mathbf{A}\mathbf{s}[n] + \mathbf{w}[n], \tag{2.1}$$

or

$$\begin{bmatrix} x_1[n] \\ x_2[n] \\ \vdots \\ x_M[n] \end{bmatrix} = \begin{bmatrix} \mathbf{a}(\theta_1) & \mathbf{a}(\theta_2) & \cdots & \mathbf{a}(\theta_D) \end{bmatrix} \begin{bmatrix} s_1[n] \\ s_2[n] \\ \vdots \\ s_D[n] \end{bmatrix} + \begin{bmatrix} w_1[n] \\ w_2[n] \\ \vdots \\ w_M[n] \end{bmatrix}, \tag{2.2}$$

where,

$$\mathbf{a}(\theta_i) = \begin{bmatrix} 1, & e^{j2\pi d/\lambda \sin(\theta_i)}, & \cdots, & e^{j2\pi(M-1)d/\lambda \sin(\theta_i)} \end{bmatrix}^T, \tag{2.3}$$

$\mathbf{s}[n]$ is a vector of incident complex signal at time n, $\mathbf{w}[n]$ is a noise vector at each array element m with zero mean, variance of σ_n^2, $\mathbf{a}(\theta_i)$ is M-element array steering vector for the θ_i DOA, and $\mathbf{A}$ is $M \times D$ matrix of steering vectors

$\mathbf{a}(\theta_i)$. It is initially assumed that the number of the targets $D < M$.

Based on above signal model, covariance matrix of received signal is given by

$$\begin{aligned}\mathbf{R}_T &= E[\mathbf{x}[\mathrm{n}]\mathbf{x}^H[\mathrm{n}]] = \mathbf{A}E[\mathbf{s}[\mathrm{n}]\mathbf{s}^H[\mathrm{n}]]\mathbf{A}^H + E[\mathbf{w}[\mathrm{n}]\mathbf{w}^H[\mathrm{n}]] \\ &= \mathbf{A}\mathbf{R}_{ss}\mathbf{A}^H + \sigma^2\mathbf{I}_M\end{aligned}, \qquad (2.4)$$

In general, $D < M$, $\mathbf{A}\mathbf{R}_{ss}\mathbf{A}^H$ is a singular matrix and non-negative definite. The array covariance matrix is calculated by the expectation of array output. However, we cannot find exact statistics for the signals and noise. Therefore, we assume that the process has ergodic properties, so we can approximate the correlation by use of a time-averaged correlation. Then, (2.4) can be represented by

$$\mathbf{R}_T = \frac{1}{N}\sum_{n=1}^{N}\mathbf{x}[\mathrm{n}]\mathbf{x}^H[\mathrm{n}]. \qquad (2.5)$$

From (2.4), we can find that the eigenvalue of $\mathbf{R}_T$ is exactly equal to summation of the eigenvalue of $\mathbf{A}\mathbf{R}_{ss}\mathbf{A}^H$ and the noise variance σ_n^2. Since the rank of $\mathbf{A}\mathbf{R}_{ss}\mathbf{A}^H$ is D, we can separate D eigenvalues larger than σ_n^2 and $M - D$ eigenvalues with a value of σ_n^2. We can also choose the D eigenvectors associated with the signal and $M - D$ eigenvectors associated with the noise. Then we can construct the $M \times D$ dimensional subspace spanned by the signal eigenvectors and $M \times (M - D)$ dimensional subspace spanned by the noise eigenvectors, respectively.

$$\mathbf{E} = [\mathbf{E}_S \ \mathbf{E}_N], \qquad (2.6)$$

where,

$$\begin{aligned}\mathbf{E}_N &= [\mathbf{e}_1\ \mathbf{e}_2\ \cdots\ \mathbf{e}_{M-D}] \\ \mathbf{E}_S &= [\mathbf{e}_{M-D+1}\ \mathbf{e}_{M-D+2}\ \cdots\ \mathbf{e}_M].\end{aligned} \tag{2.6}$$

The noise subspace eigenvectors are orthogonal to the array steering vectors at the direction of arrival $\theta_1,\ \theta_2,\ \cdots,\ \theta_D$. The relation is expressed as follows,

$$\begin{aligned}&\mathbf{A} \perp \mathbf{E}_N \\ &\mathbf{A}^H \perp \mathbf{e}_i \quad i = 1,\ 2,\ \cdots, M-D\end{aligned}. \tag{2.7}$$

Placing this relation in the denominator creates sharp peaks at the DOA. Thus, the MUSIC pseudo-spectrum is given as

$$P_{MUSIC}(\theta) = \frac{1}{\left|\mathbf{a}(\theta)^H \mathbf{E}_N \mathbf{E}^H{}_N \mathbf{a}(\theta)\right|}. \tag{2.8}$$

The peak value of pseudo-spectrum determined as DOA of target objects by using peak detection algorithm such as constant false alarm rate (CFAR). Parametric approach such as MUSIC takes advantage of a prior knowledge such as the number of frequency components. Because the precise number of frequency D value is not available in practical systems, it must be estimated. As information theoretic criteria, MDL or the Akaike information criterion (AIC) have been widely used to estimate the number of frequencies [26]. In this work, we employ the MDL criterion to estimate M. This is expressed as [27],

$$\mathrm{MDL}(k) = -\log\left(\frac{\prod_{i=k}^{L-1}\lambda_i^{\frac{1}{L-k}}}{\frac{1}{L-k}\sum_{i=k}^{L-1}\lambda_i}\right)^{(k-L)Q} + \frac{1}{2}k(2L-k)\log Q, \qquad (2.9)$$

after which the estimate of M can be obtained by

$$\hat{M} = \arg_k \min \mathrm{MDL}(k) + 1, \qquad (2.10)$$

where, $k = 0,1,\cdots,L-1$.

The flowchart of MUSIC algorithm is summarized in Figure 2.2.

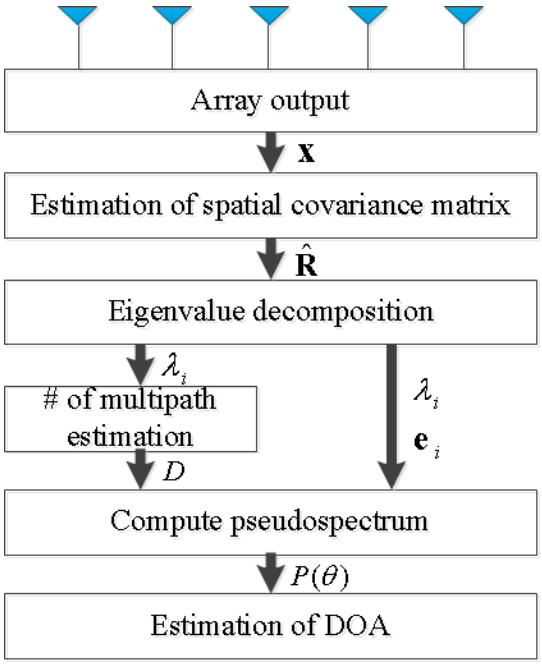

Figure 2.2 Flowchart of the MUSIC algorithm

2.2.2 DOA Estimation in the Frequency-domain Processing

As described above section 2.2.1, DOA estimation in time-domain gives only the sequence of estimated angles. To apply multi-target environment for automotive radars, respective DOA of targets should be paired with those of distance and velocity. Therefore, a proper pairing solution should be considered. However, if the number of targets increases, the computational load to combine each DOA with range and velocity.

In this section, we propose the DOA estimation in frequency-domain processing to provide natural pairing solution for automotive radar system. The proposed method is based on an observation that each target has different beat frequency. Thus, the DOA estimation is performed by using beat frequency component of target.

Let us define the spectrum of received signal obtained from fast Fourier transform (FFT). N_{FFT} discrete-time samples for M array output is defined by

$$\begin{aligned} \mathbf{X}_T &= [\mathbf{x}_1[n]\ \mathbf{x}_2[n]\ \cdots\ \mathbf{x}_M[n]]^T \\ \mathbf{S}_T &= [\mathbf{s}_1[n]\ \mathbf{s}_2[n]\ \cdots\ \mathbf{s}_D[n]]^T \\ \mathbf{W}_T &= [\mathbf{w}_1[n]\ \mathbf{w}_2[n]\ \cdots\ \mathbf{w}_M[n]]^T \end{aligned}, \qquad (2.11)$$

where,

$$\begin{aligned} \mathbf{x}_m[n] &= [x_m[0]\ x_m[1]\ \cdots\ x_m[N_{FFT}]\ ]^T, \ \text{for } m=1, 2, \cdots, M \\ \mathbf{s}_d[n] &= [s_d[0]\ s_d[1]\ \cdots\ s_d[N_{FFT}]\ ]^T, \ \text{for } d=1, 2, \cdots, D \\ \mathbf{w}_m[n] &= [w_m[0]\ w_m[1]\ \cdots\ w_m[N_{FFT}]\ ]^T \end{aligned}, \qquad (2.12)$$

$(\bullet)_T$ denotes sampled data in time-domain, $\mathbf{X}_T$ and $\mathbf{W}_T$ are $M \times N_{FFT}$

dimensional matrix, and $\mathbf{S}_T$ is $D \times N_{FFT}$ dimensional matrix. Fast Fourier transform matrix with length of N_{FFT} is represented as follows

$$\begin{aligned} [\mathbf{F}]_{n,k} &= \frac{1}{N_{FFT}} e^{-j2\pi(k-1)(n-1)/N_{FFT}} \\ \mathbf{f}(f_d) &= \mathbf{F}(:, k_d+1) = \mathbf{F}(:, \frac{f_d}{\Delta f}+1) \end{aligned} , \qquad (2.13)$$

where, $\mathbf{f}(f_d)$ denotes Fourier operator for the beat frequency of d th target, k_d is frequency index of d th target, f_d is beat frequency of d th target, and Δf is frequency resolution. From (2.13), coefficient of Fourier transform for the f_d is expressed by

$$\begin{aligned} \mathbf{x}_F(f_d) &= \sum_{i=1}^{D} \mathbf{a}(\theta_i)\mathbf{S}_T(i, :)\mathbf{f}(f_d) + \mathbf{W}_T\mathbf{f}(f_d) \\ &= \mathbf{a}(\theta_d)\mathbf{S}_T(d, :)\mathbf{f}(f_d) + \mathbf{W}_T\mathbf{f}(f_d) \\ &= \mathbf{a}(\theta_d)s_F(f_d) + \mathbf{w}_F(f_d) \end{aligned} , \qquad (2.14)$$

where, $\mathbf{x}_F(f_d)$ is a $M \times 1$ vector including complex magnitude of beat frequency f_d for each array element. For the D targets, the total matrix representation is given as

$$\begin{aligned} \mathbf{X} &= [\mathbf{x}_F(f_1)\ \mathbf{x}_F(f_2)\ \cdots\ \mathbf{x}_F(f_D)]^T \\ \mathbf{S} &= Diag[s_F(f_1)\ s_F(f_2)\ \cdots\ s_F(f_D)]^T \\ \mathbf{W} &= [\mathbf{w}_F(f_1)\ \mathbf{w}_F(f_2)\ \cdots\ \mathbf{w}_F(f_D)]^T \end{aligned} , \qquad (2.15)$$

where,

$$\begin{aligned}\mathbf{x}_F(f_d) &= [x_{f,1}[f_d]\, x_{f,2}[f_d] \cdots x_{f,M}[f_d]]^T, \text{ for } d=1, 2, \cdots, D \\ \mathbf{w}_F(f_d) &= [w_{f,1}[f_d]\, w_{f,2}[f_d] \cdots w_{f,M}[f_d]]^T\end{aligned}, \quad (2.16)$$

and compact matrix form is expressed by

$$\mathbf{X} = \mathbf{AS} + \mathbf{W}. \quad (2.17)$$

In order to estimate DOA with respect to f_d, covariance matrix for each beat frequency is defined as

$$\mathbf{R}_{F,i} = E[\mathbf{x}_F(f_i)\mathbf{x}_F{}^H(f_i)], \quad \text{for } i=1, 2, \cdots, D. \quad (2.18)$$

Since $rank(\mathbf{R}_{F,i}) = 1$ in general case, $\mathbf{R}_{F,i}$ has one eigenvalue in signal subspace, and $M-1$ eigenvalues in noise subspace. From the pseudo-spectrum (2.8), estimated DOA component θ_i is exactly paired with distance and velocity corresponding to f_i. Therefore, the DOA estimation in frequency domain resolves paring problem for multi-target detection automatically.

2.3 Simulation Result

2.3.1 Simulation Setup

To analyze the performance of DOA algorithm with two different approaches, Monte Carlo simulations were performed. The received signal was generated by the FMCW signal model. The parameters used in this simulation for FMCW are summarized in Table 2.1.

Table 2.1 Parameters used in simulation for FMCW

Parameters	value
Carrier frequency, f_c	76.5 GHz
Sweep time, Δt	5 ms
Sweep bandwidth, BW	500 MHz
Maximum target range, $R_{\max}$	200 m
Maximum target velocity, $V_{\mathrm{r,max}}$	300 km/h
Sampling frequency, f_s	440 kHz
The number of time sample	1024
The number of FFT point, N_{FFT}	1024
The number of Antenna	8
Antenna spacing	$\lambda / 2 = c / 2 f_c$

It is assumed that 77GHz FMCW radar with single transmitting antenna and 8 receiving array antenna with equally spaced elements. Maximum beat frequency is derived by

$$f_{b,\max} = f_{r,\max} + f_{d,\max} = \frac{BW}{\Delta t}\frac{2R_{\max}}{c} + \frac{2f_c}{c}V_{r,\max} \quad , \tag{2.19}$$

where, $f_{r,\max} = \frac{BW}{\Delta t}\frac{2R_{\max}}{c}$ is the maximum frequency difference by the maximum target range, and $f_{d,\max} = \frac{2f_c}{c}V_{r,\max}$ is the maximum Doppler frequency shift by the maximum relative velocity of target. By the Nyquist sampling theorem, sampling frequency is determined by

$$f_s > 2 \cdot f_{b,\max} . \tag{2.20}$$

For convenience of operation, we set the number of the sample in time-domain equal to those in frequency-domain.

2.3.2 Performance Comparison of the DOA Estimation in Time- and Frequency-domain Processing

To evaluate performance of DOA estimation, we employed the measure of RMSE under various conditions such as signal to noise ratio (SNR), the number of antenna elements, and angular separation of closed two targets. The RMSE of estimated DOA is defined as

$$RMSE = E[(\hat{\theta} - \theta_{real})^2], \tag{2.21}$$

where, $\hat{\theta}$ is the estimated DOA, and θ_{real} is the real DOA for the target location. From (2.21), we can find that the RMSE means the standard deviation of estimator.

The RMSE is evaluated against SNR. It is assumed that there exist two targets with -7 and 8 degree. In general, the DOA of target represents the angle from the perpendicular direction of the radar sensor. SNR is varied from 0 dB to 20 dB with 1000 independent trials, respectively. MUSIC estimate in time-domain uses the number of time sample, which is snapshot, for $N = 300,\ 500,\ 1000$.

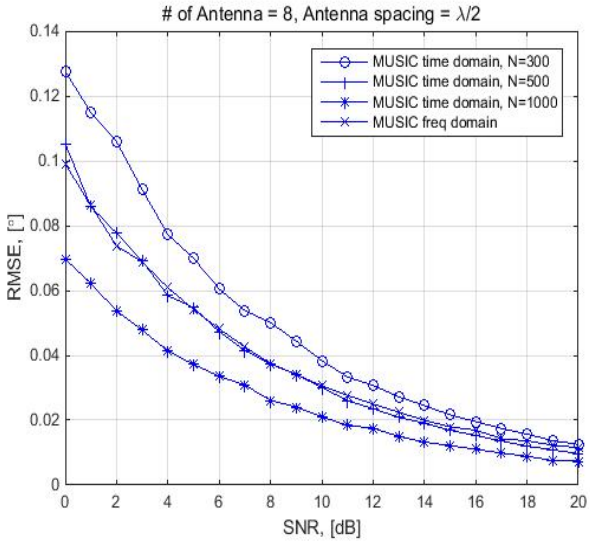

Figure 2.3 RMSE versus SNR

Figure 2.3 shows the RMSE performance of the algorithms in terms of the number of time samples for the two targets. In general, many of the DOA algorithms rely on the array covariance matrix. Since we use time average for estimating covariance matrix, large time sample performs better in comparison. However, large snapshot

affects computational time, results in longer cycle time for processing. On the other hand, MUSIC estimate in frequency domain shows good performance with relatively small computational load.

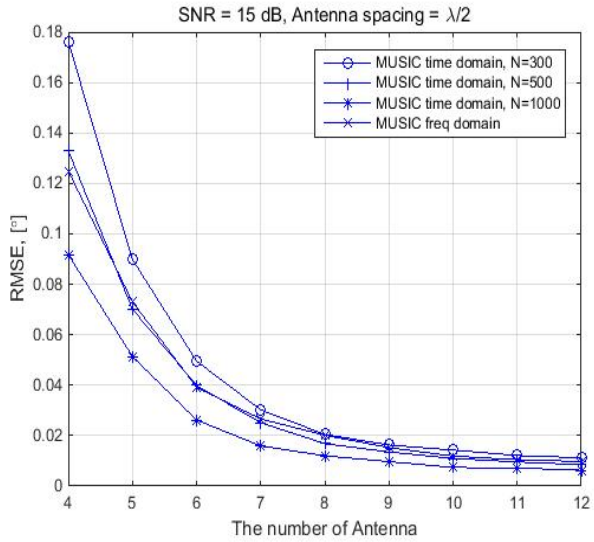

Figure 2.4 RMSE versus the number of antenna

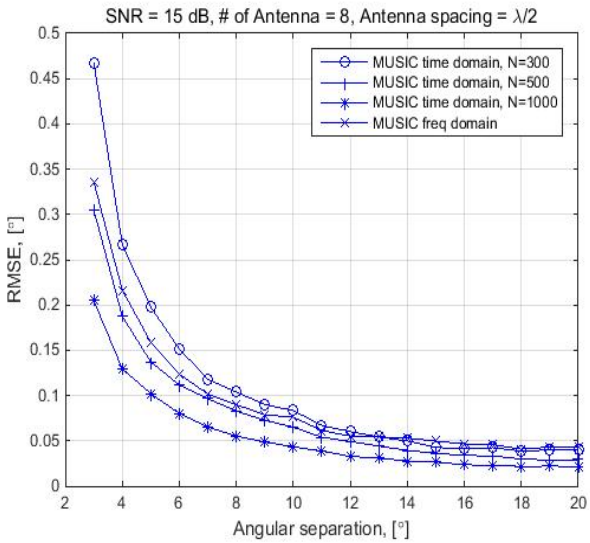

Figure 2.5 RMSE versus angular separation.

Figure 2.4 shows the RMSE performance in terms of the number of antenna elements. The SNR is 10 dB, the number of antenna elements varies from 4 to 12, and rest of simulation parameter is same as Figure 2.3. The number of antenna determines the size of covariance matrix, which is a square matrix. As the number of antenna elements increase, beam pattern of the array is sharper, and the more power of receiving antenna is concentrated on specific direction. Moreover, MUSIC algorithm uses the orthogonality between steering vector of incoming signal and eigenvectors in noise subspace. Thus large antenna elements make large size of eigenvectors in noise subspace, results in reducing correlation of signal and noise.

To evaluate angular resolution of the algorithm, the RMSE performance in terms of angular separation is analyzed as shown in Figure 2.5. The SNR is 10 dB, the number of antenna is 8, and the angular separation of two targets varies from 3 to 20 degree.

MUSIC estimate in frequency domain shows similar performance with MUSIC estimate in time domain with N =300.

From above observation, it is proved that the DOA estimate in frequency domain is almost same performance as one in time domain, whereas frequency domain approach provides efficient pairing solution.

2.3.3 Performance Analysis of the DOA Estimation in Frequency-domain

The frequency domain approach utilizes the beat frequency of the target which is derived from Fourier analysis of the received signal. Thus, better estimation of the beat frequency leads to better performance of DOA estimate. The frequency resolution of the FMCW radar is determined by sampling frequency f_s and length of FFT N_{FFT} as follows

$$\Delta f = \frac{f_s}{N_{FFT}}. \qquad (2.21)$$

Thus, large FFT points gives more precise complex magnitude of beat frequency, which results in better performance of DOA estimate. Figure 2.6, Figure 2.7, and Figure 2.8 show the RMSE performance versus SNR, the number of antenna elements, and the angular separation of two targets, respectively. These simulated results are performed with same condition as previous section 2.3.2. It is commonly observed that larger FFT point shows better performance of RMSE with expense of computational load, which is $n \log_2 n$.

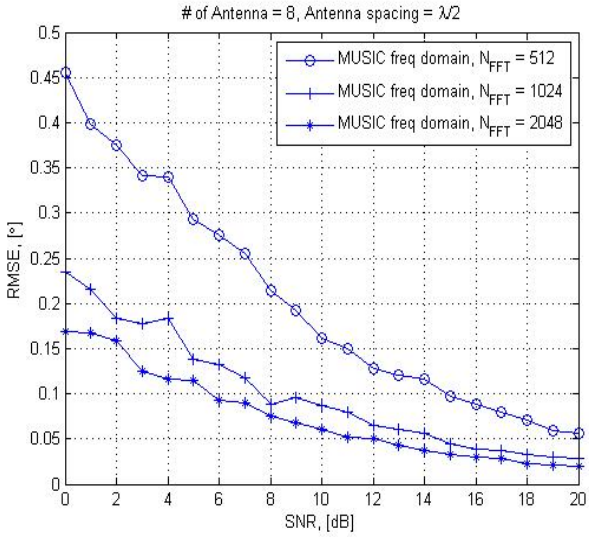

Figure 2.6 RMSE versus SNR according to the number of FFT length

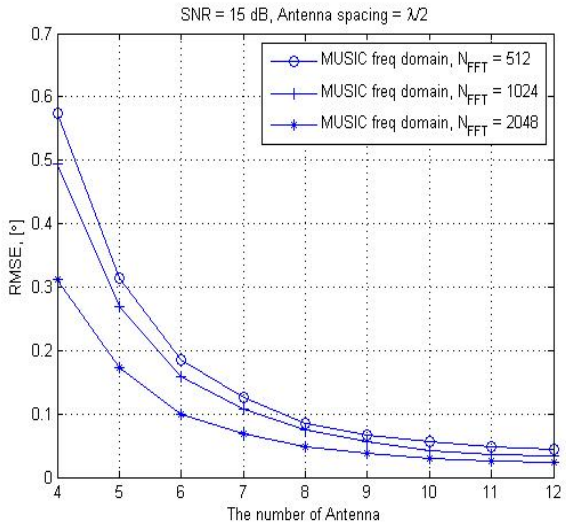

Figure 2.7 RMSE versus the number of antenna according to the number of FFT length

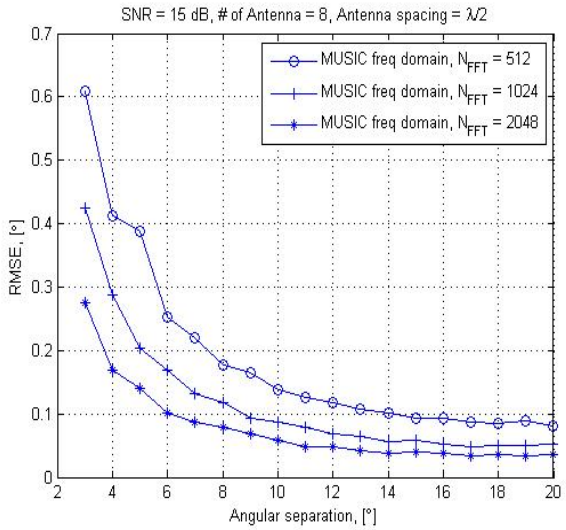

Figure 2.8 RMSE versus angular separation according to the number of FFT length

2.4 Conclusion

Conventional DOA estimation method is performed in time-domain, and gives only the directions of targets as a sequence. Thus, additional process should be established to pair DOA and distance/velocity. If there are many targets in field of view for a radar system, a very large amount of computation for precise pairing is required. To cope with the restriction of cycle time for the radar system, it is essential to suggest a simple but efficient pairing technique.

In this chapter, the efficient high-resolution DOA estimation method for automotive radar systems is proposed. We analyze high-resolution DOA estimation algorithm by use of beat frequency of target. By comparing to conventional time domain processing, we evaluated the suitability of the proposed method by simulation results. The frequency domain approach also provides a simple and efficient target pairing solution, which combine DOA information with distance and velocity of the target.

Chapter 3

Clutter Suppression Method of Iron Tunnel using Cepstral Analysis for Automotive Radars

3.1 Introduction

Clutter suppression is regarded as a relatively simple problem, however, in particular for iron-tunnel environments, the clutters are known to severely degrade the target detection performance because of the signal reflection from iron structures.

In the literature, several techniques have been presented in an effort to characterize the clutter structure on roads [28]-[29], whereas they are appropriate only for ultra-wideband pulse radars. Other studies have analyzed the stationary targets located in bridges and guard rails [30]-[31]. However, it is noteworthy that unlike the bridges and guard rails, iron structures are densely distributed to induce large reflections in iron-tunnel environments. So far, many of research have been descriptive under normal road conditions. Meanwhile, authors in [22] have introduced a technique to recognize the structure of iron tunnel. They employed measurement of the entropy based on the

short time Fourier transform analysis, and showed performance improvement by adjusting CFAR threshold. Note that this technique is tailored only for the recognition of iron-tunnel environments and not for the clutter suppression.

The main purpose of this study is to develop an understanding of the clutter effect of the iron tunnel and to establish an efficient clutter suppression algorithm under the iron tunnel environment. First, we derive a signal model for frequency modulated continuous waveform (FMCW) radars in iron-tunnel conditions, considering that iron pillars are located apart at equal distances, which leads to linear-increment of beat frequency with respect to the distance of clutters. Here, we focus on the periodic properties of the clutters induced by iron structures uniformly located in the tunnel. In order to analyze these properties, we employ cepstral analysis, which is used in wide areas for pitch detection [32]-[34]. By comparing radar signals in cepstrum domain under various road conditions, we prove that the existence of certain family of peaks in cepstral domain is a unique characteristic of iron-tunnel environments, which represents periodical beat frequency of clutters. Based on the above finding, we propose a clutter suppression method for iron-tunnel environments with liftering corresponding filtering in the spectral domain. To verify the proposed method, a 77 GHz forward-looking FMCW radar for ACC is employed. Measured results show that the proposed method efficiently suppresses the clutter of iron tunnel and extracts the parameter of the target object. It is shown that the proposed method provides significant performance enhancement even for early target detection.

The overall structure of the study organized as follows. Section 3.2 begins by modeling radar signal under an iron-tunnel condition. The cepstral characteristic and the method to suppress clutter are also discussed in section 3.2. Section 3.3 analyzes

the experimental results of the proposed method. Finally, conclusion is presented in section 3.4.

3.2 Clutter Suppression under Iron Tunnels

In this section, a radar signal model with iron-tunnel clutters is briefly described. We analyze cepstral characteristics under various road conditions, and propose an efficient method to suppress the clutter effect of iron tunnel by the cepstrum editing process.

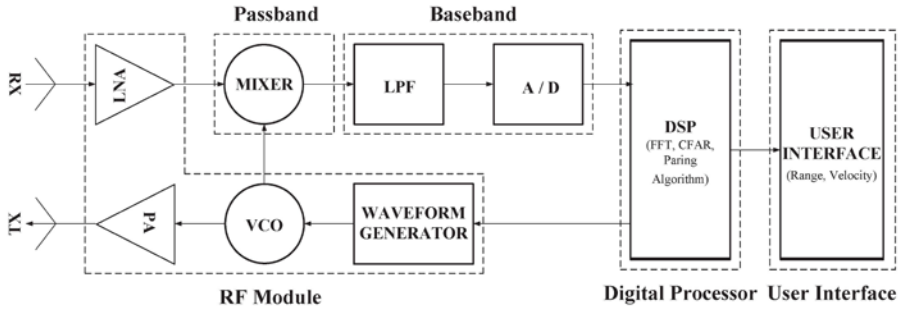

Figure 3.1 Schematic diagram of a typical FMCW radar

3.2.1 Radar Model of an Iron Tunnel

A 77 GHz forward-looking FMCW long range radar is employed in this work. The antenna module consists of linear patch antennas implemented on a printed circuit board, which has single transmitting antenna and K receiving antennas. A sinusoid signal of the waveform generator is modulated as a chirp signal by a voltage-controlled oscillator. The amplified signal is transmitted into the air, and reflected signal from the target is received with a time delay and Doppler frequency shift. Using a mixer and low pass filter, the received signal is converted to baseband signal. The range and velocity are obtained by digital processor of discrete-time signal derived from the

analog to digital converter (ADC). The unit time, which includes all of the above process, is called scan, and has a value of 50 ms in this work. With the linear frequency modulation, the received signal after ADC from k -th array can be simplified by [30]

$$x_k(n) = s_k(n) + e_k(n) = \sum_{i=1}^{T} a_k(i)\cos(2\pi f_k(i)n + \phi_k(i)) + e_k(n), \qquad (3.1)$$

where, $n = 0,1,\cdots,N-1$, N is the number of time samples, and T is the number of targets existing on the field of view. $s_k(n)$ contains sinusoids returned from each target, $e_k(n)$ represents the white noise signal with zero mean and variance of σ^2. $a_k(i)$, $f_k(i)$ and $\phi_k(i)$ are the amplitude, beat frequency and phase of the i -th target, respectively. The beat frequency, $f_k(i)$, means the frequency difference between the transmitted and the received signal for i -th target. $f_k(i)$ is composed of $f_{k,r}(i)$ (which is frequency difference by the distance of target) and $f_{k,d}(i)$ (which is Doppler frequency shift by relative velocity), and each of them is represented as

$$f_{k,r}(i) = \frac{2\alpha}{c} R(i) = \frac{2B}{cT_c} R(i), \qquad (3.2)$$

and

$$f_{k,d}(i) = \frac{2f_c}{c} v_r(i) = \frac{2}{\lambda} v_r(i), \qquad (3.3)$$

where, $\alpha = \frac{B}{T_c} = \frac{Bandwidth}{Chirp\,duration}$ is the chirp slope, f_c is the center frequency. c is speed of light and λ is the wavelength of center frequency. $R(i)$ and $v_r(i)$ are the range and relative velocity of the i-th target, respectively. When considering that the iron clutters of tunnel are densely distributed, (3.1) can be expressed as follows,

$$x_k(n) = \sum_{i=1}^{T} a_k(i)\cos(2\pi f_k(i)n + \phi_k(i)) + \sum_{j=1}^{C} a_{k,c}(j)\cos(2\pi f_{k,c}(j)n + \phi_{k,c}(j)) + e_k(n) \quad , \tag{3.4}$$

where, C is the number of clutters, $a_{k,c}(j)$, $f_{k,c}(j)$, and $\phi_{k,c}(j)$ are the amplitude, beat frequency, and phase of the j-th clutter, respectively. Assuming that the iron clutters have a uniform space, frequency difference by the distance of clutter, $f_{k,r,c}(j)$, is given by

$$f_{k,r,c}(j) = \frac{2B}{cT_c} R_c(j) = \frac{2B}{cT_c}(R_c(1) + (j-1)l) = f_{k,r,c}(1) + (j-1)\Delta f \quad , \tag{3,5}$$

where, $R_c(1)$ is the distance of the first iron clutter and l represents distance of the inter-clutter. $f_{k,r,c}(1) = \frac{2B}{cT_c} R_c(1)$ is frequency difference by the distance of the first

clutter. $\Delta f = \frac{2Bl}{cT_c}$ is frequency difference by the distance of the inter-clutter. Iron clutter is a stationary target, which has a constant Doppler frequency, so iron-tunnel condition presents periodic frequency components of the iron clutters. Under an iron tunnel, reflected signal from clutters is much larger than those from targets, which results in the detection failure of the target from clutters. To suppress clutter effect, periodicity of clutters in frequency domain needs to be analyzed. To accomplish this object, a cepstrum is employed in this work.

3.2.2 Cepstral Analysis of an Iron Tunnel

The cepstrum, derived from an anagram of spectrum, is a signal processing technique for identifying harmonic families in spectrum and removing the certain spectral components [35]. Cepstrum is used in wide research areas including speech signal processing and fault diagnosis. The cepstrum is originally defined as the power spectrum of the logarithmic power spectrum. However, various definitions for cepstrum are presented in literatures with different functionalities. For the given discrete time signal of $x_k(n)$, representative definitions of cepstrum are expressed as follows [36]

$$C_{power}(n) = \sum_{n=0}^{N-1} log(|\sum_{n=0}^{N-1} x_k(n) e^{-j\frac{2\pi}{N}kn}|^2) e^{j\frac{2\pi}{N}kn}, \quad (3.6)$$

$$C_{real}(n) = \sum_{n=0}^{N-1} log(|\sum_{n=0}^{N-1} x_k(n) e^{-j\frac{2\pi}{N}kn}|) e^{j\frac{2\pi}{N}kn}, \quad (3.7)$$

and

$$C_{complex}(n) = \sum_{n=0}^{N-1} log(\sum_{n=0}^{N-1} x_k(n) e^{-j\frac{2\pi}{N}kn}) e^{j\frac{2\pi}{N}kn}, \quad (3.8)$$

where, $|\cdot|$ denotes absolute value, $C_{power}(n)$, $C_{real}(n)$, and $C_{complex}(n)$ represent power, real and complex cepstrum, respectively. The operations of both forward and inverse Fourier transform are involved in the calculation of the cepstrum. The transformation of cepstrum concentrates on the periodic spectrum components, such as families of equally spaced harmonics. The essential observation leading to the cepstrum analysis is that the logarithmic spectrum can be treated as an input waveform and subjected to further inverse Fourier transform. The magnitude of the spectrum of $x_k(n)$ varies as the frequency changes. By the log operation, however, it is possible to compress the dynamic range of magnitude and reduce magnitude differences in the harmonic components. Table 3.1 lists the terminologies in the cepstrum domain with the one corresponding in the spectrum domain.

Table 3.1 Terminology of cepstral- and spectral domain

Cepstral domain	Spectral domain
quefrency	frequency
gamnitude	magnitude
rahmonic	harmonic
lifter	filter
saphe	phase

To characterize the radar signal under the iron-tunnel environment, we analyze the cepstral results. The real cepstrum is employed in this work. Discrete-time Fourier transform is replaced by fast Fourier transform (FFT), which is computationally efficient. Data acquisition is performed in various road conditions, such as an expressway, guardrail, normal tunnel and iron tunnel. Figure 3.2 shows the magnitude response of the cepstrum under each road condition. Under general road conditions including expressway, guardrail, and normal tunnel, any peak value of quefrency does not exist clearly. It means that there is no periodicity between the beat frequencies of the targets having different ranges and velocities. It is shown that the magnitude response has certain peak values of the quefrency only under iron-tunnel condition, which are rahmonic components. The first rahmonic peak is exactly same as the inverse of fundamental period in frequency domain, Δf . From this analysis, we verify that the periodicity of the clutter frequencies is an inherent property of the iron-tunnel condition.

(a) Express way

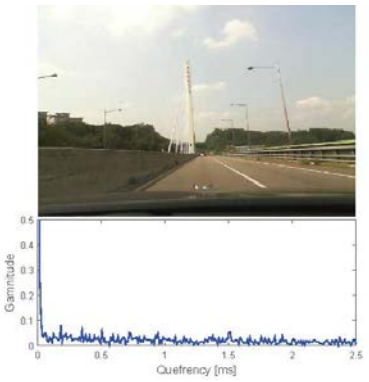

(b) Guard rail

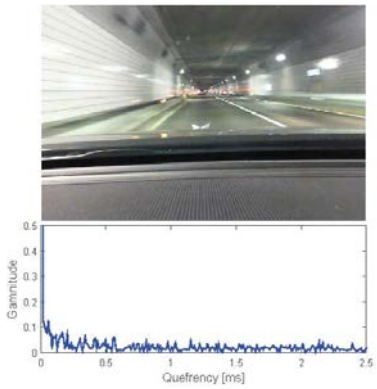

(c) Normal tunnel

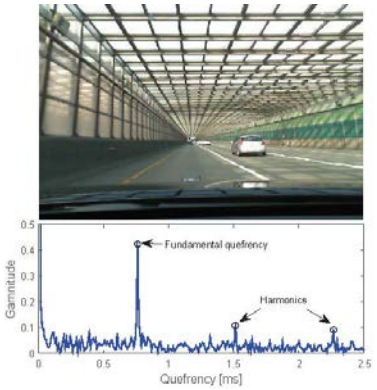

(d) Iron tunnel

Figure 3.1 Schematic diagram of typical FMCW radar

3.2.3 Cepstrum Based Clutter Suppression Method

To extract the hidden frequency of target objects from periodic frequency of clutter, an effective technique to suppress the clutter frequency is necessary. Since Fourier transform is complex domain operation, the cepstrum is represented in complex

domain. Therefore, the complex cepstrum has its inverse transformation, and the time domain signal can be reconstructed by using a modified cepstrum. However, complex cepstrum requires the continuity of phase to be unwrapped. So, it is not applicable to stationary random components where the phase is random.

On the other hand, if the input waveform of inverse Fourier transform has no phase information such as magnitude of spectrum, the cepstrum is real-valued. Despite of real-valued cepstrum, reconstruction to the time domain can be achieved by using the amplitude of the modified spectrum combined with the original phase spectrum. Moreover, we can lifter a rahmonic family in the quefrency domain and obtain an edited spectrum. Based on this real cepstral analysis, a simple rejection and reconstruction of the spectrum are employed in this work [37]. As shown in Figure 3.3, we propose to remove harmonics of clutters through the following steps: Step 1) once the received signal is transformed into the frequency domain by the fast Fourier transform (FFT), we perform the log operation to separate the amplitude and phase components. Step 2) using the log amplitude only with inverse FFT, real cepstrum is obtained. Step 3) the peak values in the cepstrum, representing a rahmonic family, are simply rejected by setting those gamnitude to zero, which acts as an ideal band-rejection lifter in the cepstral domain. Step 4) edited cepstrum is reversely transformed to spectral domain, which is an edited log amplitude. Step 5) edited log spectrum is composed of edited log amplitude and phase of the original spectrum. Step 6) with exponentiation of the edited log spectrum, finally, the edited spectrum is obtained, from which the target frequencies are extracted.

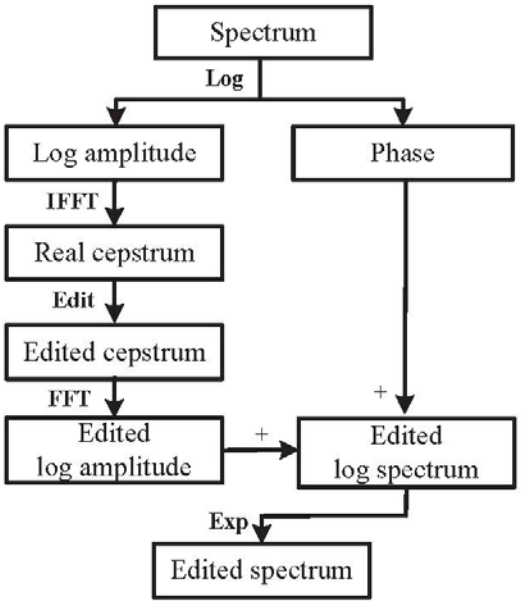

Figure 3.3 Procedure of cepstrum method for removing the harmonic family

3.3 Experimental Result

In this section, we present our experimental results based on the measured data in real driving environments. The FMCW radar sensor for ACC was installed at front of the test vehicle. The parameters of the FMCW radar are with 76.5 GHz of center frequency and 200 m of maximum operating range. The FFT algorithm is used for frequency estimation, and the cell average (CA)-CFAR is employed to detect target frequency [38]. To validate the proposed method, measurement tests were performed under various iron tunnels. Moreover, all of the measured data is obtained in a real driving situation. To recognize an iron tunnel, the method based on spectrum spreading in [22], is applied. The proposed method, therefore, operates only when iron tunnel is recognized. The profile of the representative two iron tunnels, used in this work, is summarized in Table 3.2.

Table 3.2 Iron-tunnel profile

Case	Geographic coordinate (latitude, longitude)	Length (km)	Experiment Date
A	(37.27, 127.08)	1.0	Sep.09.2015
B	(37.17, 127.03)	0.7	Sep.05.2015

The measured results for the proposed suppression method are shown in Figure 3.4 and Figure 3.5 for case A and B in Table 3.2, respectively. Figure 3.4.a depicts the original spectrum of the received signal before applying the proposed algorithm. The component represented by an asterisk stands for beat frequency of the target vehicle in the same lane with the ego-vehicle. Because of the periodical frequencies of the iron clutters, the hidden frequency of the target is not identified clearly. Although the target indicates the peak frequency, the frequency of target may be filtered by a CFAR threshold. The magnitude response of the log spectrum is shown in Figure 3.4.b. The log magnitude maintains periodicity of the original spectrum, while it smoothens the variation of magnitude with respect to frequency. Figure 3.4.c shows the cepstrum of the received signal with fundamental period and its rahmonics, resulted from the periodic peaks in the spectrum. The peak at rahmonic of 0.76 ms in Figure 3.4.c is equal to the inverse of 1.31 kHz, the fundamental period of the peak in the spectrum. After peaks of quefrencies are removed, edited spectrum in Figure 3.4.d still has residual periodic components. Compared with the original spectrum, nevertheless, frequency of the target is identified definitely, and also clutter effect is suppressed clearly. Figure 3.5 in case B of the iron tunnel also shows very similar results with Figure 3.4. Because the iron structures of the case B are almost same as those of A, identical fundamental frequency and harmonics in the quefrency domain are presented.

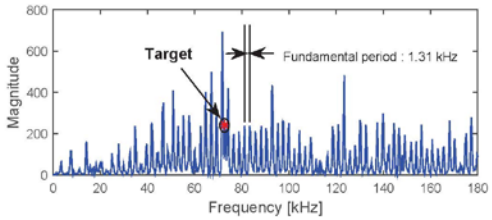

(a) Magnitude of original spectrum

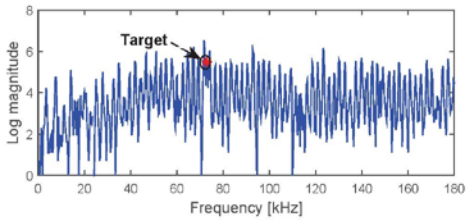

(b) Log magnitude of original spectrum

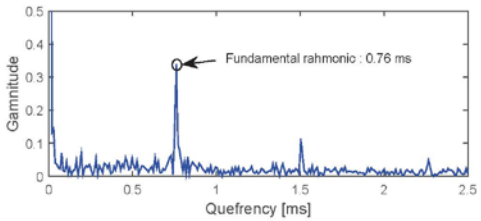

(c) Cepstrum analysis

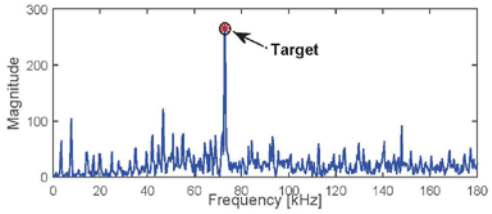

(d) Edited spectrum

Figure 3.4 Clutter suppression using cepstral analysis for the iron tunnel of case A

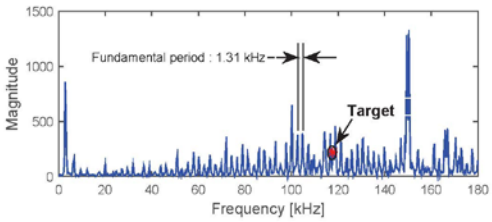

(a) Magnitude of original spectrum

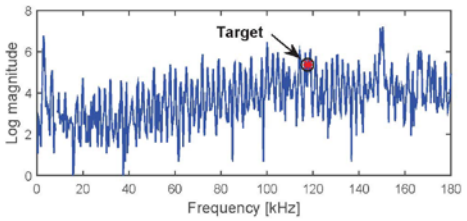

(b) Log magnitude of original spectrum

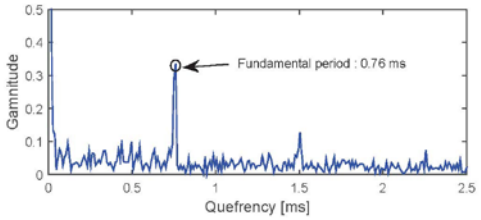

(c) Cepstrum analysis

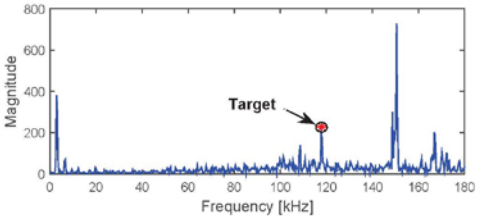

(d) Edited spectrum

Figure 3.5 Clutter suppression using cepstral analysis for the iron tunnel of case B

Figure 3.6 presents detection results before and after the clutter suppression. Figure 3.6.a and Figure 3.6.b shows the original spectrum and edited spectrum in frequency domain, respectively. The dotted line represents the threshold value obtained by CFAR. The spectral components larger than CFAR threshold are expressed by an asterisk. These peaks include the target in the same lane with ego-vehicle, the targets in others lane, and also clutters with high power. Although residual clutters are detected after suppression, they can be rejected by target pairing and tracking procedure. It is beyond the scope of this study to examine the pairing and tracking algorithm. It is noteworthy that the target in the same lane with the ego-vehicle is extracted from clutters, which provides essential information so as to control the ego-vehicle automatically. Figure 3.6.c depicts the trajectory comparison of the target vehicle in the same lane. The trajectory of the target is calculated by using the estimated target distance, location of ego-vehicle, and wheel speed of ego-vehicle. It represents the change of the estimated position with a marker at every five scans. It is shown that when the suppression algorithm is applied, the target vehicle is detected at an earlier time.

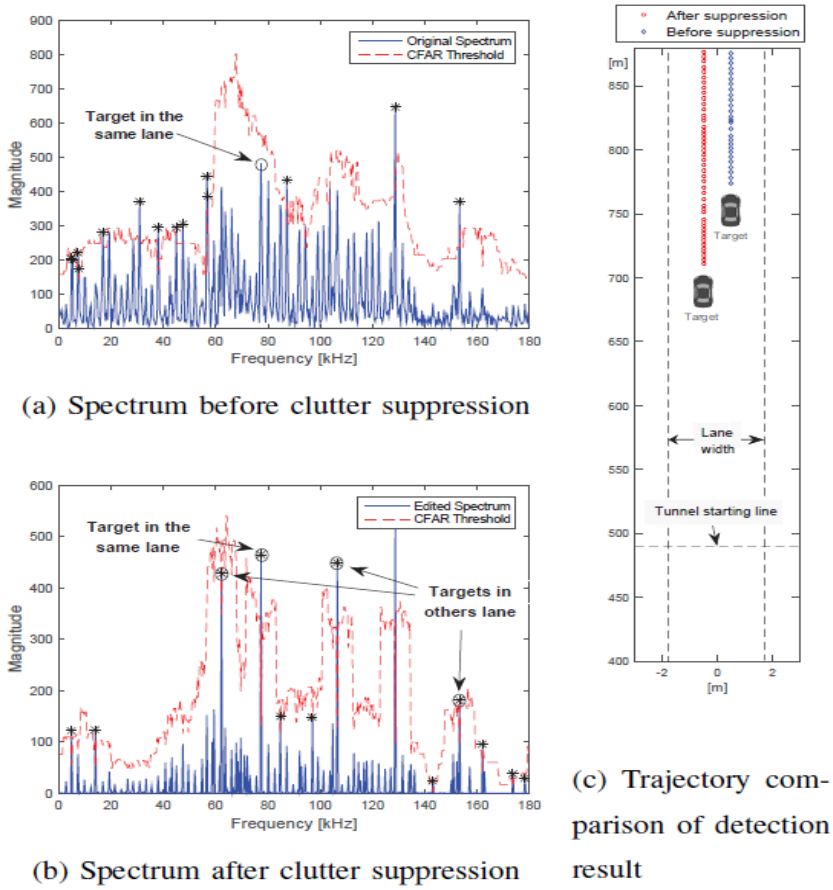

Figure 3.6 Detection result before and after clutter suppression

To evaluate the performance of the proposed method quantitatively, experiments are performed to determine the distance of early target detection, which is a measure of the initial distance to detect a target vehicle in the lane of the ego-vehicle. The initial detection of the target is a very important indicator for the ACC application. If the initial detection of the target is late, the ego-vehicle brakes suddenly, which increases the probability of collision with the vehicle in the front or rear. For each iron-tunnel

condition, some factors are considered including a type of the target vehicle and different velocity of the ego-vehicle. Table II summarizes the results of distance of early target detection for each iron tunnel. The average distance of the early target detection is improved by more than 55 m for the proposed method. Although the proposed method performs additional computation of both FFT and inverse FFT, it shows performance enhancement without adjusting any CFAR threshold with respect to the road condition.

Table 3.3 Evaluation of the distance of early target

Case	Geographic coordinate (latitude, longitude)	Length (km)	Before suppression (m)	After suppression (m)	Ego-vehicle speed (mps)	Relative speed (mps)	Vehicle type	Experiment Date
A	(37.27, 127.08)	1.0	79.7	133.4	37.3	-8.21	SUV	Sep.09.2015
A	(37.27, 127.08)	1.0	57.3	118.1	34.1	-9.99	compact car	Sep.09.2015
B	(37.17, 127.03)	0.7	64.5	125.1	27.1	-6.97	Sedan	Sep.05.2015
B	(37.17, 127.03)	0.7	60.1	109.7	40.1	-23.16	compact car	Sep.05.2015

3.4 Conclusion

In many applications of automotive radar systems, a technique to suppress clutter effect is essential, particularly for the iron-tunnel environments. In this paper, we modeled a FMCW radar signal under iron tunnels in which iron structures are uniformly and densely distributed. From cepstral analysis, we proved that the periodic property of iron clutters is revealed in the cepstral domain. Based on this observation, we proposed an efficient clutter suppression method using real cepstrum to remove the clutter effects in the cepstral domain. Experimental results present that the proposed method provides significant enhancement in the target detection performance. This proves that the proposed method is successfully applied for clutter suppression.

Chapter 4

Interference Mitigation by High-Resolution Frequency Estimation for Automotive Radars

4.1 Introduction

Mutual interference is a crucial issue that must be resolved for improved safety functions [16], [23]. Given the increasing number of automotive radar sensors operating at the same instant, the probability that radar sensors may receive signals from other radar sensors gradually increases. In such a situation, the system may fail to detect the correct target given the serious interference. Effective countermeasures, therefore, have to be considered. In the literature, several techniques have been presented in an effort mitigate the performance degradation issue caused by interference in radar or communications systems [39], [40]. To avoid overlap in the frequency domain, one method to minimize interference shifts the frequency of the transmitted signal pseudo-randomly [39]. Other authors [40] propose frequency ramps from short PN-coded sequences as a spread-spectrum technique. With these methods, however, the radars must share the same set of codes. Efficient strategies to distribute codes are required beforehand for collision avoidance.

Another study [16] qualitatively analyzed the mutual interference between millimeter-wave radar sensors and examined interference scenarios when considering spatial, temporal and frequency overlap. Interference from neighboring sensors appears to result in an increase in the noise level in the frequency domain. Therefore, it is important to estimate beat frequency accurately in a high interference environment. Conventional FMCW radar systems use the fast Fourier transform (FFT) algorithm for beat frequency estimation [41]. However, the traditional FFT algorithm is associated with high probability of failing to separate target objects from interferers. This motivates us to exploit high-resolution estimation techniques in interference-limited automotive radar environments.

This chapter proposes a beat frequency estimator for use in automotive FMCW radar systems based on high-resolution techniques to suppress mutual interference by means of a frequency domain analysis. The proposed method can be considered as the application of a subspace method known as MUSIC and ESPRIT, which solve the generalized eigenvalue problem using an autocorrelation matrix of received signal [17], [18]. The proposed method employs an estimator of a correlation matrix with forward-backward spatial smoothing (FBSS) [42] and a frequency signal dimension order (FSDO) estimator with the minimum description length (MDL) criteria [27]. The proposed method improves the frequency resolution and reduces the influence of interference relative to the FFT method. Moreover, ESPRIT is more computationally efficient than MUSIC [43], as ESPRIT directly calculates the frequency components in a given frequency range, whereas MUSIC requires a peak detection process from the spectral analysis.

To verify proposed methods, measurement was performed in a test field. The

experimental data used in the paper are obtained from a 77 GHz forward-looking FMCW radar for adaptive cruise control (ACC). The results show that the missing problem of a target vehicle under interference environments is improved by proposed methods in the detection performance.

The rest of this chapter is organized as follows. The characteristics and a mathematical representation of FMCW radar systems are presented in section 4.2. Based on the system model, beat frequency estimations using MUSIC and ESPRIT are discussed in section 4.3. Experimental results are presented in section 4.4 to verify the performance enhancement when using the proposed schemes. Finally, conclusions are given in section 4.5.

4.2 Automotive FMCW Radars in an Interference Environment

A signal transmitted using a linearly increasing or decreasing signal in the frequency domain can be represented as [30]

$$\begin{aligned} f(t) &= A\cos(2\pi\phi) \\ &= A\cos\left(2\pi\int_0^t (f_0 + \alpha t)dt\right) = A\cos\left(2\pi(f_0 t + \frac{1}{2}\alpha t^2)\right), \end{aligned} \tag{4.1}$$

where, A and ϕ are the amplitude and phase of the transmitted signal, respectively; f_0 is the transmitted signal frequency at time $t = 0$; and $\alpha = \frac{BW}{\Delta t} = \frac{\text{sweepbandwidth}}{\text{sweeptime}}$ is the chirp rate (chirp slope). The received signals returning from multiple targets are delayed and attenuated. If the targets are moving, they include an additional frequency shift term as follows:

$$g(t) = \sum_{i=1}^{m} B_i \cos\left(2\pi\left((f_0 + f_{d,i})(t - t_{d,i}) + \frac{1}{2}\alpha(t - t_{d,i})^2\right)\right), \tag{4.2}$$

Here, m is the number of targets; B_i is the amplitude of the received signal; and

$f_{d,i}$ and $t_{d,i}$ are the Doppler frequency and the delay time respectively. The transmitted and received signals are mixed by multiplication in the time domain. With the trigonometric identity of the sum of the cosines, the product of the two signals has distinct sinusoidal components. One of these will be at a frequency that is approximately twice the carrier frequency, which will be cut off by a low-pass filter (LPF). The other term, i.e., the mixer output after LPF processing, is given by

$$s(t) = \sum_{i=1}^{m} C_i \cos\left(2\pi(\alpha t_{d,i} - f_{d,i})t + 2\pi(f_0 + f_{d,i})t_{d,i} - \pi\alpha t_{d,i}^2\right), \qquad (4.3)$$

where $C_i = AB_i$ is the amplitude of the mixed output. $f_{b,i} = \alpha t_{d,i} - f_{d,i}$ is the beat frequency (or frequency difference), which is analyzed by the FFT algorithm. The range and velocity of each target are obtained from the beat frequency component with a peak detection algorithm such as the CFAR technique [44].

Considering that many vehicles may be equipped with FMCW radar sensors, it is essential to analyze the interference mechanism. Two simple scenarios can be regarded, as shown in Figure 4.1. One is direct interference from a vehicle in the opposite direction and the other is a returned interference from a vehicle traveling in the same direction (which is indirect interference). There are many factors affecting radar sensitivity, such as interfering source levels, the side-lobe effect, the target shape, the

operating band, and the sweep time.

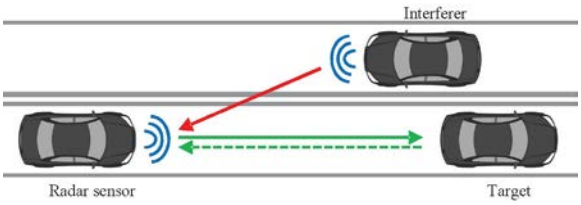

(a) Direct interference

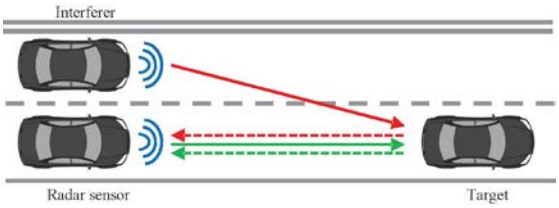

(b) In-direct interference

Figure 4.1 Simple interference scenarios in automotive radar environment

As an issue that acts between FMCW radars, interference can be divided into in-band-region interference and out-of-band interference depending on the delay time, resulting in a ghost target and a uniform increase of the noise floor respectively [16]. In-band-region interference not only occurs with a very low probability, but it can also be removed by means of multi-target detection and tracking algorithms [45]. For the out-of-band interference, however, the detection of the targets fails due to the increase in the noise floor. Figure 4.2 shows the influence of an interference signal that is 30dB larger than the signal from the target when the target is present at the 70m. The target

signal-to-noise-ratio (SNR) is reduced considerably. It is an important issue, therefore, to identify the signal from a result which contains an increase in the noise floor. The out-of-band interference is modeled in the following two cases according to the delay time of the interference signal.

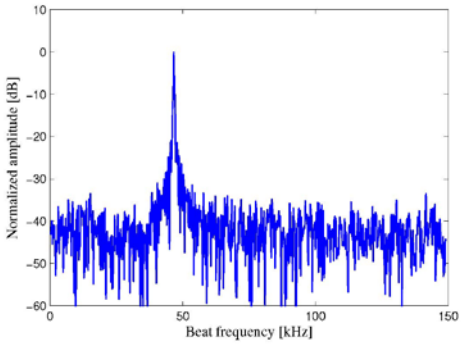

(a) Spectrum of a target without interference

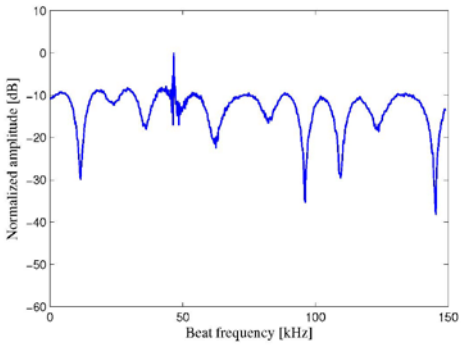

(b) Spectrum of a target with interference

Figure 4.2 The spectrum of FFT output for an out-of-band region interference with a magnitude 30 dB larger than signal returned from target object.

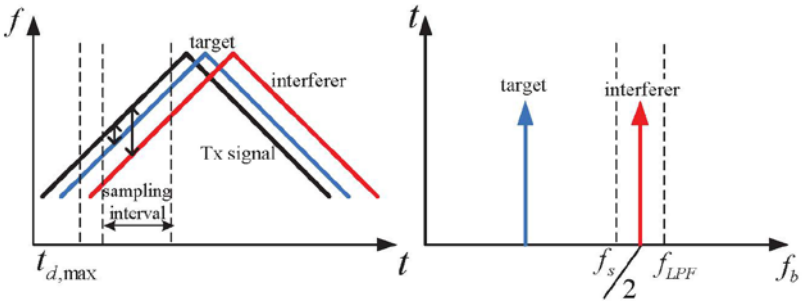

(a) Same sign-chirp case

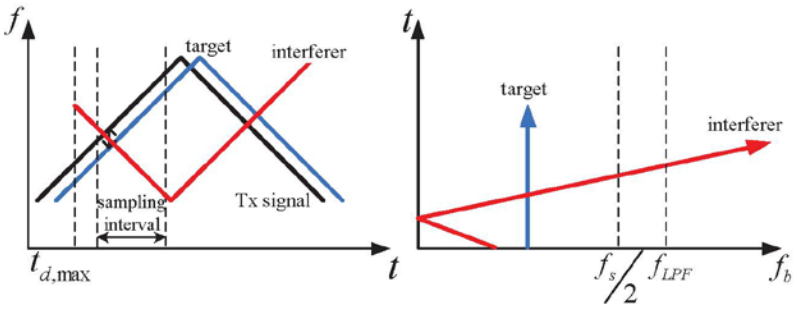

(b) Different sign-chirp case

Figure 4.3 Two cases of out-of-band interference, where f_s is the sampling rate and f_{LPF} is the cut-off frequency of LPF.

4.2.1 The Same Sign-Chirp Case

Assuming there are multiple interferers equipped with FMCW radar in the field of view, with parallel increasing chirps in the transmitted signal and with the interference

signal in the sampling interval (Figure 4.3(a)), the received signal can be expressed as follows:

$$\begin{aligned} g(t) &= g_s(t) + g_I(t) + n(t) \\ &= \sum_{i=1}^{m} B_i \cos\left(2\pi\left((f_0 + f_{d,i})(t - t_{d,i}) + \frac{1}{2}\alpha(t - t_{d,i})^2\right)\right) \\ &\quad + \sum_{j=1}^{k} B_{I_j} \cos\left(2\pi\left((f_0 + f_{d,I_j})(t - t_{d,I_j}) + \frac{1}{2}\alpha(t - t_{d,I_j})^2\right)\right) + n(t). \end{aligned} \tag{4.4}$$

Here, $t_{d,max} < t_{d,I_j}$; $t_{d,max}$ is the round-trip time for the maximum operating range of 200m, I_j is the index of the interferer, t_{d,I_j} is the delay time of the interferer, k is the number of interferers, and $n(t)$ is white noise. The mixed output after low-pass filtering is as follows:

$$\begin{aligned} x(t) &= f(t)g(t) = f(t)\left(g_s(t) + g_I(t) + n(t)\right) = s(t) + I(t) + w(t) \\ &= \sum_{i=1}^{m} C_i \cos\left(2\pi(\alpha t_{d,i} - f_{d,i})t + (2\pi(f_0 + f_{d,i})t_{d,i} - \pi\alpha t_{d,i}^2\right) \\ &\quad + \sum_{j=1}^{k} C_{I_j} \cos\left(2\pi(\alpha t_{d,I_j} - f_{d,I_j})t + (2\pi(f_0 + f_{d,I_j})t_{d,I_j} - \pi\alpha t_{d,I_j}^2\right) + w(t). \end{aligned} \tag{4.5}$$

In this case, the influence of interference signal is presented in the form of a ghost target with a constant frequency. Because the beat frequency of the interferer is larger

than the maximum beat frequency corresponding to the maximum operating range, it can be ignored by the sampling rate, f_s.

4.2.2 The Different Sign-Chirp Case

In contrast to the above case, with an increasing chirp of transmitted signal and a decreasing chirp of interfering signal, the received signal is expressed as follow:

$$\begin{aligned} g(t) &= g_s(t) + g_I(t) + n(t) \\ &= \sum_{i=1}^{m} B_i \cos\left(2\pi\left((f_0 + f_{d,i})(t - t_{d,i}) + \frac{1}{2}\alpha(t - t_{d,i})^2\right)\right) \\ &+ \sum_{j=1}^{k} B_{I_j} \cos\left(2\pi\left((f_0 + BW + f_{d,I_j})(t - t_{d,I_j}) - \frac{1}{2}\alpha(t - t_{d,I_j})^2\right)\right) + n(t), \end{aligned} \tag{4.6}$$

The mixed output is, therefore, given by

$$\begin{aligned} x(t) &= f(t)g(t) = f(t)\left(g_s(t) + g_I(t) + n(t)\right) = s(t) + I(t) + w(t) \\ &= \sum_{i=1}^{m} C_i \cos\left(2\pi(\alpha t_{d,i} - f_{d,i})t + (2\pi(f_0 + f_{d,i})t_{d,i} - \pi\alpha t_{d,i}^2\right) \\ &+ \sum_{j=1}^{k} C_{I_j} \cos\left[-2\pi(\alpha t_{d,I_j} + BW + f_{d,I_j})t + 2\pi\alpha t^2 + 2\pi(f_0 + BW + f_{d,I_j})t_{d,I_j} + \pi\alpha t_{d,i}^2\right] + w(t). \end{aligned} \tag{4.7}$$

Because the interfering signal comes with a short pulse and time-varying frequency components as shown in Figure 4.3(b), it would appear as an increase in the noise floor with a very wide spectral width. The amount of the increase in the noise floor is proportional to the time duration of the interfering signal or the interfering source power. Considering that the interfering signals are also treated as noise, (4.7) can also be represented as shown below.

$$\begin{aligned} x(t) &= s(t) + \big(I(t) + w(t)\big) = s(t) + e(t) \\ &= \sum_{i=1}^{m} C_i \cos\left[2\pi(\alpha t_{d,i} - f_{d,i})t + (2\pi(f_0 + f_{d,i})t_{d,i} - \pi\alpha t_{d,i}^2\right] + e(t), \end{aligned} \tag{4.8}$$

Here, $e(t)=I(t)+w(t)$.

4.3 High-Resolution Frequency Estimation Methods

In this section, the proposed high-resolution beat frequency estimation scheme is described. Figure 4.4 shows a functional block diagram of the proposed scheme, which employs a FBSS and a FSDO estimator. We present a data model for subspace-based algorithms and describe an effective method to estimate the correlation matrix. Based on the data model, a theory encompassing MUSIC and ESPRIT is investigated and the FSDO estimator, as a part of MUSIC and ESPRIT, is presented to provide the number of frequency components.

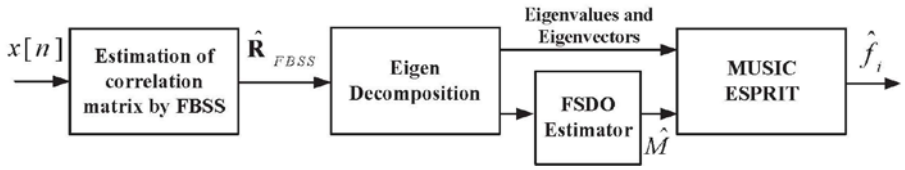

Figure 4.4 Functional block diagram of the high-resolution beat frequency estimation algorithm

4.3.1 Data Model

Let us a consider sampled version of radar mixed output as a discrete-time sinusoid signal having amplitude, frequency, and phase components, as follows,

$$x[n] = s[n] + e[n] = \sum_{i=1}^{m} a_i \cos(2\pi f_i n + \phi_i) + e[n], \qquad (4.9)$$

where n=0,1,2,$\cdots$,N–1; $s[n]$ contains sinusoids returned from each target; $e[n]$ represents the noise signal from other FMCW radars, including white noise with a zero mean and variance of σ^2; m is the number of sinusoids; N is the number of sampled data points; and a_i, f_i and ϕ_i are the amplitude, beat frequency, and phase of the i-th sinusoid, respectively. According to Euler's formula, $\cos(2\pi f_i n+\phi_i)$ can be expressed as $\frac{1}{2}(e^{j(2\pi f_i n+\phi_i)}+e^{j(-2\pi f_i n+\phi_i)})$. Then, (4.9) can be represented in complex exponential form, as

$$x[n]=s[n]+e[n]=\sum_{i=1}^{M}\overline{A_i}e^{j(2\pi \overline{f_i}n+\phi_i)}+e[n], \tag{4.10}$$

with

$$\begin{aligned}
&\overline{A_i}=\frac{a_i}{2}e^{j\pi_i},\quad \overline{f_i}=f_i \quad \text{for } 1\le i\le m\\
&\overline{A_i}=\frac{a_i}{2}e^{-j\pi_i},\ \overline{f_i}=-f_i \quad \text{for } m+1\le i\le 2m,\\
&M=2m
\end{aligned} \tag{4.11}$$

By defining the i-th complex sinusoid component, $\overline{A_i}e^{j2\pi \overline{f_i}n}$ as $s_i(n)$, (4.10) is expressed as follows:

$$x[n] = \sum_{i=1}^{M} s_i[n] + e[n], \qquad n = 0,1,2,\cdots,N-1, \tag{4.12}$$

From L discrete-time samples, a compact matrix form is obtained by

$$\mathbf{x}(n) = \sum_{i=1}^{M} \mathbf{s}_i(n) + \mathbf{e}(n), \tag{4.13}$$

where $L > M$; $\mathbf{x}(n) = [x[n]\, x[n+1] \cdots x[n-L+1]]^T$, $\mathbf{s}_i(n) = [s_i[n]\, s_i[n+1] \cdots s_i[n-L+1]]^T = [1\, e^{j2\pi \overline{f_i}} \cdots e^{j2\pi(L-1)\overline{f_i}}]^T \times \overline{A_i} e^{j2\pi \overline{f_i} n}$; and $\mathbf{e}(n) = [e[n]\, e[n+1] \cdots e[n-L+1]]^T$. Then, a low-rank matrix representation for subspace methods can be represented as

$$\mathbf{x}(n) = \mathbf{F}\mathbf{A}(n) + \mathbf{e}(n), \tag{4.14}$$

where $\mathbf{F} = [\mathbf{f}(\overline{f_1})\mathbf{f}(\overline{f_2}) \cdots \mathbf{f}(\overline{f_M})]$ is a $L \times M$ Vandermonde matrix of rank M , $\mathbf{A}(n) = [\overline{A_1} e^{j2\pi \overline{f_1} n}\, \overline{A_2} e^{j2\pi \overline{f_2} n} \cdots \overline{A_M} e^{j2\pi \overline{f_M} n}]$, and $\mathbf{f}(\overline{f_i}) = [e^{j2\pi \overline{f_i}} \cdots e^{j2\pi(L-1)\overline{f_i}}]^T$ for $i = 1,2,\cdots,M$ is a frequency mode vector with frequency $\overline{f_i}$. The autocorrelation matrix of mixed output $\mathbf{R}_{xx}$ is expressed as

$$\mathbf{R}_{xx} = E\left[\mathbf{x}(n)\mathbf{x}(n)^H\right], \tag{4.15}$$

where $E[\cdot]$ denotes the expected value. By using eigenvalue decomposition, the eigenvalues and corresponding eigenvectors of $\mathbf{R}_{xx}$ are obtained according to $\{\lambda_1 \geq \lambda_2 \geq \cdots \geq \lambda_L\}$ and respectively. If $\mathbf{R}_{xx}$ has the full rank of M, the eigenvalues are given by

$$\lambda_1 \geq \lambda_2 \geq \cdots \geq \lambda_M > \lambda_{M-1} = \lambda_{M-2} = \cdots = \lambda_L = var[e[n]], \tag{4.16}$$

where $var[e[n]]$ denotes the noise variance. From the eigenvalues and eigenvectors of $\mathbf{R}_{xx}$, we define a signal subspace matrix $\mathbf{V}_S = [\mathbf{v}_1 \mathbf{v}_2 \cdots \mathbf{v}_M]$ corresponding to the largest M eigenvalues, and a noise subspace matrix $\mathbf{V}_N = [\mathbf{v}_{M+1} \mathbf{v}_{M+2} \cdots \mathbf{v}_L]$ that contains the remaining eigenvectors.

4.3.2 Estimation of the Correlation Matrix

The correlation matrix of the received signal is found by the expected value of the absolute values squared. However, we cannot identify the exact statistics for the signal and noise. Assuming that the process is ergodic, we can approximate the correlation matrix by means of time-averaged correlation as follows:

$$\hat{\mathbf{R}}_{xx} = \frac{1}{N-L+1}\sum_{k=1}^{N-L+1}\mathbf{x}(n)\mathbf{x}(n)^H . \quad (4.17)$$

Here, $N > L$, N denotes the sequentially decimated time samples $\{x[n]x[n+1]\cdots x[n+N-1]\}^T$. When the number of time samples is limited, the rank sparsity of the correlation matrix degrades the performance. To improve the performance of subspace methods, FBSS method is used in this paper [42]. FBSS is used to calculate the $L \times L$ matrix, as

$$\hat{\mathbf{R}}_{FBSS} = \frac{1}{2Q}\sum_{k=1}^{Q}(\hat{\mathbf{R}}_{\mathbf{n}} + \mathbf{J}\hat{\mathbf{R}}_{\mathbf{n}}{}^T\mathbf{J}), \quad (4.18)$$

where $Q = N-L+1$; $\hat{\mathbf{R}}_{\mathbf{n}} = \mathbf{x}(n)\mathbf{x}(n)^H$, and $\mathbf{J}$ is the $L \times L$ reversal matrix, for which the elements are unity along the anti-diagonal and are zero elsewhere.

4.3.3 Application of the MUSIC Algorithm

The MUSIC algorithm uses the basic assumption that the frequency mode vector corresponding to its frequency component is orthogonal to the noise subspace formed by the noise eigenvectors. This is expressed, as

$$\mathbf{f}^H(\overline{f}_i)\mathbf{v}_k = 0, \quad (4.19)$$

where $i = 1, 2, \cdots, M$ and $k = M+1, M+2, \cdots, L$

By using the orthogonality of the frequency mode vectors to the noise eigenvectors, the MUSIC pseudo-spectrum is then defined as follows [17]:

$$P_{MUSIC}(f) = \frac{1}{\sum_{k=m+1}^{M} |\mathbf{f}^H(f)\mathbf{v}_k|^2}, \tag{4.20}$$

A peak value occurs in the pseudo-spectrum when $f = \overline{f_i}$, and the estimated frequency is obtained by CFAR[44].

4.3.4 Application of the ESPRIT Algorithm

ESPRIT is based on the naturally existing shift-invariance between discrete-time series samples which leads to rotational invariance between the corresponding signal subspaces [18]. Let us define two subsamples $\mathbf{x}_1(n) = [x[n]\, x[n+1] \cdots x[n+L-2]]^T$ and $\mathbf{x}_2(n) = [x[n+1]\, x[n+2] \cdots x[n+L-1]]^T$ for $L-1 > M$. From $s_i[n+1] = s_i[n]e^{j2\pi\overline{f_i}}$ in (4.13), $\mathbf{x}_1(n)$ and $\mathbf{x}_2(n)$ can be represented by

$$\begin{aligned} \mathbf{x}_1(n) &= \mathbf{F}\mathbf{A}(n) + \mathbf{e}_1(n) \\ \mathbf{x}_2(n) &= \mathbf{F}\mathbf{\Phi}\mathbf{A}(n) + \mathbf{e}_2(n), \end{aligned} \tag{4.21}$$

where $\mathbf{\Phi}$ is a $(L-1)\times(L-1)$ diagonal matrix whose i-th component is $\phi_i = e^{j2\pi\bar{f}_i}$. By defining $\mathbf{V}_{S1}$ and $\mathbf{V}_{S2}$ as the signal subspace eigenvectors from the auto-correlation of $\mathbf{x}_1(n)$ and $\mathbf{x}_2(n)$, respectively, the subspaces of the eigenvectors are related by a unique non-singular transformation matrix $\mathbf{\Psi}$ such that

$$\mathbf{V}_{S1}\mathbf{\Psi} = \mathbf{V}_{S2}. \tag{4.22}$$

Because $\mathbf{F}$ and $\mathbf{V}_{S1}$, $\mathbf{V}_{S2}$ span the same signal subspace, there is also a unique non-singular transformation matrix $\mathbf{T}$ such that

$$\begin{aligned} \mathbf{V}_{S1} &= \mathbf{F}\mathbf{T} \\ \mathbf{V}_{S2} &= \mathbf{F}\mathbf{\Phi}\mathbf{T}. \end{aligned} \tag{4.23}$$

By substituting (4.23) into (4.22), we can derive the following relationship:

$$\mathbf{\Psi} = \mathbf{T}^{-1}\mathbf{\Phi}\mathbf{T}. \tag{4.24}$$

Thus, the largest M eigenvalues of $\mathbf{\Psi}$ are equal to the diagonal elements of $\mathbf{\Phi}$ such that $\psi_1 = e^{j2\pi\bar{f}_1}, \psi_2 = e^{j2\pi\bar{f}_2}, \cdots, \psi_M = e^{j2\pi\bar{f}_M}$. The frequency estimates $\hat{\bar{f}}_i$ for $1 \le i \le M$ are then calculated as

$$\hat{\bar{f}}_i = \frac{\angle(\psi_i)}{2\pi}, \tag{4.25}$$

where $\angle\cdot$ denotes the phase of the argument, with the sampling frequency of the

data used to calculate $\widehat{\widehat{f_i}}$. The MUSIC algorithm needs to search the peaks of the spatial spectrum at a cost of computational load, whereas ESPRIT exploits the rotational invariance structure of the signal subspace and avoids searching any spatial spectrum.

4.3.5 Number of Frequency Estimation

MUSIC and ESPRIT take advantage of a prior knowledge such as the number of frequency components. Because the precise number of frequency M value is not available in practical systems, it must be estimated. As information theoretic criteria, MDL or the AIC have been widely used to estimate the number of frequencies. In this paper, we employ the MDL criterion to estimate M. This is expressed as [27],

$$\mathrm{MDL}(k) = -\log\left(\frac{\prod_{i=k}^{L-1}\lambda_i^{\frac{1}{L-k}}}{\frac{1}{L-k}\sum_{i=k}^{L-1}\lambda_i}\right)^{(k-L)Q} + \frac{1}{2}k(2L-k)\log Q, \qquad (4.26)$$

after which the estimate of M can be obtained by

$$\hat{M} = \arg_k \min \mathrm{MDL}(k) + 1, \qquad (4.27)$$

where, $k = 0,1,\cdots,L-1$.

4.4 Experimental Result

Table 4.1 Parameters of a FMCW radar for the experiment

Parameter	Specification
Frequency	76.25-76.75 GHz
Sweep bandwidth	500 MHz
Sweep time	5 ms
Output power	10 mW
Maximum range	200 m
FFT points	2048
Sampling rate	298 kHz

In this section, we present our measurement setup and analyze the proposed method as compared to the conventional FFT algorithm. To validate performance of the proposed methods, measurement performed with two interference scenario (Figure 4.1). The FMCW radar sensor, used for ACC, was installed in the test vehicle which is produced by a Korea company. All of the experiments were performed in an open space on flat ground. The interfering and target vehicles have 10dBsm radar cross section (RCS). The parameters of the FMCW radar used in this study are summarized in the Table 1. For a sweep bandwidth of 500 MHz, a sweep time of 5 ms and a maximum operating range of 200 m, the maximum round trip time is 1.33 μs and the maximum beat frequency is 133 kHz. The cut-off frequency of the LPF was set to 1 MHz.

In order to evaluate the quantitative performance of the frequency estimation in an interference environment, probability of resolution is analyzed according to SIR. The SIR is determined by the distance from the radar sensor to the target and the interferer. The SIR is distributed up to about -31 dB and -63 dB for the indirect interference and direct interference respectively.

The mixer outputs of the FMCW radar were analyzed using the conventional FFT, the MUSIC and the ESPRIT methods. To detect the peak values from the FFT and MUSIC spectral results, the ordered statistic (OS) CFAR algorithm was adopted [44], where the probability of a false alarm is 10^{-6}. The beat frequency of the target is determined by the spectral component higher than a threshold.

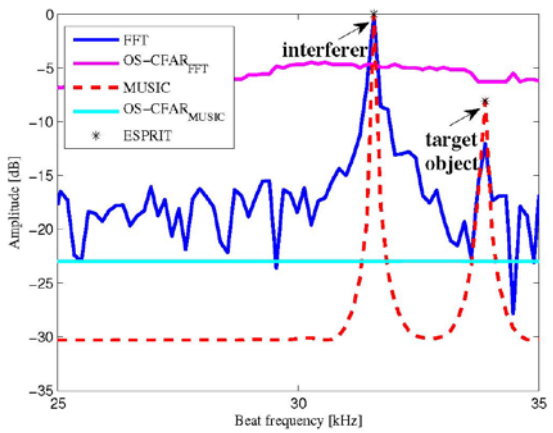

Figure 4.5 Sample result for the beat frequency estimation when the target object exists at a range of 50m (For a direct interference scenario)

Figure 4.5 shows a snapshot (which means a scan) for the beat frequency estimation when the target object exists at a range of 50 m. In this example, the SIR is -30 dB (i.e., the direct interferer is 30 m away from the radar sensor). This result shows that the proposed method is more capable of identifying the beat frequency than the conventional FFT method. Although, the FFT result indicates a peak value for the target object, it is not larger than the threshold, leading to a detection failure of the target object.

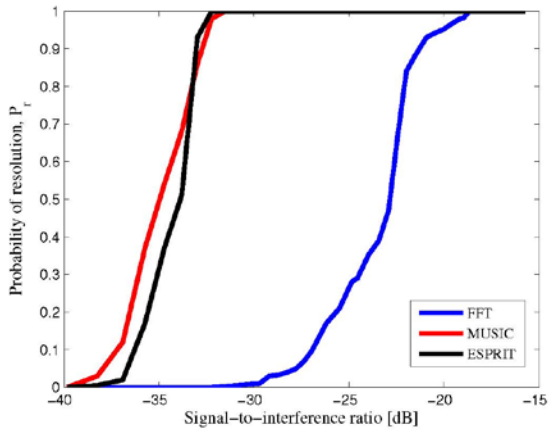

Figure 4.6 Probability of resolution versus SIR

The results are based on 1600 independent periods of measured data for each distance using the subsample size set to $L = 100$ for the FBSS. As shown in Figure 4.6, the proposed method operates up to a SIR of -32.5 dB, whereas the FFT shows a

performance limit of -17.9 dB SIR. These subspace-based methods are entirely robust for at least indirect interference scenarios. For a short range of less than 50 m, Furthermore, it can be said the proposed methods can identify the beat frequencies of targets regardless of the SIR. The MUSIC and ESPRIT algorithms show similar performance levels. However, ESPRIT has better computational efficiency because it avoids the peak-search process.

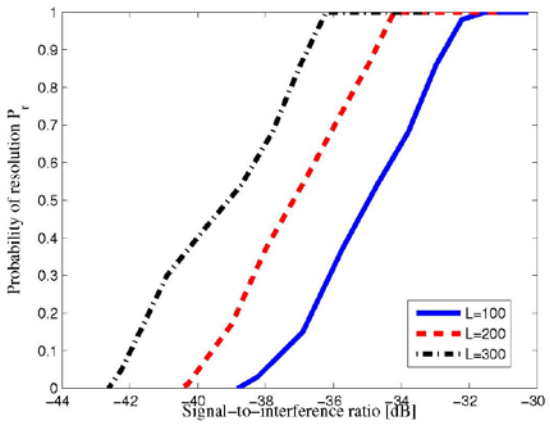

Figure 4.7 Probability of resolution versus the number of subsample for FBSS

The performance of the proposed algorithm versus the number of subsamples for the FBSS was also assessed. The conditions for estimation are same to those in Figure 4.7, except that the number of subsamples is varied from $L = 100$ to $L = 300$. Figure 4.7 shows that when the number of samples is increased to 200 and 300, the

performance of the MUSIC algorithm shows additional margin of SIR, about 2.4 dB and 4.1 dB, respectively. This improvement occurs because large number of subsamples, L , makes the rank property of the correlation matrix effective.

4.4 Conclusion

The conventional FFT approach is vulnerable in interference-limited environments. In this paper, the performance limitation of the existing system was evaluated quantitatively. Also, we proposed a subspace-based method to identify the beat frequency of the targets while suppressing the interference signals. Experimental results show that the proposed method has a SIR margin of at least about 14 dB compared to the conventional FFT algorithm. The proposed method provides a significant performance enhancement even in a direct interference environment, which proves that the proposed estimation method can be successfully applied for the beat frequency analysis in an interference environment. Thus, it is concluded that MUSIC and ESPRIT are essential for minimizing the interference effects in the automotive radar field. Moreover the overall method will be useful for eliminating the influence of interference when used in conjunction with other mitigation techniques.

Bibliography

[1] D. Geronimo. A. Lopez, A.D. Sappa, and T. Graf, "Survey of pedestrian detection for advanced driver assistance systems," *IEEE trans. on Pattern Analysis and Machine Intelligence*, vol.32, no.7, 1239-1258, 2010.

[2] G. Leen and D. Heffernan, "Expanding automotive electronic systems," *IEEE trans. on Computer*, vol.35, no.1, pp.88-93, 2002.

[3] S. J. Prosser, "Automotive sensors: past, present and future," *Journal of Physics*, vol.76, no.1, pp.1-6, 2007.

[4] A. Vahidi, and A. Eskandarian, "Research advances in intelligent collision avoidance and adaptive cruise control," *IEEE trans. on Intelligent Transportation Systems*, vol.4, no.3, pp.143-153, 2003.

[5] M. Broy, "Challenges in automotive software engineering," in *Proc. Int. conference on Software engineering, ACM*, pp.33-42, 2006.

[6] H. Winner, and M. Schopper, "Adaptive cruise control," *Handbuch Fahrerassistenzsysteme. Springer Fachmedien Wiesbaden*, pp.859-891, 2015.

[7] J. Wenger, "Automotive radar-status and perspectives," In *Proc. compound Semicondoctor integrated Circuit Symposium, CSIC'05, IEEE*, pp.1-4, 2005.

[8] A. Kawakubo, S. Tokoro, Y. Yamada, and T. Kawasaki, "Electronically-scanning millimeter-wave Radar for forward objects detection," *SAE*

Congress, pp.127-134, 2004.

[9] R. H. Rasshofer and K. Gresser, "Automotive radar and lidar systems for next generation driver assistance functions," *Adv. Radio Sci.*, vol. 3, pp.205-209, 2005.

[10] M. Schneider, "Automotive radar–status and trends," In *Proc. German microwave conference*, pp. 144–147, 2005.

[11] W. Menzel, "Millimeter-wave radar for civil applications," in *Proc. IEEE Radar Conference (EuRAD)*, pp. 89–92, 2010.

[12] M. E. Russell, A. Crain, A. Curran, R. A. Campbell, C. A. Drubin, and W. F. Miccioli, "Millimeter-wave radar sensor for automotive intelligent cruise control (icc)," *IEEE trans. on Microwave Theory and Techniques*, vol.45, no.12, pp.2444–2453, 1997.

[13] S. H. Jeong, J. N. Oh, and K. H. Lee, "Design of 24 GHz radar with subspace-based digital beam forming for acc stop-and-go system," *ETRI journal*, vol.32, no.5, pp.827–830, 2010.

[14] E. Hyun and J. H. Lee, "A meothod for multi-target range and velocity detection in automotive fmcw radar," in *Proc. IEEE Int. Conference on Intelligent Transportation Systems, ITSC'09*, pp. 1–5, 2009.

[15] M. Reiher and B. Yang, "On the occurrence of ghost targets in linear fmcw radar: A worst case study," in *Proc. IEEE Int. Radar Symposium*, pp. 1–4, 2008.

[16] G. M. Brooker, "Mutual interference of millimeter-wave radar systems," *IEEE trans. on Electromagnetic Compatibility*, vol.49, no.1, pp.170–181, 2007.

[17] R. Schmidt, "Multiple emitter location and signal parameter estimation,"

IEEE trans. on Antennas and Propagation, vol.34, no.3, pp.276–280, 1986.

[18] R. Roy and T. Kailath, “Esprit-estimation of signal parameters via rotational invariance techniques,” *IEEE trans. on Acoustics, Speech and Signal Processing*, vol. 37, no. 7, pp. 984–995, 1989.

[19] A.G. Jaffer, “Maximum likelihood direction finding of stochastic sources: A separable solution, “ *in Proc. ICASSP 88*, vol.5, pp.2893,2896, 1988.

[20] M. Reiher, and B. Yang, “On the occurrence of ghost targets in linear FMCW radar: A worst case study,” in *Proc. IEEE Int. Radar Symposium*, pp.1-4, 2008.

[21] E. Conte, and M. Longo, “Characterisation of radar clutter as a spherically invariant random process,” *in IEE Proc. F (Communications, Radar and Signal Processing)*, vol.134, no.2, pp.191-197, 1984.

[22] J. E. Lee, et al. “Enhanced iron-tunnel recognition for automotive radars,” *IEEE trans. on Vehicular Technology*, 2015.

[23] M. Goppelt, H. Bl¨ocher, and W. Menzel, “Automotive radar–investigation of mutual interference mechanisms,” *Advances in Radio Science*, vol. 8, pp. 55–60, 2010.

[24] H. Krim, and M. Viberg, “Two decades of array signal processing research: the parametric approach,” *IEEE signal Processing Magazine*, vol.13, no.4, pp.65-94, 1996.

[25] R. Okuda, Y. Kajiwara, and K. Terashima, “"A survey of technical trend of adas and autonomous driving,”" in *Proc. IEEE VLSI Technology, Systems and Application (VLSI-TSA), Proceedings of Technical Program-2014 International Symposium on*, pp.1-4, 2014

[26] H. Akaike, “A new look at the statistical model identification,” *IEEE trans.*

on Automatic Control, vol.19, no.6, pp716-723, 1974.

[27] M. Wax and T. Kailath, "Detection of signals by information theoretic criteria," *IEEE trans. on Acoustics, Speech and Signal Processing*, vol. 33, no. 2, pp. 387–392, 1985.

[28] I. Matsunami and A. Kajiwara: "Clutter suppression scheme for vehicle radar," in *Proc. IEEE Radio and Wireless Symposium (RWS)*, pp. 320-323, 2010.

[29] R. Kapoor, G. Tsihrintzis, and N. Nandhakumar: "Detection of obscured targets in heavy-tailed radar clutter using an ultra-wideband (UWB)," in *Proc. IEEE conf. Signals, Systems and Computers, Pacific Grove*, pp. 863-867, 1996.

[30] A. G. Stove: "Linear FMCW radar techniques," *IEE Proceedings F (Radar and Signal Processing*), vol.139, no.5, pp. 343-350, 1992.

[31] M. I. Skolnik : "Introduction to radar systems," (McGraw-Hill, 3rd edn. 2001)

[32] T. Abe, T. Kobayashi, and S. Imai: "Harmonics tracking and pitch extraction based on instantaneous frequency," in *Proc. IEEE Int. Conf. Acoustics, Speech, and Signal Processing (ICASSP)*, pp. 756-759, 1995.

[33] R. D. Kent: "Acoustic analysis of speech," (Singular Publishing Group, 2002)

[34] P. Borghesani, P. Pennacchi, R. Randall, N. Sawalhi, and R. Ricci: "Application of cepstrum pre-whitening for the diagnosis of bearing faults under variable speed conditions," *Mechanical Systems and Signal Processing*, vol.36, no.2, pp. 370-384, 2013.

[35] B. Borgert, M. Healy, and J. Tukey: "The quefrency analysis of time series

for echoes: cepstrum, pseudo-autocovariance, cross-cepstrum and saphe craking, " in *Proc. symp. on time series analysis*, pp. 209-243, 1963.

[36] R. Randall, "A history of cepstrum analysis and its application to mechanical problems," in *Proc. Int. Conf. Surveillance 7*, pp. 1-16, 2013.

[37] R. Randall, N. Sawalhi, and M. Coats: "A comparison of methods for separation of deterministic and random signals," *International Journal of Condition Monitoring*, vol.1, no.1, pp. 11-19, 2011.

[38] S. Watts, "Cell-averaging CFAR gain in spatially correlated k-distributed clutter," *IEE Proceedings-Radar, Sonar and Navigation*, vol.143, no.5, pp. 321-327, 1996.

[39] L. Mu, T. Xiangqian, S. Ming, and Y. Jun, "Research on key technologies for collision avoidance automotive radar," in *Proc. IEEE Intelligent Vehicles Symposium*, pp. 233–236, 2009.

[40] J.-H. Zhang, G.-S. Liu, H. Gu, and W.-M. Su, "A novel transmit signal based on high range-resolution concept for flar or aicc system applications," in *Proc. CIE International Conference on Radar*, 2001.

[41] H. Rohling, "Some radar topics: waveform design, range cfar and target recognition," *in Advances in Sensing with Security Applications. Springer*, pp. 293–322, 2006.

[42] A. Eriksson, P. Stoica, and T. Soderstrom, "Markov-based eigenanalysis method for frequency estimation," *IEEE trans. on Signal Processing*, vol. 42, no. 3, pp. 586–594, 1994.

[43] M. Haardt and J. A. Nossek, "Unitary esprit: How to obtain increased estimation accuracy with a reduced computational burden," *IEEE trans. on Signal Processing*, vol. 43, no. 5, pp. 1232–1242, 1995.

[44] S. Blake, “Os-cfar theory for multiple targets and nonuniform clutter,” *IEEE trans. on Aerospace and Electronic Systems*, vol. 24, no. 6, pp. 785–790, 1988.

[45] M. S. Lee and Y. H. Kim, “An efficient multi target tracking algorithm for car applications,” *IEEE trans. on Industrial Electronics*, vol. 50, no. 2, pp. 397–399, 2003.

초록

자동차 기술 분야의 안전 및 편의에 대한 수요가 증가함에 따라, 주행 보조 시스템의 많은 응용 제품들이 연구, 개발 중이다. 차량의 주행 정보를 제공하기 위해서, 라이더, 카메라, 레이더, 초음파 레이더와 같은 다양한 센서 중에서, 레이더 센서는 시계 및 기상 상황에 대해 훌륭한 성능을 보여준다. 특히, 글로벌 생태계의 긴급 제동 시스템과 같은 안전 관련 기술의 의무장착화 진행과 맞물려 차량 레이더 센서의 시장을 폭발적으로 증가할 것으로 예상된다. 최근에는, 작은 크기를 가지면서도 성능이 우수한 레이더 센서에 대한 개발이 필수적이다. 또한 기존의 단거리, 중장거리 레이더 기능을 통합하는 다중 모드 레이더의 개발이 요구된다. 따라서 고해상도 파라미터 추정, 다중 타겟 감지, 클러터 억제, 간섭 완화 등의 기법은 여전히 레이더 신호처리 분야의 도전 과제로 남아있다.

고해상도 파라미터 추정에 대해서, 타겟 차량들을 구분하기 위한 각도 추정 기법들이 연구되고 있다. 특히 복잡한 도심환경에서는 비슷한 거리 및 속도로 주행하는 차량들이 빈번히 존재한다. 이러한 근접 차량들을 구분하기 위해서는 차량용 레이더에 적합한 고해상도 각도 추정

알고리즘이 필수적이다.

한편 레이더 센서 시야 범위 내에 존재하는 다중 타겟들을 분리하는 다중 타겟 감지기법이 요구된다. 다중 타겟 감지 기법은 각각의 타겟들이 가지는 고유의 주파수 성분들을 페어링하고 결합하는 과정이다. 특정 환경에서는 잘못된 주파수 페어링을 통해서 고스트 타겟이 검출될 수 있다. 따라서 신뢰성 높은 페어링 또는 결합 기법이 요구된다.

클러터는 주변 환경으로부터 반사되는 원하지 않는 신호 성분을 말한다. 차량 주행 환경에서는 가드레일, 교통표지판, 도로 주변의 정지물체들이 될 수 있다. 클러터의 효과를 최소화하기 위해서, 기존 레이더 시스템은 클러터의 비유동적인 특성 및 저주파 특성을 가정하고 이를 필터링한다. 그러나 차량용 레이더 환경에서는 클러터들이 다양한 주파수 성분 및 에너지를 가지고 분포하므로 적용이 어렵다. 특히, 철제 구조물과 같은 특수한 환경에서는 클러터의 높은 파워로 인하여 타겟 차량이 검출되지 않는다.

상호 간섭은 차량 안전 기능 제공을 위해서 반드시 풀어야 할 문제이다. 동일한 대역, 동일한 순간에 동작하는 레이더 센서를 탑재한 차량의 수가 증가할수록, 다른 레이더 센서의 신호로부터 정확한 타겟 구분에 실패 할 확률일 점차적으로 증가한다. 따라서 이에 대한 적절한 대책이 필요하다.

본 논문에서는, 차량용 레이더 시스템을 위한 효율적인 파라미터

추정 기법을 제안한다. 제안된 기법들은 앞서 설명한 신호처리 이슈들을 각각 포함하고 있다. 먼저, 주파수 영역에서 고해상도 각도 추정 기법을 제안한다. 본 기법은 타겟 차량의 고유한 비트 주파수를 이용하여 고해상도로 각도를 추정한다. 타겟의 비트 주파수는 거리 및 속도 정보를 제공하기 때문에, 추정된 각도 정보는 자연스럽게 거리 및 속도정보와 페어링 된다. 다음으로는, 철제 터널 환경에서의 클러터 억제 기법을 제안한다. 철제 터널 환경의 클러터는 철제 구조물의 반사 신호 성분으로 타겟의 감지 성능을 매우 열화시킨다. 제안된 기법은 켑스트럼에 기반한 클러터 억제 기법으로서, 주파수 영역에서의 주기적인 클러터 특성을 이용한다. 마지막으로, 간섭 제거 기법을 제안한다. 차량용 레이더의 간섭은 대부분 주파수 영역의 잡음 전력의 증가로 나타나며, 타겟의 감지 실패로 이어진다. 따라서 우리는 간섭 환경에서의 고해상도 주파수 추정 기법을 제안하고, 성능의 개선을 제시한다.

주요어 : 차량 레이더, FMCW, 각도 추정, 간섭, 완화, 클러터, 억제, 고해상도, 신호처리

학 번 : 2009- 30928

Ph.D. DISSERTATION

EFFICIENT PARAMETER ESTIMATION METHODS FOR AUTOMOTIVE RADAR SYSTEMS

차량용 레이더 시스템을 위한
효율적인 파라미터 추정 기법 연구

By
HAN-BYUL LEE

FEBRUARY 2016

DEPARTMENT OF ELECTRICAL AND COMPUTER ENGINEERING
COLLEGE OF ENGINEERING
SEOUL NATIONAL UNIVERSITY

Abstract

EFFICIENT PARAMETER ESTIMATION METHODS FOR AUTOMOTIVE RADAR SYSTEMS

Han-Byul Lee
Department of Electrical and Computer Engineering
The Graduate School
Seoul National University

As the demand for safety and convenience in the automotive-technology field increased, many applications of advanced driving assistance systems were developed. To provide driving information, among the sensors, such as cameras sensor, light detection and ranging sensor, radar sensor, and ultrasonic sensor, a radar sensor is known to exhibit excellent performance in terms of visibility for different weather conditions. Especially

with the legislation of the adaptive cruise control system and autonomous emergency braking system in a global environment, the market of the automotive radar sensor is expected to grow explosively. At present, the development of cost-effective radar offering high performance with small size is required. In addition, the radar system should be enforced to have a simultaneous functionality for both long and short ranges. Thus, challenging issues still remain with respect to radar signal processing including high-resolution parameter estimation, multi-target detection, clutter suppression, and interference mitigation.

For high-resolution parameter estimation, direction-of-arrival (DOA) estimation method has been investigated to identify the target object under complex unban environment. To separate closely spaced target having similar range and distance, high-resolution techniques, such as multiple signal classification (MUSIC), the estimation of signal parameters via rotational invariance techniques (ESPRIT), and maximum likelihood (ML) algorithm, are applied for automotive radars. In general, cycle time for radar system, which is the processing time for one snapshot, is very short, thus to establish a high-resolution estimation algorithm with computational efficiency is additional issue.

On the other hands, multi-target detection scheme is required to identify many targets in the field of view. Multi-target detection is regarded as target pairing solution, whose task is to associate frequency components obtained from multiple targets. Under certain conditions, the association may fail and real target may be combined to ghost components. Thus, reliable paring or association method is essential for automotive radar systems.

The clutter denotes undesired echoes due to reflected wave from background environment, which includes guardrail, traffic signs, and stationary structures around the

load. To minimize the effect of clutter, conventional radar systems use high pass filter based on the assumption that the clutter is stationary with energy concentrated in the low frequency domain. However, the clutter is presented with various energy and frequency under automotive radar environment. Especially, under the specific environment with iron materials, target component is not detected due to clutter with large power.

Mutual interference is a crucial issue that must be resolved for improved safety functions. Given the increasing number of automotive radar sensors operating at the same instant, the probability that radar sensors may receive signals from other radar sensors gradually increases. In such a situation, the system may fail to detect the correct target given the serious interference. Effective countermeasures, therefore, have to be considered.

In this dissertation, we propose efficient parameter estimation methods for automotive radar system. The proposed methods include the radar signal processing issues as above described, respectively. First, the high-resolution DOA estimation method is proposed by using frequency domain analysis. The scheme is based on the MUSIC algorithm, which use distinct beat frequency of the target. The target beat frequency also gives distance and velocity. Thus, the proposed algorithm provides either high-resolution angle information of target or natural target pairing solution. Secondly, we propose the clutter suppression method under iron-tunnel conditions. The clutter in iron-tunnel environments is known to severely degrade the target detection performance because of the signal reflection from iron structures. The suppression scheme is based on cepstral analysis of received signal. By using periodical characteristic of the iron-tunnel clutter, the suppressed frequency response

is obtained. Finally, the interference mitigation scheme is studied. Mutual interference between frequency modulated continuous waveform (FMCW) radars appears in the form of increased noise levels in the frequency domain and results in a failure to separate the target object from interferer. Thus, we propose a high-resolution frequency estimation technique for use in interference environments.

Keywords : Automotive radar, FMCW, Direction-of-arrival, Interference, Mitigation, Clutter, Suppression, High-resolution, Signal processing

Student Number : 2009 - 30928

Contents

List of Tables

List of Figures

Chapter 1

Introduction

1.1 Background

Three major topics in the field of automotive technology are green, convenience, and safety. Among these issues, the goal of research on safety and convenience is to prevent accidents in a variety of dangerous situations commonly encountered by drivers. To provide safety and driving comfort, advanced driving assistance systems (ADAS) are emerging as very active issues [1]-[2]. The sensors have played a vital role in the development of ADAS and enhancement of vehicle safety. Sensor technology provides artificial sensing of the environment, which enables decision making by in-car computers [3]. These sensor enabled systems help in providing warning to drivers and regulating vehicle control to mitigate collisions that can lead to material damage as well as human injury. ADAS includes blind spot detection, adaptive cruise control (ACC), autonomous emergency braking (AEB), obstacle detection, collision avoidance systems, rear view cameras, parking assistance (PA), and lane departure warning as showing in Figure 1.1 [4]-[5]. Key sensor technologies being used in these systems are camera sensor, infrared sensors, radar, light detection and ranging, and ultrasonic sensors.

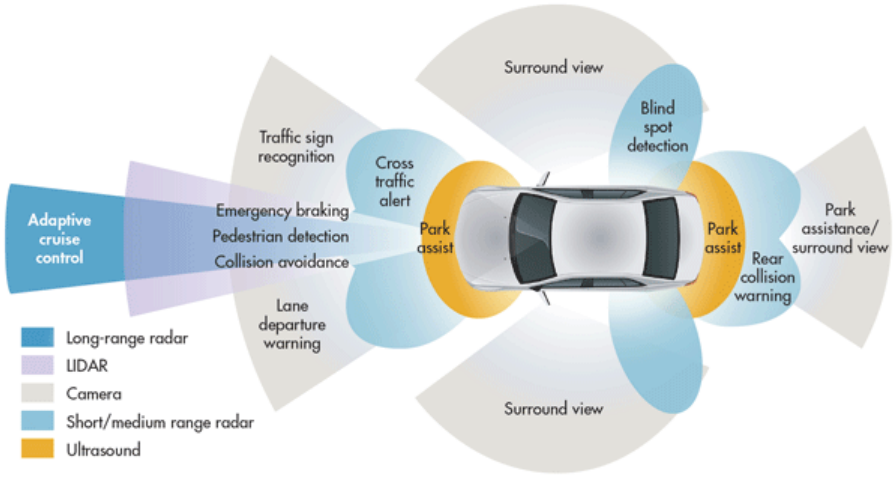

Figure 1.1 ADAS applications

1.2 ADAS Applications for Automotive Radars

ACC ensures that the automobile remains at a predefined distance away from the car ahead, reducing the speed to zero if necessary [6]. For ACC, radar sensors emit and receive radio waves and thus determine the distance of vehicles in front of the user's vehicle. ACC with stop and go facility allows the vehicle to come to a standstill if the preceding vehicle comes to a halt. The system again takes over as the preceding vehicle stars and by controlling acceleration, the predefined cruise speed is again achieved.

The blind spot detection helps the driver while attempting to pass other vehicles [7]. Sensors continuously monitor the presence, direction, and speed of vehicles in the lanes beside the ego-vehicle. If a vehicle moves into the blind spot, warning based on visual or audio signals can be generated to alert the driver of potential danger of collision. Radar sensors mounted on the real bumper or on the side rear view mirrors monitor vehicles behind or on adjacent lanes.

Forward collision warning systems are in-vehicle electronic systems that monitoring the roadway in front of the host vehicle and warn the driver when a potential collision risk exists. The system provides an audible alert when it senses a reduction in traffic speed in vehicles ahead. When the danger of a collision is detected, it provides a red warning light that flashes on the windshield. The forward collision warning is extended as an AEB recently. The system takes sudden braking in an emergency situation.

PA systems consist of visual aids, using real view cameras and side view cameras, Ultrasonic sensors provide distance information which allows the vehicle to be safety guided into the parking space without crashing into any other parked vehicle. Radar is

applied as a form of sensor fusion with camera sensors and ultrasonic techniques. Parking assistance systems will gradually make way for automatic parking systems.

1.3 Motivation and Organization

The development of automotive radar focuses on two types; short-range radar (SRR) using ultra-wide band (UWB) system at the 24 GHz and 77 GHz bands, and long-range radar (LRR) using frequency modulated continuous waveform (FMCW) systems at the 77GHz band [8]-[9]. The 77GHz band is known to be the most appropriate frequency band in global automotive radar environments, as the 24GHz band is shared with other communications systems. Furthermore, multi-mode radar sensors including the function of both SRR and LRR are obliged to miniaturize its size [10]. Considering the size of multi-mode radar sensors, 77GHz FMCW radar is a good candidate for a new automotive radar solution [11]. FMCW radar uses the waveforms of linearly increasing or decreasing frequencies, which increases reliability of radar system by providing the distance and velocity information of the target simultaneously. Moreover, the easy implementation of these radar sensors is the most significant factor making the most popular commercial system at present [12]–[13].

There remain several problems, however, related to the signal processing of automotive FMCW radar, including high-resolution parameter estimation, multi-target detection, clutter elimination and mutual interference elimination [14]–[16]. For high-resolution parameter estimation, direction-of-arrival (DOA) estimation method has been investigated to identify the target object under complex unban environment. To separate closely spaced target having similar range and distance, high-resolution techniques, such as multiple signal classification (MUSIC) [17], the estimation of signal parameters via rotational invariance techniques (ESPRIT) [18], and maximum likelihood (ML) algorithm [19], are applied for automotive radars. In general, cycle time for radar system, which is the processing time for one snapshot, is very short, thus

to establish a high-resolution estimation algorithm with computational efficiency is additional issue. On the other hands, multi-target detection scheme is required to identify many targets in the field of view. Multi-target detection is regarded as target pairing solution, whose task is to associate frequency components obtained from multiple targets. Under certain conditions, the association may fail and real target may be combined to ghost components [20]. Thus, reliable paring or association method is essential for automotive radar systems. The clutter denotes undesired echoes due to reflected wave from background environment, which includes guardrail, traffic signs, and stationary structures around the load. To minimize the effect of clutter, conventional radar systems use high pass filter based on the assumption that the clutter is stationary with energy concentrated in the low frequency domain [21]. However, the clutter is presented with various energy and frequency under automotive radar environment. Especially, under the specific environment with iron materials, target component is not detected due to clutter with large power [22]. Mutual interference is a crucial issue that must be resolved for improved safety functions. Given the increasing number of automotive radar sensors operating at the same instant, the probability that radar sensors may receive signals from other radar sensors gradually increases. In such a situation, the system may fail to detect the correct target given the serious interference [23]. Effective countermeasures, therefore, have to be considered.

This thesis has a focus on efficient parameter estimation for automotive radar signal processing. In chapter 2, high-resolution DOA estimation with having pairing function for automotive FMCW radar is presented. In the section 2 of chapter 2, the MUSIC in the time-domain and frequency-domain is analyzed, and the simulated results are presented in section 3 of chapter 2. In Chapter 3, the clutter suppression scheme for iron tunnels is presented. Radar signal model of iron tunnel,

characterization of iron tunnel, and clutter suppression scheme are presented in in section 2 of chapter 3. Experimental result is analyzed in in section 3 of chapter 3. In chapter 4, interference mitigation method is described. Qualitative analysis of interference is presented in section 2 of chapter 4. In section 3 of chapter 4, high-resolution frequency estimation scheme is presented. Experimental result is analyzed in section 4 of chapter 4. Finally, conclusion is presented in chapter 5.

Chapter 2

High-Resolution Direction of Arrival Estimation with Pairing function for Automotive Radar Systems

2.1 Introduction

Automotive radar sensors are employed for various ADAS applications such as ACC, FCW, and AEB. Conventional FMCW radar provides only range and velocity of targets which exist on field of view. The increasing demand for safety and convenience leads to efforts improving the DOA estimation to allow resolution of targets even in the similar distance-velocity information. In an urban environment, for example, DOA is essential to separate targets with having same distance and velocity. The DOA resolution using conventional beam-former is poor since automotive radars have typically a low antenna aperture due to size restriction [24]. High-resolution methods for DOA estimation such as MUSIC [17] enable radar sensors to resolve very closely spaced targets. These algorithms are well known as subspace based algorithm,

which is applied wide research area to estimate specific parameters. MUSIC is based on exploiting the eigen-structure of input covariance matrix. MUSIC makes assumption that the noise in each channel is uncorrelated making correlation matrix diagonal.

On the other hand, Target pairing is an essential for multi-target detection. FMCW radar uses increasing chirp (which is a up chirp) and decreasing chirp (which is a down chirp) signal to obtain paired beat frequency of target [25]. From these frequency pair, distance and velocity of targets are calculated. However, additional technique is required to combine estimated DOA and distance and velocity.

In this chapter, high-resolution DOA estimation algorithm in frequency domain process is proposed. The proposed method is not significantly different from the conventional MUSIC, whereas it resolves pairing issue naturally by using only beat frequency of target. To analyze detection performance of proposed method, simulation results are presented based on a 77 GHz FMCW radar system. From the simulation, proposed frequency domain approach shows RMSE performance similar to time domain approach.

2.2 High-Resolution DOA Estimation for Automotive Radars

In order to provide DOA information, an array concept with multiple antennas is employed. With a far-field assumption, which means radius of propagation is much larger than array spacing, the propagation delay with respect to array element results in linear phase shift. Array signal processing can largely be classified into spectral approach and the parametric approach. The former uses spectral peak component of estimator, including beamforming techniques and subspace based methods [24]. The latter directly computes the DOA from signal model of estimator, such as maximum likelihood (ML) [19]. In this section, we employed MUSIC algorithm for DOA estimation, well known as subspace based method.

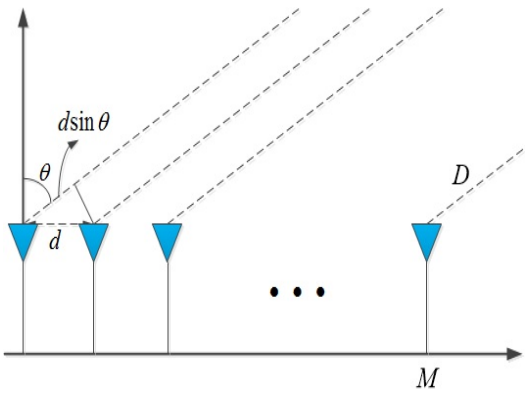

Figure 2.1 ULA structure for DOA estimation

2.2.1 DOA Estimation in the Time-domain Processing

Let us consider uniform linear array (ULA) with M antenna element, uniform spacing of d as shown in Figure 2.1. Plane wave reflected from each D target incidents on a different angle depending on the location of target. Each received signal $x_m(n)$, for $m = 0,1,\ldots,M$, includes additive zero mean, Gaussian noise. Time is represented by the n-th time sample. Thus, Array output $\mathbf{x}[n]$ is expressed as follows,

$$\mathbf{x}[n] = \mathbf{A}\mathbf{s}[n] + \mathbf{w}[n], \tag{2.1}$$

or

$$\begin{bmatrix} x_1[n] \\ x_2[n] \\ \vdots \\ x_M[n] \end{bmatrix} = \begin{bmatrix} \mathbf{a}(\theta_1) & \mathbf{a}(\theta_2) & \cdots & \mathbf{a}(\theta_D) \end{bmatrix} \begin{bmatrix} s_1[n] \\ s_2[n] \\ \vdots \\ s_D[n] \end{bmatrix} + \begin{bmatrix} w_1[n] \\ w_2[n] \\ \vdots \\ w_M[n] \end{bmatrix}, \tag{2.2}$$

where,

$$\mathbf{a}(\theta_i) = \begin{bmatrix} 1, & e^{j2\pi d/\lambda \sin(\theta_i)}, & \cdots, & e^{j2\pi(M-1)d/\lambda \sin(\theta_i)} \end{bmatrix}^T, \tag{2.3}$$

$\mathbf{s}[n]$ is a vector of incident complex signal at time n, $\mathbf{w}[n]$ is a noise vector at each array element m with zero mean, variance of σ_n^2, $\mathbf{a}(\theta_i)$ is M-element array steering vector for the θ_i DOA, and $\mathbf{A}$ is $M \times D$ matrix of steering vectors

$\mathbf{a}(\theta_i)$. It is initially assumed that the number of the targets $D < M$.

Based on above signal model, covariance matrix of received signal is given by

$$\begin{aligned}\mathbf{R}_T &= E[\mathbf{x}[\mathrm{n}]\mathbf{x}^H[\mathrm{n}]] = \mathbf{A}E[\mathbf{s}[\mathrm{n}]\mathbf{s}^H[\mathrm{n}]]\mathbf{A}^H + E[\mathbf{w}[\mathrm{n}]\mathbf{w}^H[\mathrm{n}]] \\ &= \mathbf{A}\mathbf{R}_{ss}\mathbf{A}^H + \sigma^2\mathbf{I}_M\end{aligned}, \qquad (2.4)$$

In general, $D < M$, $\mathbf{A}\mathbf{R}_{ss}\mathbf{A}^H$ is a singular matrix and non-negative definite. The array covariance matrix is calculated by the expectation of array output. However, we cannot find exact statistics for the signals and noise. Therefore, we assume that the process has ergodic properties, so we can approximate the correlation by use of a time-averaged correlation. Then, (2.4) can be represented by

$$\mathbf{R}_T = \frac{1}{N}\sum_{n=1}^{N}\mathbf{x}[\mathrm{n}]\mathbf{x}^H[\mathrm{n}]. \qquad (2.5)$$

From (2.4), we can find that the eigenvalue of $\mathbf{R}_T$ is exactly equal to summation of the eigenvalue of $\mathbf{A}\mathbf{R}_{ss}\mathbf{A}^H$ and the noise variance σ_n^2. Since the rank of $\mathbf{A}\mathbf{R}_{ss}\mathbf{A}^H$ is D, we can separate D eigenvalues larger than σ_n^2 and $M - D$ eigenvalues with a value of σ_n^2. We can also choose the D eigenvectors associated with the signal and $M - D$ eigenvectors associated with the noise. Then we can construct the $M \times D$ dimensional subspace spanned by the signal eigenvectors and $M \times (M - D)$ dimensional subspace spanned by the noise eigenvectors, respectively.

$$\mathbf{E} = [\mathbf{E}_S \ \mathbf{E}_N], \qquad (2.6)$$

where,

$$\begin{aligned}\mathbf{E}_N &= [\mathbf{e}_1\ \mathbf{e}_2\ \cdots\ \mathbf{e}_{M-D}] \\ \mathbf{E}_S &= [\mathbf{e}_{M-D+1}\ \mathbf{e}_{M-D+2}\ \cdots\ \mathbf{e}_M].\end{aligned} \tag{2.6}$$

The noise subspace eigenvectors are orthogonal to the array steering vectors at the direction of arrival $\theta_1,\ \theta_2,\ \cdots,\ \theta_D$. The relation is expressed as follows,

$$\begin{aligned}&\mathbf{A} \perp \mathbf{E}_N \\ &\mathbf{A}^H \perp \mathbf{e}_i \quad i = 1,\ 2,\ \cdots, M-D\end{aligned}. \tag{2.7}$$

Placing this relation in the denominator creates sharp peaks at the DOA. Thus, the MUSIC pseudo-spectrum is given as

$$P_{MUSIC}(\theta) = \frac{1}{\left|\mathbf{a}(\theta)^H \mathbf{E}_N \mathbf{E}^H{}_N \mathbf{a}(\theta)\right|}. \tag{2.8}$$

The peak value of pseudo-spectrum determined as DOA of target objects by using peak detection algorithm such as constant false alarm rate (CFAR). Parametric approach such as MUSIC takes advantage of a prior knowledge such as the number of frequency components. Because the precise number of frequency D value is not available in practical systems, it must be estimated. As information theoretic criteria, MDL or the Akaike information criterion (AIC) have been widely used to estimate the number of frequencies [26]. In this work, we employ the MDL criterion to estimate M. This is expressed as [27],

$$\mathrm{MDL}(k) = -\log\left(\frac{\prod_{i=k}^{L-1}\lambda_i^{\frac{1}{L-k}}}{\frac{1}{L-k}\sum_{i=k}^{L-1}\lambda_i}\right)^{(k-L)Q} + \frac{1}{2}k(2L-k)\log Q, \qquad (2.9)$$

after which the estimate of M can be obtained by

$$\hat{M} = \arg_k \min \mathrm{MDL}(k) + 1, \qquad (2.10)$$

where, $k = 0,1,\cdots,L-1$.

The flowchart of MUSIC algorithm is summarized in Figure 2.2.

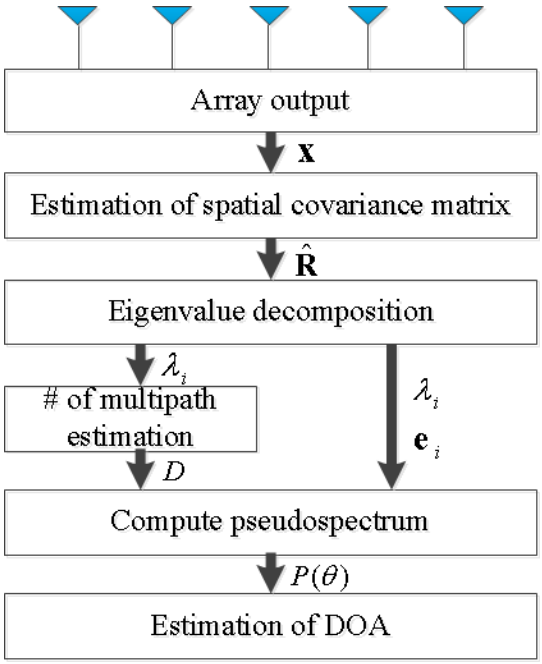

Figure 2.2 Flowchart of the MUSIC algorithm

2.2.2 DOA Estimation in the Frequency-domain Processing

As described above section 2.2.1, DOA estimation in time-domain gives only the sequence of estimated angles. To apply multi-target environment for automotive radars, respective DOA of targets should be paired with those of distance and velocity. Therefore, a proper pairing solution should be considered. However, if the number of targets increases, the computational load to combine each DOA with range and velocity.

In this section, we propose the DOA estimation in frequency-domain processing to provide natural pairing solution for automotive radar system. The proposed method is based on an observation that each target has different beat frequency. Thus, the DOA estimation is performed by using beat frequency component of target.

Let us define the spectrum of received signal obtained from fast Fourier transform (FFT). N_{FFT} discrete-time samples for M array output is defined by

$$\begin{aligned} \mathbf{X}_T &= [\mathbf{x}_1[n]\ \mathbf{x}_2[n]\ \cdots\ \mathbf{x}_M[n]]^T \\ \mathbf{S}_T &= [\mathbf{s}_1[n]\ \mathbf{s}_2[n]\ \cdots\ \mathbf{s}_D[n]]^T \\ \mathbf{W}_T &= [\mathbf{w}_1[n]\ \mathbf{w}_2[n]\ \cdots\ \mathbf{w}_M[n]]^T \end{aligned}, \qquad (2.11)$$

where,

$$\begin{aligned} \mathbf{x}_m[n] &= [x_m[0]\ x_m[1]\ \cdots\ x_m[N_{FFT}]\ ]^T, \ \text{for } m=1, 2, \cdots, M \\ \mathbf{s}_d[n] &= [s_d[0]\ s_d[1]\ \cdots\ s_d[N_{FFT}]\ ]^T, \ \text{for } d=1, 2, \cdots, D \\ \mathbf{w}_m[n] &= [w_m[0]\ w_m[1]\ \cdots\ w_m[N_{FFT}]\ ]^T \end{aligned}, \qquad (2.12)$$

$(\bullet)_T$ denotes sampled data in time-domain, $\mathbf{X}_T$ and $\mathbf{W}_T$ are $M \times N_{FFT}$

dimensional matrix, and $\mathbf{S}_T$ is $D \times N_{FFT}$ dimensional matrix. Fast Fourier transform matrix with length of N_{FFT} is represented as follows

$$\begin{aligned} [\mathbf{F}]_{n,k} &= \frac{1}{N_{FFT}} e^{-j2\pi(k-1)(n-1)/N_{FFT}} \\ \mathbf{f}(f_d) &= \mathbf{F}(:, k_d+1) = \mathbf{F}(:, \frac{f_d}{\Delta f}+1) \end{aligned} , \qquad (2.13)$$

where, $\mathbf{f}(f_d)$ denotes Fourier operator for the beat frequency of d th target, k_d is frequency index of d th target, f_d is beat frequency of d th target, and Δf is frequency resolution. From (2.13), coefficient of Fourier transform for the f_d is expressed by

$$\begin{aligned} \mathbf{x}_F(f_d) &= \sum_{i=1}^{D} \mathbf{a}(\theta_i)\mathbf{S}_T(i, :)\mathbf{f}(f_d) + \mathbf{W}_T\mathbf{f}(f_d) \\ &= \mathbf{a}(\theta_d)\mathbf{S}_T(d, :)\mathbf{f}(f_d) + \mathbf{W}_T\mathbf{f}(f_d) \\ &= \mathbf{a}(\theta_d)s_F(f_d) + \mathbf{w}_F(f_d) \end{aligned} , \qquad (2.14)$$

where, $\mathbf{x}_F(f_d)$ is a $M \times 1$ vector including complex magnitude of beat frequency f_d for each array element. For the D targets, the total matrix representation is given as

$$\begin{aligned} \mathbf{X} &= [\mathbf{x}_F(f_1)\ \mathbf{x}_F(f_2)\ \cdots\ \mathbf{x}_F(f_D)]^T \\ \mathbf{S} &= Diag[s_F(f_1)\ s_F(f_2)\ \cdots\ s_F(f_D)]^T \\ \mathbf{W} &= [\mathbf{w}_F(f_1)\ \mathbf{w}_F(f_2)\ \cdots\ \mathbf{w}_F(f_D)]^T \end{aligned} , \qquad (2.15)$$

where,

$$\begin{aligned}\mathbf{x}_F(f_d) &= [x_{f,1}[f_d]\, x_{f,2}[f_d] \cdots x_{f,M}[f_d]]^T, \text{ for } d=1, 2, \cdots, D \\ \mathbf{w}_F(f_d) &= [w_{f,1}[f_d]\, w_{f,2}[f_d] \cdots w_{f,M}[f_d]]^T\end{aligned}, \quad (2.16)$$

and compact matrix form is expressed by

$$\mathbf{X} = \mathbf{AS} + \mathbf{W}. \quad (2.17)$$

In order to estimate DOA with respect to f_d, covariance matrix for each beat frequency is defined as

$$\mathbf{R}_{F,i} = E[\mathbf{x}_F(f_i)\mathbf{x}_F{}^H(f_i)], \quad \text{for } i=1, 2, \cdots, D. \quad (2.18)$$

Since $rank(\mathbf{R}_{F,i}) = 1$ in general case, $\mathbf{R}_{F,i}$ has one eigenvalue in signal subspace, and $M-1$ eigenvalues in noise subspace. From the pseudo-spectrum (2.8), estimated DOA component θ_i is exactly paired with distance and velocity corresponding to f_i. Therefore, the DOA estimation in frequency domain resolves paring problem for multi-target detection automatically.

2.3 Simulation Result

2.3.1 Simulation Setup

To analyze the performance of DOA algorithm with two different approaches, Monte Carlo simulations were performed. The received signal was generated by the FMCW signal model. The parameters used in this simulation for FMCW are summarized in Table 2.1.

Table 2.1 Parameters used in simulation for FMCW

Parameters	value
Carrier frequency, f_c	76.5 GHz
Sweep time, Δt	5 ms
Sweep bandwidth, BW	500 MHz
Maximum target range, $R_{\max}$	200 m
Maximum target velocity, $V_{\mathrm{r,max}}$	300 km/h
Sampling frequency, f_s	440 kHz
The number of time sample	1024
The number of FFT point, N_{FFT}	1024
The number of Antenna	8
Antenna spacing	$\lambda / 2 = c / 2 f_c$

It is assumed that 77GHz FMCW radar with single transmitting antenna and 8 receiving array antenna with equally spaced elements. Maximum beat frequency is derived by

$$f_{b,\max} = f_{r,\max} + f_{d,\max} = \frac{BW}{\Delta t}\frac{2R_{\max}}{c} + \frac{2f_c}{c}V_{r,\max} \quad , \tag{2.19}$$

where, $f_{r,\max} = \frac{BW}{\Delta t}\frac{2R_{\max}}{c}$ is the maximum frequency difference by the maximum target range, and $f_{d,\max} = \frac{2f_c}{c}V_{r,\max}$ is the maximum Doppler frequency shift by the maximum relative velocity of target. By the Nyquist sampling theorem, sampling frequency is determined by

$$f_s > 2 \cdot f_{b,\max} . \tag{2.20}$$

For convenience of operation, we set the number of the sample in time-domain equal to those in frequency-domain.

2.3.2 Performance Comparison of the DOA Estimation in Time- and Frequency-domain Processing

To evaluate performance of DOA estimation, we employed the measure of RMSE under various conditions such as signal to noise ratio (SNR), the number of antenna elements, and angular separation of closed two targets. The RMSE of estimated DOA is defined as

$$RMSE = E[(\hat{\theta} - \theta_{real})^2], \tag{2.21}$$

where, $\hat{\theta}$ is the estimated DOA, and θ_{real} is the real DOA for the target location. From (2.21), we can find that the RMSE means the standard deviation of estimator.

The RMSE is evaluated against SNR. It is assumed that there exist two targets with -7 and 8 degree. In general, the DOA of target represents the angle from the perpendicular direction of the radar sensor. SNR is varied from 0 dB to 20 dB with 1000 independent trials, respectively. MUSIC estimate in time-domain uses the number of time sample, which is snapshot, for $N = 300,\ 500,\ 1000$.

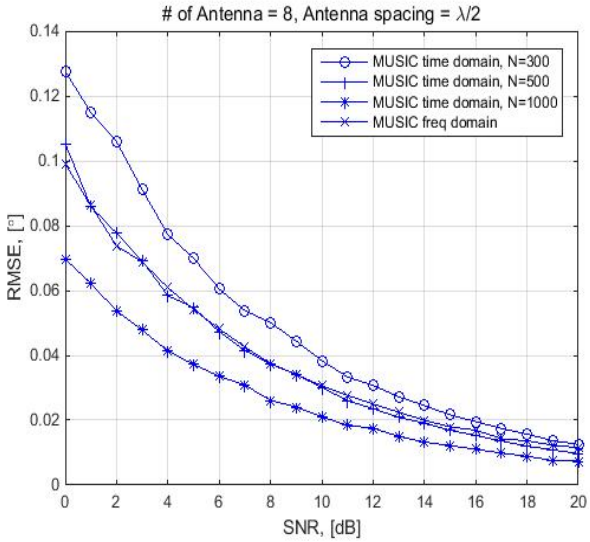

Figure 2.3 RMSE versus SNR

Figure 2.3 shows the RMSE performance of the algorithms in terms of the number of time samples for the two targets. In general, many of the DOA algorithms rely on the array covariance matrix. Since we use time average for estimating covariance matrix, large time sample performs better in comparison. However, large snapshot

affects computational time, results in longer cycle time for processing. On the other hand, MUSIC estimate in frequency domain shows good performance with relatively small computational load.

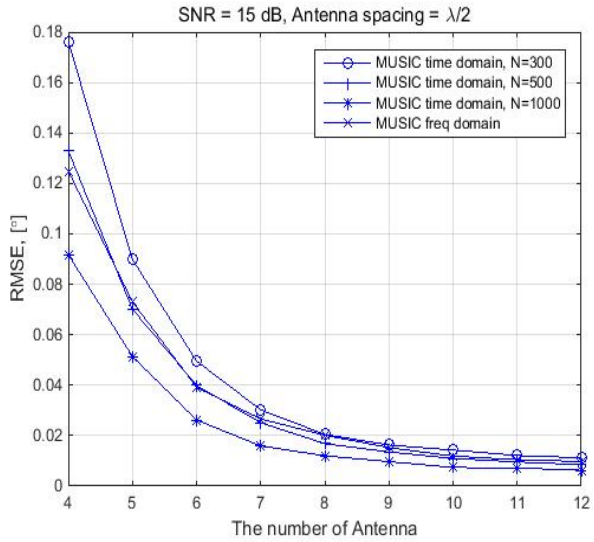

Figure 2.4 RMSE versus the number of antenna

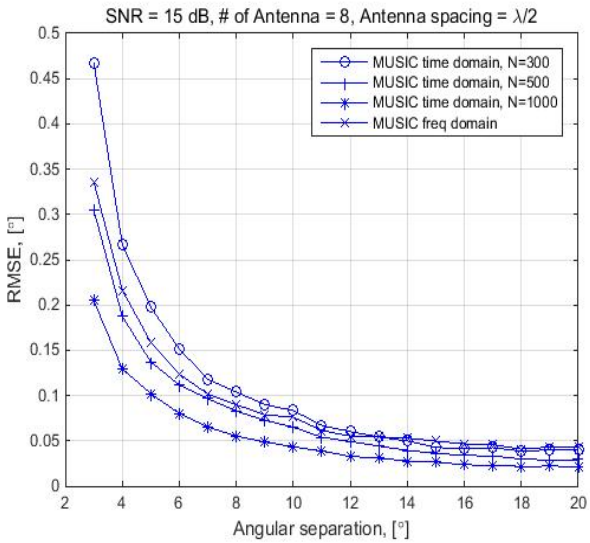

Figure 2.5 RMSE versus angular separation.

Figure 2.4 shows the RMSE performance in terms of the number of antenna elements. The SNR is 10 dB, the number of antenna elements varies from 4 to 12, and rest of simulation parameter is same as Figure 2.3. The number of antenna determines the size of covariance matrix, which is a square matrix. As the number of antenna elements increase, beam pattern of the array is sharper, and the more power of receiving antenna is concentrated on specific direction. Moreover, MUSIC algorithm uses the orthogonality between steering vector of incoming signal and eigenvectors in noise subspace. Thus large antenna elements make large size of eigenvectors in noise subspace, results in reducing correlation of signal and noise.

To evaluate angular resolution of the algorithm, the RMSE performance in terms of angular separation is analyzed as shown in Figure 2.5. The SNR is 10 dB, the number of antenna is 8, and the angular separation of two targets varies from 3 to 20 degree.

MUSIC estimate in frequency domain shows similar performance with MUSIC estimate in time domain with N =300.

From above observation, it is proved that the DOA estimate in frequency domain is almost same performance as one in time domain, whereas frequency domain approach provides efficient pairing solution.

2.3.3 Performance Analysis of the DOA Estimation in Frequency-domain

The frequency domain approach utilizes the beat frequency of the target which is derived from Fourier analysis of the received signal. Thus, better estimation of the beat frequency leads to better performance of DOA estimate. The frequency resolution of the FMCW radar is determined by sampling frequency f_s and length of FFT N_{FFT} as follows

$$\Delta f = \frac{f_s}{N_{FFT}}. \qquad (2.21)$$

Thus, large FFT points gives more precise complex magnitude of beat frequency, which results in better performance of DOA estimate. Figure 2.6, Figure 2.7, and Figure 2.8 show the RMSE performance versus SNR, the number of antenna elements, and the angular separation of two targets, respectively. These simulated results are performed with same condition as previous section 2.3.2. It is commonly observed that larger FFT point shows better performance of RMSE with expense of computational load, which is $n \log_2 n$.

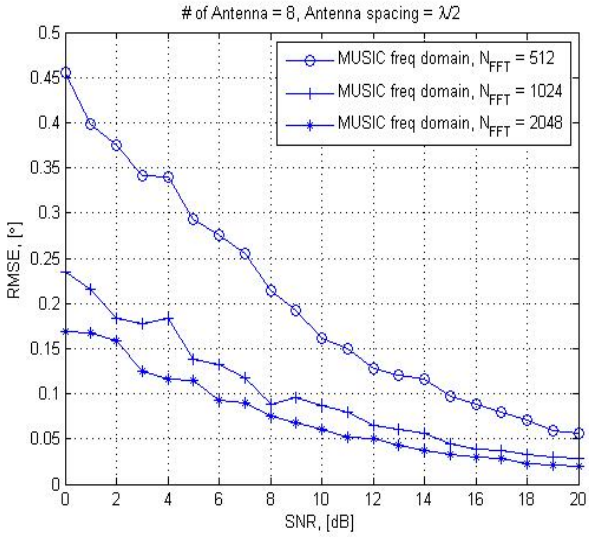

Figure 2.6 RMSE versus SNR according to the number of FFT length

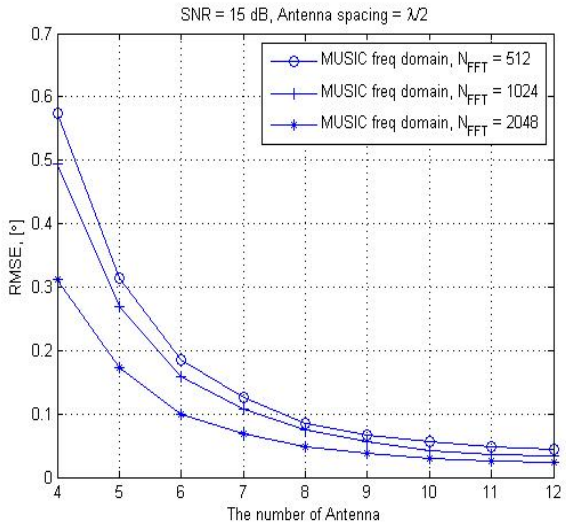

Figure 2.7 RMSE versus the number of antenna according to the number of FFT length

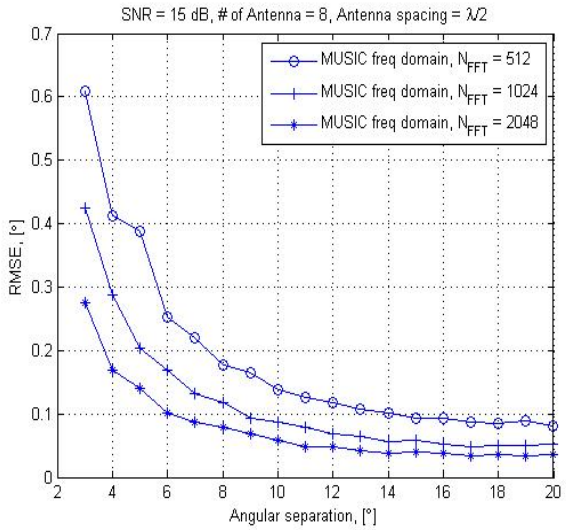

Figure 2.8 RMSE versus angular separation according to the number of FFT length

2.4 Conclusion

Conventional DOA estimation method is performed in time-domain, and gives only the directions of targets as a sequence. Thus, additional process should be established to pair DOA and distance/velocity. If there are many targets in field of view for a radar system, a very large amount of computation for precise pairing is required. To cope with the restriction of cycle time for the radar system, it is essential to suggest a simple but efficient pairing technique.

In this chapter, the efficient high-resolution DOA estimation method for automotive radar systems is proposed. We analyze high-resolution DOA estimation algorithm by use of beat frequency of target. By comparing to conventional time domain processing, we evaluated the suitability of the proposed method by simulation results. The frequency domain approach also provides a simple and efficient target pairing solution, which combine DOA information with distance and velocity of the target.

Chapter 3

Clutter Suppression Method of Iron Tunnel using Cepstral Analysis for Automotive Radars

3.1 Introduction

Clutter suppression is regarded as a relatively simple problem, however, in particular for iron-tunnel environments, the clutters are known to severely degrade the target detection performance because of the signal reflection from iron structures.

In the literature, several techniques have been presented in an effort to characterize the clutter structure on roads [28]-[29], whereas they are appropriate only for ultra-wideband pulse radars. Other studies have analyzed the stationary targets located in bridges and guard rails [30]-[31]. However, it is noteworthy that unlike the bridges and guard rails, iron structures are densely distributed to induce large reflections in iron-tunnel environments. So far, many of research have been descriptive under normal road conditions. Meanwhile, authors in [22] have introduced a technique to recognize the structure of iron tunnel. They employed measurement of the entropy based on the

short time Fourier transform analysis, and showed performance improvement by adjusting CFAR threshold. Note that this technique is tailored only for the recognition of iron-tunnel environments and not for the clutter suppression.

The main purpose of this study is to develop an understanding of the clutter effect of the iron tunnel and to establish an efficient clutter suppression algorithm under the iron tunnel environment. First, we derive a signal model for frequency modulated continuous waveform (FMCW) radars in iron-tunnel conditions, considering that iron pillars are located apart at equal distances, which leads to linear-increment of beat frequency with respect to the distance of clutters. Here, we focus on the periodic properties of the clutters induced by iron structures uniformly located in the tunnel. In order to analyze these properties, we employ cepstral analysis, which is used in wide areas for pitch detection [32]-[34]. By comparing radar signals in cepstrum domain under various road conditions, we prove that the existence of certain family of peaks in cepstral domain is a unique characteristic of iron-tunnel environments, which represents periodical beat frequency of clutters. Based on the above finding, we propose a clutter suppression method for iron-tunnel environments with liftering corresponding filtering in the spectral domain. To verify the proposed method, a 77 GHz forward-looking FMCW radar for ACC is employed. Measured results show that the proposed method efficiently suppresses the clutter of iron tunnel and extracts the parameter of the target object. It is shown that the proposed method provides significant performance enhancement even for early target detection.

The overall structure of the study organized as follows. Section 3.2 begins by modeling radar signal under an iron-tunnel condition. The cepstral characteristic and the method to suppress clutter are also discussed in section 3.2. Section 3.3 analyzes

the experimental results of the proposed method. Finally, conclusion is presented in section 3.4.

3.2 Clutter Suppression under Iron Tunnels

In this section, a radar signal model with iron-tunnel clutters is briefly described. We analyze cepstral characteristics under various road conditions, and propose an efficient method to suppress the clutter effect of iron tunnel by the cepstrum editing process.

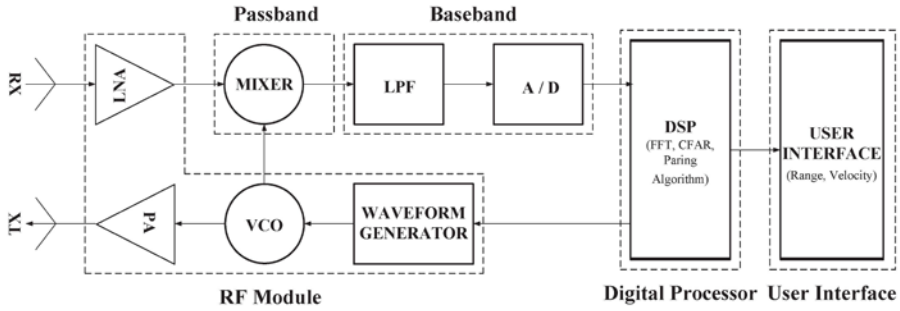

Figure 3.1 Schematic diagram of a typical FMCW radar

3.2.1 Radar Model of an Iron Tunnel

A 77 GHz forward-looking FMCW long range radar is employed in this work. The antenna module consists of linear patch antennas implemented on a printed circuit board, which has single transmitting antenna and K receiving antennas. A sinusoid signal of the waveform generator is modulated as a chirp signal by a voltage-controlled oscillator. The amplified signal is transmitted into the air, and reflected signal from the target is received with a time delay and Doppler frequency shift. Using a mixer and low pass filter, the received signal is converted to baseband signal. The range and velocity are obtained by digital processor of discrete-time signal derived from the

analog to digital converter (ADC). The unit time, which includes all of the above process, is called scan, and has a value of 50 ms in this work. With the linear frequency modulation, the received signal after ADC from k -th array can be simplified by [30]

$$x_k(n) = s_k(n) + e_k(n) = \sum_{i=1}^{T} a_k(i)\cos(2\pi f_k(i)n + \phi_k(i)) + e_k(n), \qquad (3.1)$$

where, $n = 0,1,\cdots,N-1$, N is the number of time samples, and T is the number of targets existing on the field of view. $s_k(n)$ contains sinusoids returned from each target, $e_k(n)$ represents the white noise signal with zero mean and variance of σ^2. $a_k(i)$, $f_k(i)$ and $\phi_k(i)$ are the amplitude, beat frequency and phase of the i -th target, respectively. The beat frequency, $f_k(i)$, means the frequency difference between the transmitted and the received signal for i -th target. $f_k(i)$ is composed of $f_{k,r}(i)$ (which is frequency difference by the distance of target) and $f_{k,d}(i)$ (which is Doppler frequency shift by relative velocity), and each of them is represented as

$$f_{k,r}(i) = \frac{2\alpha}{c} R(i) = \frac{2B}{cT_c} R(i), \qquad (3.2)$$

and

$$f_{k,d}(i) = \frac{2f_c}{c} v_r(i) = \frac{2}{\lambda} v_r(i), \qquad (3.3)$$

where, $\alpha = \frac{B}{T_c} = \frac{Bandwidth}{Chirp\,duration}$ is the chirp slope, f_c is the center frequency. c is speed of light and λ is the wavelength of center frequency. $R(i)$ and $v_r(i)$ are the range and relative velocity of the i-th target, respectively. When considering that the iron clutters of tunnel are densely distributed, (3.1) can be expressed as follows,

$$x_k(n) = \sum_{i=1}^{T} a_k(i)\cos(2\pi f_k(i)n + \phi_k(i)) + \sum_{j=1}^{C} a_{k,c}(j)\cos(2\pi f_{k,c}(j)n + \phi_{k,c}(j)) + e_k(n) \quad , \tag{3.4}$$

where, C is the number of clutters, $a_{k,c}(j)$, $f_{k,c}(j)$, and $\phi_{k,c}(j)$ are the amplitude, beat frequency, and phase of the j-th clutter, respectively. Assuming that the iron clutters have a uniform space, frequency difference by the distance of clutter, $f_{k,r,c}(j)$, is given by

$$f_{k,r,c}(j) = \frac{2B}{cT_c} R_c(j) = \frac{2B}{cT_c}(R_c(1) + (j-1)l) = f_{k,r,c}(1) + (j-1)\Delta f \quad , \tag{3,5}$$

where, $R_c(1)$ is the distance of the first iron clutter and l represents distance of the inter-clutter. $f_{k,r,c}(1) = \frac{2B}{cT_c} R_c(1)$ is frequency difference by the distance of the first

clutter. $\Delta f = \frac{2Bl}{cT_c}$ is frequency difference by the distance of the inter-clutter. Iron clutter is a stationary target, which has a constant Doppler frequency, so iron-tunnel condition presents periodic frequency components of the iron clutters. Under an iron tunnel, reflected signal from clutters is much larger than those from targets, which results in the detection failure of the target from clutters. To suppress clutter effect, periodicity of clutters in frequency domain needs to be analyzed. To accomplish this object, a cepstrum is employed in this work.

3.2.2 Cepstral Analysis of an Iron Tunnel

The cepstrum, derived from an anagram of spectrum, is a signal processing technique for identifying harmonic families in spectrum and removing the certain spectral components [35]. Cepstrum is used in wide research areas including speech signal processing and fault diagnosis. The cepstrum is originally defined as the power spectrum of the logarithmic power spectrum. However, various definitions for cepstrum are presented in literatures with different functionalities. For the given discrete time signal of $x_k(n)$, representative definitions of cepstrum are expressed as follows [36]

$$C_{power}(n) = \sum_{n=0}^{N-1} log(|\sum_{n=0}^{N-1} x_k(n) e^{-j\frac{2\pi}{N}kn}|^2) e^{j\frac{2\pi}{N}kn}, \quad (3.6)$$

$$C_{real}(n) = \sum_{n=0}^{N-1} log(|\sum_{n=0}^{N-1} x_k(n) e^{-j\frac{2\pi}{N}kn}|) e^{j\frac{2\pi}{N}kn}, \quad (3.7)$$

and

$$C_{complex}(n) = \sum_{n=0}^{N-1} log(\sum_{n=0}^{N-1} x_k(n) e^{-j\frac{2\pi}{N}kn}) e^{j\frac{2\pi}{N}kn}, \quad (3.8)$$

where, $|\cdot|$ denotes absolute value, $C_{power}(n)$, $C_{real}(n)$, and $C_{complex}(n)$ represent power, real and complex cepstrum, respectively. The operations of both forward and inverse Fourier transform are involved in the calculation of the cepstrum. The transformation of cepstrum concentrates on the periodic spectrum components, such as families of equally spaced harmonics. The essential observation leading to the cepstrum analysis is that the logarithmic spectrum can be treated as an input waveform and subjected to further inverse Fourier transform. The magnitude of the spectrum of $x_k(n)$ varies as the frequency changes. By the log operation, however, it is possible to compress the dynamic range of magnitude and reduce magnitude differences in the harmonic components. Table 3.1 lists the terminologies in the cepstrum domain with the one corresponding in the spectrum domain.

Table 3.1 Terminology of cepstral- and spectral domain

Cepstral domain	Spectral domain
quefrency	frequency
gamnitude	magnitude
rahmonic	harmonic
lifter	filter
saphe	phase

To characterize the radar signal under the iron-tunnel environment, we analyze the cepstral results. The real cepstrum is employed in this work. Discrete-time Fourier transform is replaced by fast Fourier transform (FFT), which is computationally efficient. Data acquisition is performed in various road conditions, such as an expressway, guardrail, normal tunnel and iron tunnel. Figure 3.2 shows the magnitude response of the cepstrum under each road condition. Under general road conditions including expressway, guardrail, and normal tunnel, any peak value of quefrency does not exist clearly. It means that there is no periodicity between the beat frequencies of the targets having different ranges and velocities. It is shown that the magnitude response has certain peak values of the quefrency only under iron-tunnel condition, which are rahmonic components. The first rahmonic peak is exactly same as the inverse of fundamental period in frequency domain, Δf . From this analysis, we verify that the periodicity of the clutter frequencies is an inherent property of the iron-tunnel condition.

(a) Express way

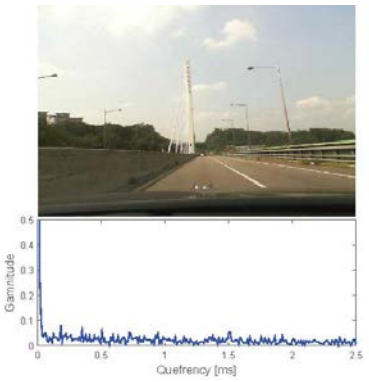

(b) Guard rail

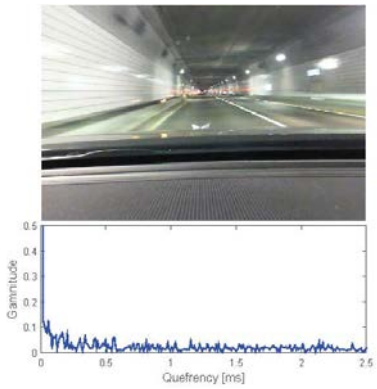

(c) Normal tunnel

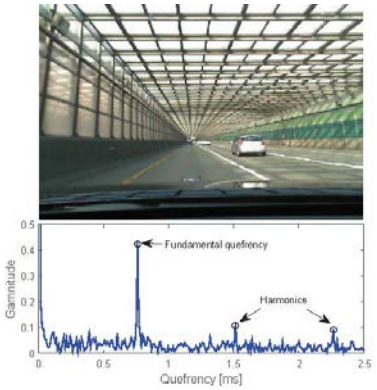

(d) Iron tunnel

Figure 3.1 Schematic diagram of typical FMCW radar

3.2.3 Cepstrum Based Clutter Suppression Method

To extract the hidden frequency of target objects from periodic frequency of clutter, an effective technique to suppress the clutter frequency is necessary. Since Fourier transform is complex domain operation, the cepstrum is represented in complex

domain. Therefore, the complex cepstrum has its inverse transformation, and the time domain signal can be reconstructed by using a modified cepstrum. However, complex cepstrum requires the continuity of phase to be unwrapped. So, it is not applicable to stationary random components where the phase is random.

On the other hand, if the input waveform of inverse Fourier transform has no phase information such as magnitude of spectrum, the cepstrum is real-valued. Despite of real-valued cepstrum, reconstruction to the time domain can be achieved by using the amplitude of the modified spectrum combined with the original phase spectrum. Moreover, we can lifter a rahmonic family in the quefrency domain and obtain an edited spectrum. Based on this real cepstral analysis, a simple rejection and reconstruction of the spectrum are employed in this work [37]. As shown in Figure 3.3, we propose to remove harmonics of clutters through the following steps: Step 1) once the received signal is transformed into the frequency domain by the fast Fourier transform (FFT), we perform the log operation to separate the amplitude and phase components. Step 2) using the log amplitude only with inverse FFT, real cepstrum is obtained. Step 3) the peak values in the cepstrum, representing a rahmonic family, are simply rejected by setting those gamnitude to zero, which acts as an ideal band-rejection lifter in the cepstral domain. Step 4) edited cepstrum is reversely transformed to spectral domain, which is an edited log amplitude. Step 5) edited log spectrum is composed of edited log amplitude and phase of the original spectrum. Step 6) with exponentiation of the edited log spectrum, finally, the edited spectrum is obtained, from which the target frequencies are extracted.

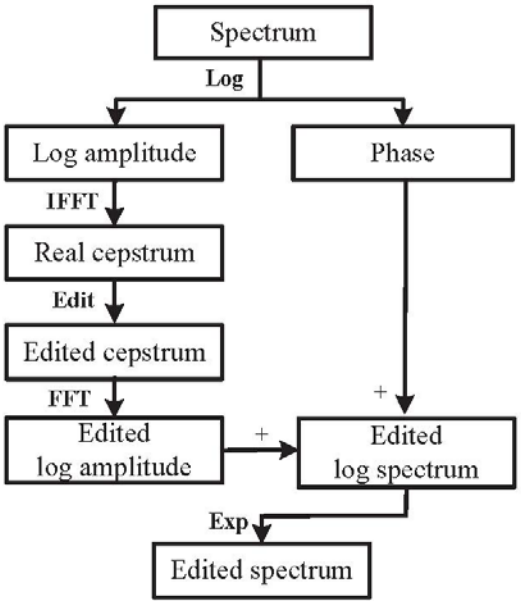

Figure 3.3 Procedure of cepstrum method for removing the harmonic family

3.3 Experimental Result

In this section, we present our experimental results based on the measured data in real driving environments. The FMCW radar sensor for ACC was installed at front of the test vehicle. The parameters of the FMCW radar are with 76.5 GHz of center frequency and 200 m of maximum operating range. The FFT algorithm is used for frequency estimation, and the cell average (CA)-CFAR is employed to detect target frequency [38]. To validate the proposed method, measurement tests were performed under various iron tunnels. Moreover, all of the measured data is obtained in a real driving situation. To recognize an iron tunnel, the method based on spectrum spreading in [22], is applied. The proposed method, therefore, operates only when iron tunnel is recognized. The profile of the representative two iron tunnels, used in this work, is summarized in Table 3.2.

Table 3.2 Iron-tunnel profile

Case	Geographic coordinate (latitude, longitude)	Length (km)	Experiment Date
A	(37.27, 127.08)	1.0	Sep.09.2015
B	(37.17, 127.03)	0.7	Sep.05.2015

The measured results for the proposed suppression method are shown in Figure 3.4 and Figure 3.5 for case A and B in Table 3.2, respectively. Figure 3.4.a depicts the original spectrum of the received signal before applying the proposed algorithm. The component represented by an asterisk stands for beat frequency of the target vehicle in the same lane with the ego-vehicle. Because of the periodical frequencies of the iron clutters, the hidden frequency of the target is not identified clearly. Although the target indicates the peak frequency, the frequency of target may be filtered by a CFAR threshold. The magnitude response of the log spectrum is shown in Figure 3.4.b. The log magnitude maintains periodicity of the original spectrum, while it smoothens the variation of magnitude with respect to frequency. Figure 3.4.c shows the cepstrum of the received signal with fundamental period and its rahmonics, resulted from the periodic peaks in the spectrum. The peak at rahmonic of 0.76 ms in Figure 3.4.c is equal to the inverse of 1.31 kHz, the fundamental period of the peak in the spectrum. After peaks of quefrencies are removed, edited spectrum in Figure 3.4.d still has residual periodic components. Compared with the original spectrum, nevertheless, frequency of the target is identified definitely, and also clutter effect is suppressed clearly. Figure 3.5 in case B of the iron tunnel also shows very similar results with Figure 3.4. Because the iron structures of the case B are almost same as those of A, identical fundamental frequency and harmonics in the quefrency domain are presented.

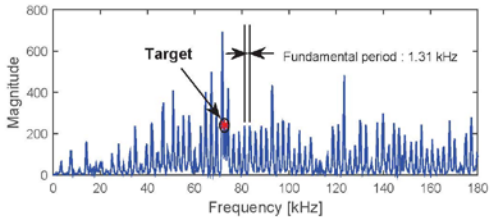

(a) Magnitude of original spectrum

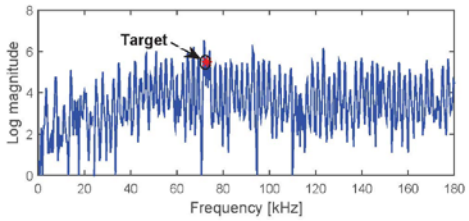

(b) Log magnitude of original spectrum

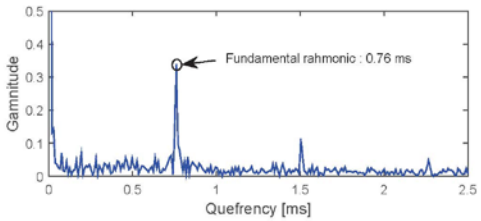

(c) Cepstrum analysis

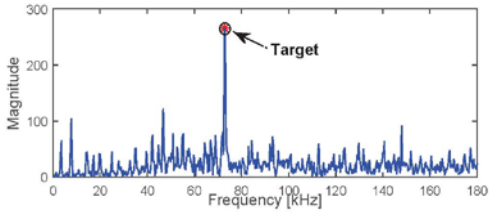

(d) Edited spectrum

Figure 3.4 Clutter suppression using cepstral analysis for the iron tunnel of case A

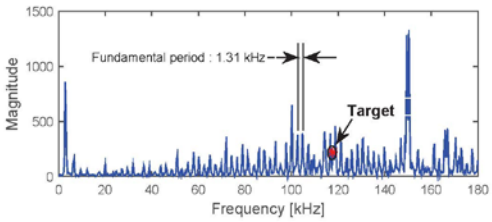

(a) Magnitude of original spectrum

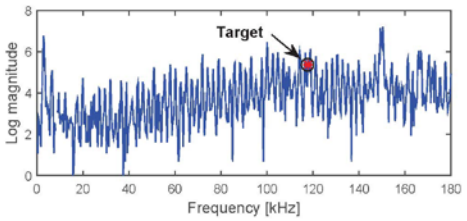

(b) Log magnitude of original spectrum

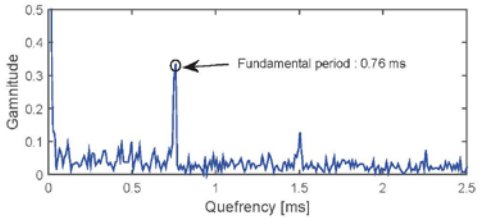

(c) Cepstrum analysis

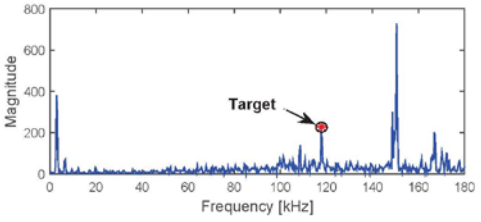

(d) Edited spectrum

Figure 3.5 Clutter suppression using cepstral analysis for the iron tunnel of case B

Figure 3.6 presents detection results before and after the clutter suppression. Figure 3.6.a and Figure 3.6.b shows the original spectrum and edited spectrum in frequency domain, respectively. The dotted line represents the threshold value obtained by CFAR. The spectral components larger than CFAR threshold are expressed by an asterisk. These peaks include the target in the same lane with ego-vehicle, the targets in others lane, and also clutters with high power. Although residual clutters are detected after suppression, they can be rejected by target pairing and tracking procedure. It is beyond the scope of this study to examine the pairing and tracking algorithm. It is noteworthy that the target in the same lane with the ego-vehicle is extracted from clutters, which provides essential information so as to control the ego-vehicle automatically. Figure 3.6.c depicts the trajectory comparison of the target vehicle in the same lane. The trajectory of the target is calculated by using the estimated target distance, location of ego-vehicle, and wheel speed of ego-vehicle. It represents the change of the estimated position with a marker at every five scans. It is shown that when the suppression algorithm is applied, the target vehicle is detected at an earlier time.

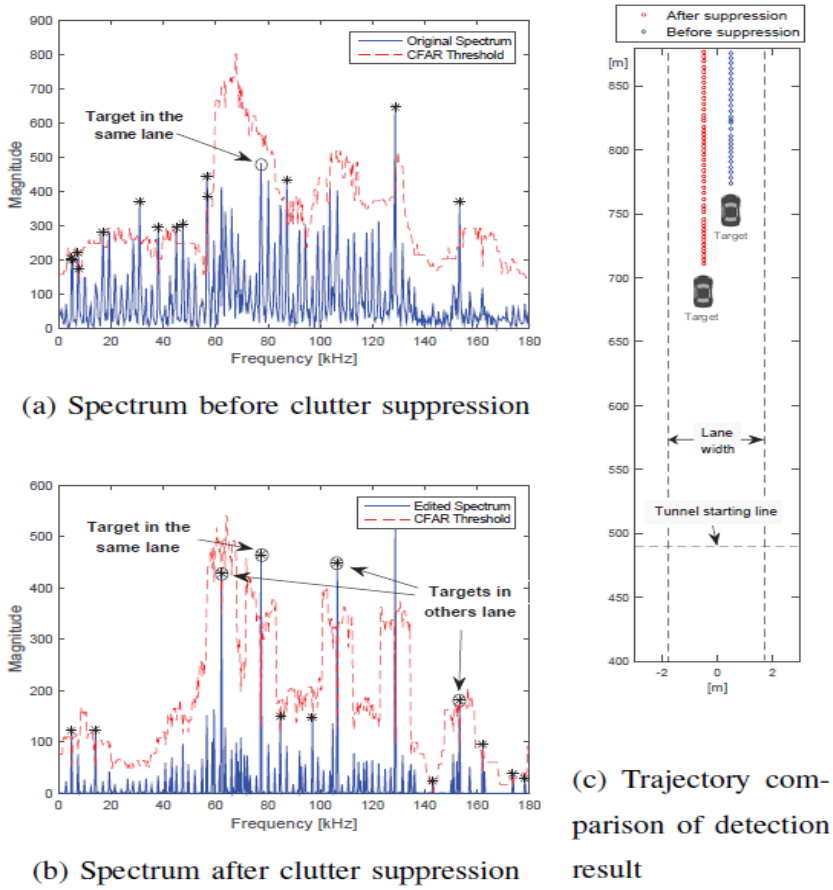

Figure 3.6 Detection result before and after clutter suppression

To evaluate the performance of the proposed method quantitatively, experiments are performed to determine the distance of early target detection, which is a measure of the initial distance to detect a target vehicle in the lane of the ego-vehicle. The initial detection of the target is a very important indicator for the ACC application. If the initial detection of the target is late, the ego-vehicle brakes suddenly, which increases the probability of collision with the vehicle in the front or rear. For each iron-tunnel

condition, some factors are considered including a type of the target vehicle and different velocity of the ego-vehicle. Table II summarizes the results of distance of early target detection for each iron tunnel. The average distance of the early target detection is improved by more than 55 m for the proposed method. Although the proposed method performs additional computation of both FFT and inverse FFT, it shows performance enhancement without adjusting any CFAR threshold with respect to the road condition.

Table 3.3 Evaluation of the distance of early target

Case	Geographic coordinate (latitude, longitude)	Length (km)	Before suppression (m)	After suppression (m)	Ego-vehicle speed (mps)	Relative speed (mps)	Vehicle type	Experiment Date
A	(37.27, 127.08)	1.0	79.7	133.4	37.3	-8.21	SUV	Sep.09.2015
A	(37.27, 127.08)	1.0	57.3	118.1	34.1	-9.99	compact car	Sep.09.2015
B	(37.17, 127.03)	0.7	64.5	125.1	27.1	-6.97	Sedan	Sep.05.2015
B	(37.17, 127.03)	0.7	60.1	109.7	40.1	-23.16	compact car	Sep.05.2015

3.4 Conclusion

In many applications of automotive radar systems, a technique to suppress clutter effect is essential, particularly for the iron-tunnel environments. In this paper, we modeled a FMCW radar signal under iron tunnels in which iron structures are uniformly and densely distributed. From cepstral analysis, we proved that the periodic property of iron clutters is revealed in the cepstral domain. Based on this observation, we proposed an efficient clutter suppression method using real cepstrum to remove the clutter effects in the cepstral domain. Experimental results present that the proposed method provides significant enhancement in the target detection performance. This proves that the proposed method is successfully applied for clutter suppression.

Chapter 4

Interference Mitigation by High-Resolution Frequency Estimation for Automotive Radars

4.1 Introduction

Mutual interference is a crucial issue that must be resolved for improved safety functions [16], [23]. Given the increasing number of automotive radar sensors operating at the same instant, the probability that radar sensors may receive signals from other radar sensors gradually increases. In such a situation, the system may fail to detect the correct target given the serious interference. Effective countermeasures, therefore, have to be considered. In the literature, several techniques have been presented in an effort mitigate the performance degradation issue caused by interference in radar or communications systems [39], [40]. To avoid overlap in the frequency domain, one method to minimize interference shifts the frequency of the transmitted signal pseudo-randomly [39]. Other authors [40] propose frequency ramps from short PN-coded sequences as a spread-spectrum technique. With these methods, however, the radars must share the same set of codes. Efficient strategies to distribute codes are required beforehand for collision avoidance.

Another study [16] qualitatively analyzed the mutual interference between millimeter-wave radar sensors and examined interference scenarios when considering spatial, temporal and frequency overlap. Interference from neighboring sensors appears to result in an increase in the noise level in the frequency domain. Therefore, it is important to estimate beat frequency accurately in a high interference environment. Conventional FMCW radar systems use the fast Fourier transform (FFT) algorithm for beat frequency estimation [41]. However, the traditional FFT algorithm is associated with high probability of failing to separate target objects from interferers. This motivates us to exploit high-resolution estimation techniques in interference-limited automotive radar environments.

This chapter proposes a beat frequency estimator for use in automotive FMCW radar systems based on high-resolution techniques to suppress mutual interference by means of a frequency domain analysis. The proposed method can be considered as the application of a subspace method known as MUSIC and ESPRIT, which solve the generalized eigenvalue problem using an autocorrelation matrix of received signal [17], [18]. The proposed method employs an estimator of a correlation matrix with forward-backward spatial smoothing (FBSS) [42] and a frequency signal dimension order (FSDO) estimator with the minimum description length (MDL) criteria [27]. The proposed method improves the frequency resolution and reduces the influence of interference relative to the FFT method. Moreover, ESPRIT is more computationally efficient than MUSIC [43], as ESPRIT directly calculates the frequency components in a given frequency range, whereas MUSIC requires a peak detection process from the spectral analysis.

To verify proposed methods, measurement was performed in a test field. The

experimental data used in the paper are obtained from a 77 GHz forward-looking FMCW radar for adaptive cruise control (ACC). The results show that the missing problem of a target vehicle under interference environments is improved by proposed methods in the detection performance.

The rest of this chapter is organized as follows. The characteristics and a mathematical representation of FMCW radar systems are presented in section 4.2. Based on the system model, beat frequency estimations using MUSIC and ESPRIT are discussed in section 4.3. Experimental results are presented in section 4.4 to verify the performance enhancement when using the proposed schemes. Finally, conclusions are given in section 4.5.

4.2 Automotive FMCW Radars in an Interference Environment

A signal transmitted using a linearly increasing or decreasing signal in the frequency domain can be represented as [30]

$$\begin{aligned} f(t) &= A\cos(2\pi\phi) \\ &= A\cos\left(2\pi\int_0^t (f_0 + \alpha t)dt\right) = A\cos\left(2\pi(f_0 t + \frac{1}{2}\alpha t^2)\right), \end{aligned} \tag{4.1}$$

where, A and ϕ are the amplitude and phase of the transmitted signal, respectively; f_0 is the transmitted signal frequency at time $t = 0$; and $\alpha = \frac{BW}{\Delta t} = \frac{\text{sweepbandwidth}}{\text{sweeptime}}$ is the chirp rate (chirp slope). The received signals returning from multiple targets are delayed and attenuated. If the targets are moving, they include an additional frequency shift term as follows:

$$g(t) = \sum_{i=1}^{m} B_i \cos\left(2\pi\left((f_0 + f_{d,i})(t - t_{d,i}) + \frac{1}{2}\alpha(t - t_{d,i})^2\right)\right), \tag{4.2}$$

Here, m is the number of targets; B_i is the amplitude of the received signal; and

$f_{d,i}$ and $t_{d,i}$ are the Doppler frequency and the delay time respectively. The transmitted and received signals are mixed by multiplication in the time domain. With the trigonometric identity of the sum of the cosines, the product of the two signals has distinct sinusoidal components. One of these will be at a frequency that is approximately twice the carrier frequency, which will be cut off by a low-pass filter (LPF). The other term, i.e., the mixer output after LPF processing, is given by

$$s(t) = \sum_{i=1}^{m} C_i \cos\left(2\pi(\alpha t_{d,i} - f_{d,i})t + 2\pi(f_0 + f_{d,i})t_{d,i} - \pi\alpha t_{d,i}^2\right), \qquad (4.3)$$

where $C_i = AB_i$ is the amplitude of the mixed output. $f_{b,i} = \alpha t_{d,i} - f_{d,i}$ is the beat frequency (or frequency difference), which is analyzed by the FFT algorithm. The range and velocity of each target are obtained from the beat frequency component with a peak detection algorithm such as the CFAR technique [44].

Considering that many vehicles may be equipped with FMCW radar sensors, it is essential to analyze the interference mechanism. Two simple scenarios can be regarded, as shown in Figure 4.1. One is direct interference from a vehicle in the opposite direction and the other is a returned interference from a vehicle traveling in the same direction (which is indirect interference). There are many factors affecting radar sensitivity, such as interfering source levels, the side-lobe effect, the target shape, the

operating band, and the sweep time.

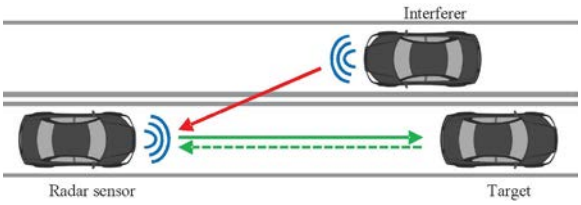

(a) Direct interference

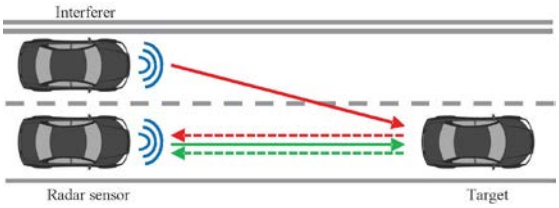

(b) In-direct interference

Figure 4.1 Simple interference scenarios in automotive radar environment

As an issue that acts between FMCW radars, interference can be divided into in-band-region interference and out-of-band interference depending on the delay time, resulting in a ghost target and a uniform increase of the noise floor respectively [16]. In-band-region interference not only occurs with a very low probability, but it can also be removed by means of multi-target detection and tracking algorithms [45]. For the out-of-band interference, however, the detection of the targets fails due to the increase in the noise floor. Figure 4.2 shows the influence of an interference signal that is 30dB larger than the signal from the target when the target is present at the 70m. The target

signal-to-noise-ratio (SNR) is reduced considerably. It is an important issue, therefore, to identify the signal from a result which contains an increase in the noise floor. The out-of-band interference is modeled in the following two cases according to the delay time of the interference signal.

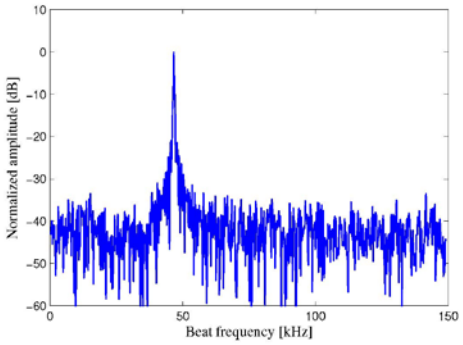

(a) Spectrum of a target without interference

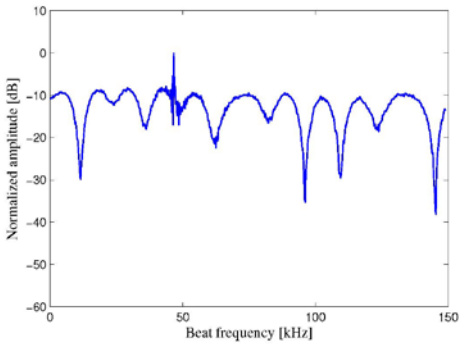

(b) Spectrum of a target with interference

Figure 4.2 The spectrum of FFT output for an out-of-band region interference with a magnitude 30 dB larger than signal returned from target object.

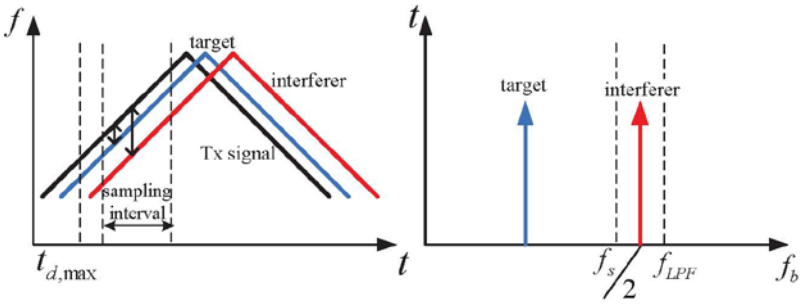

(a) Same sign-chirp case

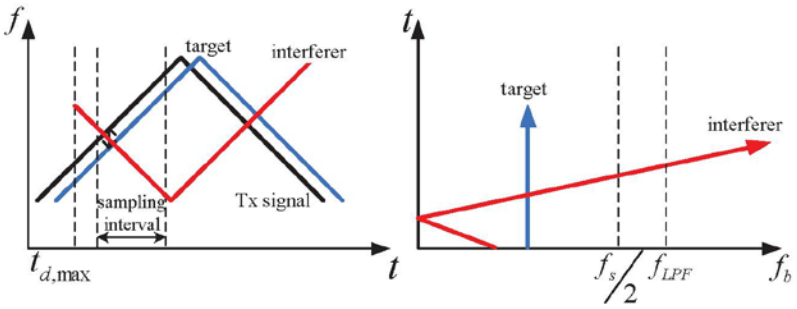

(b) Different sign-chirp case

Figure 4.3 Two cases of out-of-band interference, where f_s is the sampling rate and f_{LPF} is the cut-off frequency of LPF.

4.2.1 The Same Sign-Chirp Case

Assuming there are multiple interferers equipped with FMCW radar in the field of view, with parallel increasing chirps in the transmitted signal and with the interference

signal in the sampling interval (Figure 4.3(a)), the received signal can be expressed as follows:

$$\begin{aligned} g(t) &= g_s(t) + g_I(t) + n(t) \\ &= \sum_{i=1}^{m} B_i \cos\left(2\pi\left((f_0 + f_{d,i})(t - t_{d,i}) + \frac{1}{2}\alpha(t - t_{d,i})^2\right)\right) \\ &\quad + \sum_{j=1}^{k} B_{I_j} \cos\left(2\pi\left((f_0 + f_{d,I_j})(t - t_{d,I_j}) + \frac{1}{2}\alpha(t - t_{d,I_j})^2\right)\right) + n(t). \end{aligned} \tag{4.4}$$

Here, $t_{d,max} < t_{d,I_j}$; $t_{d,max}$ is the round-trip time for the maximum operating range of 200m, I_j is the index of the interferer, t_{d,I_j} is the delay time of the interferer, k is the number of interferers, and $n(t)$ is white noise. The mixed output after low-pass filtering is as follows:

$$\begin{aligned} x(t) &= f(t)g(t) = f(t)\left(g_s(t) + g_I(t) + n(t)\right) = s(t) + I(t) + w(t) \\ &= \sum_{i=1}^{m} C_i \cos\left(2\pi(\alpha t_{d,i} - f_{d,i})t + (2\pi(f_0 + f_{d,i})t_{d,i} - \pi\alpha t_{d,i}^2\right) \\ &\quad + \sum_{j=1}^{k} C_{I_j} \cos\left(2\pi(\alpha t_{d,I_j} - f_{d,I_j})t + (2\pi(f_0 + f_{d,I_j})t_{d,I_j} - \pi\alpha t_{d,I_j}^2\right) + w(t). \end{aligned} \tag{4.5}$$

In this case, the influence of interference signal is presented in the form of a ghost target with a constant frequency. Because the beat frequency of the interferer is larger

than the maximum beat frequency corresponding to the maximum operating range, it can be ignored by the sampling rate, f_s.

4.2.2 The Different Sign-Chirp Case

In contrast to the above case, with an increasing chirp of transmitted signal and a decreasing chirp of interfering signal, the received signal is expressed as follow:

$$\begin{aligned} g(t) &= g_s(t) + g_I(t) + n(t) \\ &= \sum_{i=1}^{m} B_i \cos\left(2\pi\left((f_0 + f_{d,i})(t - t_{d,i}) + \frac{1}{2}\alpha(t - t_{d,i})^2\right)\right) \\ &+ \sum_{j=1}^{k} B_{I_j} \cos\left(2\pi\left((f_0 + BW + f_{d,I_j})(t - t_{d,I_j}) - \frac{1}{2}\alpha(t - t_{d,I_j})^2\right)\right) + n(t), \end{aligned} \tag{4.6}$$

The mixed output is, therefore, given by

$$\begin{aligned} x(t) &= f(t)g(t) = f(t)\left(g_s(t) + g_I(t) + n(t)\right) = s(t) + I(t) + w(t) \\ &= \sum_{i=1}^{m} C_i \cos\left(2\pi(\alpha t_{d,i} - f_{d,i})t + (2\pi(f_0 + f_{d,i})t_{d,i} - \pi\alpha t_{d,i}^2\right) \\ &+ \sum_{j=1}^{k} C_{I_j} \cos\left[-2\pi(\alpha t_{d,I_j} + BW + f_{d,I_j})t + 2\pi\alpha t^2 + 2\pi(f_0 + BW + f_{d,I_j})t_{d,I_j} + \pi\alpha t_{d,i}^2\right] + w(t). \end{aligned} \tag{4.7}$$

Because the interfering signal comes with a short pulse and time-varying frequency components as shown in Figure 4.3(b), it would appear as an increase in the noise floor with a very wide spectral width. The amount of the increase in the noise floor is proportional to the time duration of the interfering signal or the interfering source power. Considering that the interfering signals are also treated as noise, (4.7) can also be represented as shown below.

$$\begin{aligned} x(t) &= s(t) + \big(I(t) + w(t)\big) = s(t) + e(t) \\ &= \sum_{i=1}^{m} C_i \cos\left[2\pi(\alpha t_{d,i} - f_{d,i})t + (2\pi(f_0 + f_{d,i})t_{d,i} - \pi\alpha t_{d,i}^2\right] + e(t), \end{aligned} \tag{4.8}$$

Here, $e(t)=I(t)+w(t)$.

4.3 High-Resolution Frequency Estimation Methods

In this section, the proposed high-resolution beat frequency estimation scheme is described. Figure 4.4 shows a functional block diagram of the proposed scheme, which employs a FBSS and a FSDO estimator. We present a data model for subspace-based algorithms and describe an effective method to estimate the correlation matrix. Based on the data model, a theory encompassing MUSIC and ESPRIT is investigated and the FSDO estimator, as a part of MUSIC and ESPRIT, is presented to provide the number of frequency components.

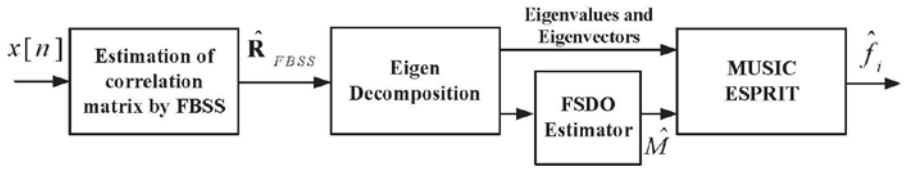

Figure 4.4 Functional block diagram of the high-resolution beat frequency estimation algorithm

4.3.1 Data Model

Let us a consider sampled version of radar mixed output as a discrete-time sinusoid signal having amplitude, frequency, and phase components, as follows,

$$x[n] = s[n] + e[n] = \sum_{i=1}^{m} a_i \cos(2\pi f_i n + \phi_i) + e[n], \qquad (4.9)$$

where n=0,1,2,$\cdots$,N–1; $s[n]$ contains sinusoids returned from each target; $e[n]$ represents the noise signal from other FMCW radars, including white noise with a zero mean and variance of σ^2; m is the number of sinusoids; N is the number of sampled data points; and a_i, f_i and ϕ_i are the amplitude, beat frequency, and phase of the i-th sinusoid, respectively. According to Euler's formula, $\cos(2\pi f_i n+\phi_i)$ can be expressed as $\frac{1}{2}(e^{j(2\pi f_i n+\phi_i)}+e^{j(-2\pi f_i n+\phi_i)})$. Then, (4.9) can be represented in complex exponential form, as

$$x[n]=s[n]+e[n]=\sum_{i=1}^{M}\overline{A_i}e^{j(2\pi \overline{f_i}n+\phi_i)}+e[n], \tag{4.10}$$

with

$$\begin{aligned}
&\overline{A_i}=\frac{a_i}{2}e^{j\pi_i},\quad \overline{f_i}=f_i \quad \text{for } 1\le i\le m\\
&\overline{A_i}=\frac{a_i}{2}e^{-j\pi_i},\ \overline{f_i}=-f_i \quad \text{for } m+1\le i\le 2m,\\
&M=2m
\end{aligned} \tag{4.11}$$

By defining the i-th complex sinusoid component, $\overline{A_i}e^{j2\pi \overline{f_i}n}$ as $s_i(n)$, (4.10) is expressed as follows:

$$x[n] = \sum_{i=1}^{M} s_i[n] + e[n], \qquad n = 0,1,2,\cdots,N-1, \tag{4.12}$$

From L discrete-time samples, a compact matrix form is obtained by

$$\mathbf{x}(n) = \sum_{i=1}^{M} \mathbf{s}_i(n) + \mathbf{e}(n), \tag{4.13}$$

where $L > M$; $\mathbf{x}(n) = [x[n]\, x[n+1] \cdots x[n-L+1]]^T$, $\mathbf{s}_i(n) = [s_i[n]\, s_i[n+1] \cdots s_i[n-L+1]]^T = [1\, e^{j2\pi \overline{f_i}} \cdots e^{j2\pi(L-1)\overline{f_i}}]^T \times \overline{A_i} e^{j2\pi \overline{f_i} n}$; and $\mathbf{e}(n) = [e[n]\, e[n+1] \cdots e[n-L+1]]^T$. Then, a low-rank matrix representation for subspace methods can be represented as

$$\mathbf{x}(n) = \mathbf{F}\mathbf{A}(n) + \mathbf{e}(n), \tag{4.14}$$

where $\mathbf{F} = [\mathbf{f}(\overline{f_1})\mathbf{f}(\overline{f_2}) \cdots \mathbf{f}(\overline{f_M})]$ is a $L \times M$ Vandermonde matrix of rank M , $\mathbf{A}(n) = [\overline{A_1} e^{j2\pi \overline{f_1} n}\, \overline{A_2} e^{j2\pi \overline{f_2} n} \cdots \overline{A_M} e^{j2\pi \overline{f_M} n}]$, and $\mathbf{f}(\overline{f_i}) = [e^{j2\pi \overline{f_i}} \cdots e^{j2\pi(L-1)\overline{f_i}}]^T$ for $i = 1,2,\cdots,M$ is a frequency mode vector with frequency $\overline{f_i}$. The autocorrelation matrix of mixed output $\mathbf{R}_{xx}$ is expressed as

$$\mathbf{R}_{xx} = E\left[\mathbf{x}(n)\mathbf{x}(n)^H\right], \tag{4.15}$$

where $E[\cdot]$ denotes the expected value. By using eigenvalue decomposition, the eigenvalues and corresponding eigenvectors of $\mathbf{R}_{xx}$ are obtained according to $\{\lambda_1 \geq \lambda_2 \geq \cdots \geq \lambda_L\}$ and respectively. If $\mathbf{R}_{xx}$ has the full rank of M, the eigenvalues are given by

$$\lambda_1 \geq \lambda_2 \geq \cdots \geq \lambda_M > \lambda_{M-1} = \lambda_{M-2} = \cdots = \lambda_L = var[e[n]], \tag{4.16}$$

where $var[e[n]]$ denotes the noise variance. From the eigenvalues and eigenvectors of $\mathbf{R}_{xx}$, we define a signal subspace matrix $\mathbf{V}_S = [\mathbf{v}_1 \mathbf{v}_2 \cdots \mathbf{v}_M]$ corresponding to the largest M eigenvalues, and a noise subspace matrix $\mathbf{V}_N = [\mathbf{v}_{M+1} \mathbf{v}_{M+2} \cdots \mathbf{v}_L]$ that contains the remaining eigenvectors.

4.3.2 Estimation of the Correlation Matrix

The correlation matrix of the received signal is found by the expected value of the absolute values squared. However, we cannot identify the exact statistics for the signal and noise. Assuming that the process is ergodic, we can approximate the correlation matrix by means of time-averaged correlation as follows:

$$\hat{\mathbf{R}}_{xx} = \frac{1}{N-L+1}\sum_{k=1}^{N-L+1}\mathbf{x}(n)\mathbf{x}(n)^H . \quad (4.17)$$

Here, $N > L$, N denotes the sequentially decimated time samples $\{x[n]x[n+1]\cdots x[n+N-1]\}^T$. When the number of time samples is limited, the rank sparsity of the correlation matrix degrades the performance. To improve the performance of subspace methods, FBSS method is used in this paper [42]. FBSS is used to calculate the $L \times L$ matrix, as

$$\hat{\mathbf{R}}_{FBSS} = \frac{1}{2Q}\sum_{k=1}^{Q}(\hat{\mathbf{R}}_{\mathbf{n}} + \mathbf{J}\hat{\mathbf{R}}_{\mathbf{n}}{}^T\mathbf{J}), \quad (4.18)$$

where $Q = N-L+1$; $\hat{\mathbf{R}}_{\mathbf{n}} = \mathbf{x}(n)\mathbf{x}(n)^H$, and $\mathbf{J}$ is the $L \times L$ reversal matrix, for which the elements are unity along the anti-diagonal and are zero elsewhere.

4.3.3 Application of the MUSIC Algorithm

The MUSIC algorithm uses the basic assumption that the frequency mode vector corresponding to its frequency component is orthogonal to the noise subspace formed by the noise eigenvectors. This is expressed, as

$$\mathbf{f}^H(\overline{f}_i)\mathbf{v}_k = 0, \quad (4.19)$$

where $i = 1, 2, \cdots, M$ and $k = M+1, M+2, \cdots, L$

By using the orthogonality of the frequency mode vectors to the noise eigenvectors, the MUSIC pseudo-spectrum is then defined as follows [17]:

$$P_{MUSIC}(f) = \frac{1}{\sum_{k=m+1}^{M} |\mathbf{f}^H(f)\mathbf{v}_k|^2}, \tag{4.20}$$

A peak value occurs in the pseudo-spectrum when $f = \overline{f_i}$, and the estimated frequency is obtained by CFAR[44].

4.3.4 Application of the ESPRIT Algorithm

ESPRIT is based on the naturally existing shift-invariance between discrete-time series samples which leads to rotational invariance between the corresponding signal subspaces [18]. Let us define two subsamples $\mathbf{x}_1(n) = [x[n]\, x[n+1] \cdots x[n+L-2]]^T$ and $\mathbf{x}_2(n) = [x[n+1]\, x[n+2] \cdots x[n+L-1]]^T$ for $L-1 > M$. From $s_i[n+1] = s_i[n]e^{j2\pi\overline{f_i}}$ in (4.13), $\mathbf{x}_1(n)$ and $\mathbf{x}_2(n)$ can be represented by

$$\begin{aligned} \mathbf{x}_1(n) &= \mathbf{F}\mathbf{A}(n) + \mathbf{e}_1(n) \\ \mathbf{x}_2(n) &= \mathbf{F}\mathbf{\Phi}\mathbf{A}(n) + \mathbf{e}_2(n), \end{aligned} \tag{4.21}$$

where $\mathbf{\Phi}$ is a $(L-1)\times(L-1)$ diagonal matrix whose i-th component is $\phi_i = e^{j2\pi\bar{f}_i}$. By defining $\mathbf{V}_{S1}$ and $\mathbf{V}_{S2}$ as the signal subspace eigenvectors from the auto-correlation of $\mathbf{x}_1(n)$ and $\mathbf{x}_2(n)$, respectively, the subspaces of the eigenvectors are related by a unique non-singular transformation matrix $\mathbf{\Psi}$ such that

$$\mathbf{V}_{S1}\mathbf{\Psi} = \mathbf{V}_{S2}. \tag{4.22}$$

Because $\mathbf{F}$ and $\mathbf{V}_{S1}$, $\mathbf{V}_{S2}$ span the same signal subspace, there is also a unique non-singular transformation matrix $\mathbf{T}$ such that

$$\begin{aligned} \mathbf{V}_{S1} &= \mathbf{F}\mathbf{T} \\ \mathbf{V}_{S2} &= \mathbf{F}\mathbf{\Phi}\mathbf{T}. \end{aligned} \tag{4.23}$$

By substituting (4.23) into (4.22), we can derive the following relationship:

$$\mathbf{\Psi} = \mathbf{T}^{-1}\mathbf{\Phi}\mathbf{T}. \tag{4.24}$$

Thus, the largest M eigenvalues of $\mathbf{\Psi}$ are equal to the diagonal elements of $\mathbf{\Phi}$ such that $\psi_1 = e^{j2\pi\bar{f}_1}, \psi_2 = e^{j2\pi\bar{f}_2}, \cdots, \psi_M = e^{j2\pi\bar{f}_M}$. The frequency estimates $\hat{\bar{f}}_i$ for $1 \le i \le M$ are then calculated as

$$\hat{\bar{f}}_i = \frac{\angle(\psi_i)}{2\pi}, \tag{4.25}$$

where $\angle\cdot$ denotes the phase of the argument, with the sampling frequency of the

data used to calculate $\widehat{\widehat{f_i}}$. The MUSIC algorithm needs to search the peaks of the spatial spectrum at a cost of computational load, whereas ESPRIT exploits the rotational invariance structure of the signal subspace and avoids searching any spatial spectrum.

4.3.5 Number of Frequency Estimation

MUSIC and ESPRIT take advantage of a prior knowledge such as the number of frequency components. Because the precise number of frequency M value is not available in practical systems, it must be estimated. As information theoretic criteria, MDL or the AIC have been widely used to estimate the number of frequencies. In this paper, we employ the MDL criterion to estimate M. This is expressed as [27],

$$\mathrm{MDL}(k) = -\log\left(\frac{\prod_{i=k}^{L-1}\lambda_i^{\frac{1}{L-k}}}{\frac{1}{L-k}\sum_{i=k}^{L-1}\lambda_i}\right)^{(k-L)Q} + \frac{1}{2}k(2L-k)\log Q, \qquad (4.26)$$

after which the estimate of M can be obtained by

$$\hat{M} = \arg_k \min \mathrm{MDL}(k) + 1, \qquad (4.27)$$

where, $k = 0,1,\cdots,L-1$.

4.4 Experimental Result

Table 4.1 Parameters of a FMCW radar for the experiment

Parameter	Specification
Frequency	76.25-76.75 GHz
Sweep bandwidth	500 MHz
Sweep time	5 ms
Output power	10 mW
Maximum range	200 m
FFT points	2048
Sampling rate	298 kHz

In this section, we present our measurement setup and analyze the proposed method as compared to the conventional FFT algorithm. To validate performance of the proposed methods, measurement performed with two interference scenario (Figure 4.1). The FMCW radar sensor, used for ACC, was installed in the test vehicle which is produced by a Korea company. All of the experiments were performed in an open space on flat ground. The interfering and target vehicles have 10dBsm radar cross section (RCS). The parameters of the FMCW radar used in this study are summarized in the Table 1. For a sweep bandwidth of 500 MHz, a sweep time of 5 ms and a maximum operating range of 200 m, the maximum round trip time is 1.33 μs and the maximum beat frequency is 133 kHz. The cut-off frequency of the LPF was set to 1 MHz.

In order to evaluate the quantitative performance of the frequency estimation in an interference environment, probability of resolution is analyzed according to SIR. The SIR is determined by the distance from the radar sensor to the target and the interferer. The SIR is distributed up to about -31 dB and -63 dB for the indirect interference and direct interference respectively.

The mixer outputs of the FMCW radar were analyzed using the conventional FFT, the MUSIC and the ESPRIT methods. To detect the peak values from the FFT and MUSIC spectral results, the ordered statistic (OS) CFAR algorithm was adopted [44], where the probability of a false alarm is 10^{-6}. The beat frequency of the target is determined by the spectral component higher than a threshold.

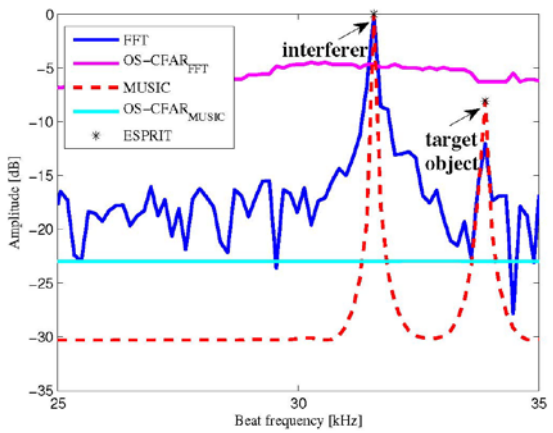

Figure 4.5 Sample result for the beat frequency estimation when the target object exists at a range of 50m (For a direct interference scenario)

Figure 4.5 shows a snapshot (which means a scan) for the beat frequency estimation when the target object exists at a range of 50 m. In this example, the SIR is -30 dB (i.e., the direct interferer is 30 m away from the radar sensor). This result shows that the proposed method is more capable of identifying the beat frequency than the conventional FFT method. Although, the FFT result indicates a peak value for the target object, it is not larger than the threshold, leading to a detection failure of the target object.

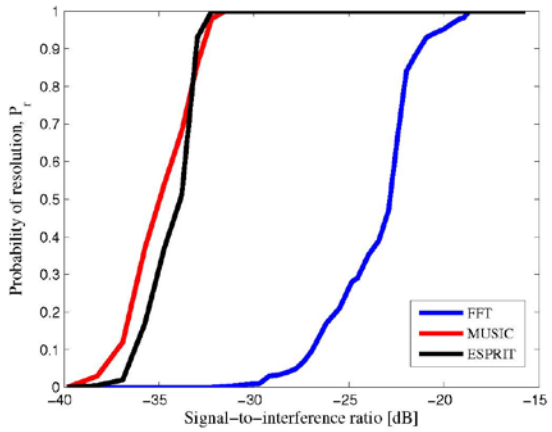

Figure 4.6 Probability of resolution versus SIR

The results are based on 1600 independent periods of measured data for each distance using the subsample size set to $L = 100$ for the FBSS. As shown in Figure 4.6, the proposed method operates up to a SIR of -32.5 dB, whereas the FFT shows a

performance limit of -17.9 dB SIR. These subspace-based methods are entirely robust for at least indirect interference scenarios. For a short range of less than 50 m, Furthermore, it can be said the proposed methods can identify the beat frequencies of targets regardless of the SIR. The MUSIC and ESPRIT algorithms show similar performance levels. However, ESPRIT has better computational efficiency because it avoids the peak-search process.

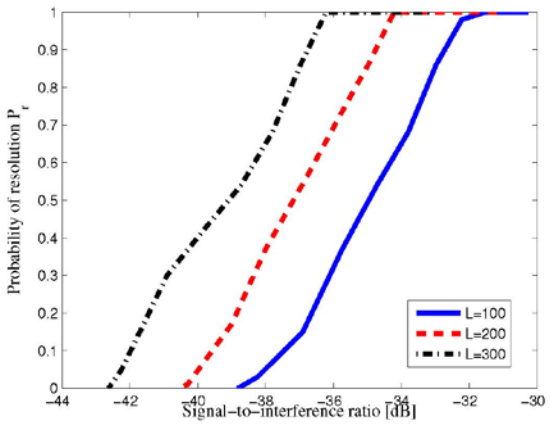

Figure 4.7 Probability of resolution versus the number of subsample for FBSS

The performance of the proposed algorithm versus the number of subsamples for the FBSS was also assessed. The conditions for estimation are same to those in Figure 4.7, except that the number of subsamples is varied from $L = 100$ to $L = 300$. Figure 4.7 shows that when the number of samples is increased to 200 and 300, the

performance of the MUSIC algorithm shows additional margin of SIR, about 2.4 dB and 4.1 dB, respectively. This improvement occurs because large number of subsamples, L , makes the rank property of the correlation matrix effective.

4.4 Conclusion

The conventional FFT approach is vulnerable in interference-limited environments. In this paper, the performance limitation of the existing system was evaluated quantitatively. Also, we proposed a subspace-based method to identify the beat frequency of the targets while suppressing the interference signals. Experimental results show that the proposed method has a SIR margin of at least about 14 dB compared to the conventional FFT algorithm. The proposed method provides a significant performance enhancement even in a direct interference environment, which proves that the proposed estimation method can be successfully applied for the beat frequency analysis in an interference environment. Thus, it is concluded that MUSIC and ESPRIT are essential for minimizing the interference effects in the automotive radar field. Moreover the overall method will be useful for eliminating the influence of interference when used in conjunction with other mitigation techniques.

Bibliography

[1] D. Geronimo. A. Lopez, A.D. Sappa, and T. Graf, "Survey of pedestrian detection for advanced driver assistance systems," *IEEE trans. on Pattern Analysis and Machine Intelligence*, vol.32, no.7, 1239-1258, 2010.

[2] G. Leen and D. Heffernan, "Expanding automotive electronic systems," *IEEE trans. on Computer*, vol.35, no.1, pp.88-93, 2002.

[3] S. J. Prosser, "Automotive sensors: past, present and future," *Journal of Physics*, vol.76, no.1, pp.1-6, 2007.

[4] A. Vahidi, and A. Eskandarian, "Research advances in intelligent collision avoidance and adaptive cruise control," *IEEE trans. on Intelligent Transportation Systems*, vol.4, no.3, pp.143-153, 2003.

[5] M. Broy, "Challenges in automotive software engineering," in *Proc. Int. conference on Software engineering, ACM*, pp.33-42, 2006.

[6] H. Winner, and M. Schopper, "Adaptive cruise control," *Handbuch Fahrerassistenzsysteme. Springer Fachmedien Wiesbaden*, pp.859-891, 2015.

[7] J. Wenger, "Automotive radar-status and perspectives," In *Proc. compound Semicondoctor integrated Circuit Symposium, CSIC'05, IEEE*, pp.1-4, 2005.

[8] A. Kawakubo, S. Tokoro, Y. Yamada, and T. Kawasaki, "Electronically-scanning millimeter-wave Radar for forward objects detection," *SAE*

Congress, pp.127-134, 2004.

[9] R. H. Rasshofer and K. Gresser, "Automotive radar and lidar systems for next generation driver assistance functions," *Adv. Radio Sci.*, vol. 3, pp.205-209, 2005.

[10] M. Schneider, "Automotive radar–status and trends," In *Proc. German microwave conference*, pp. 144–147, 2005.

[11] W. Menzel, "Millimeter-wave radar for civil applications," in *Proc. IEEE Radar Conference (EuRAD)*, pp. 89–92, 2010.

[12] M. E. Russell, A. Crain, A. Curran, R. A. Campbell, C. A. Drubin, and W. F. Miccioli, "Millimeter-wave radar sensor for automotive intelligent cruise control (icc)," *IEEE trans. on Microwave Theory and Techniques*, vol.45, no.12, pp.2444–2453, 1997.

[13] S. H. Jeong, J. N. Oh, and K. H. Lee, "Design of 24 GHz radar with subspace-based digital beam forming for acc stop-and-go system," *ETRI journal*, vol.32, no.5, pp.827–830, 2010.

[14] E. Hyun and J. H. Lee, "A meothod for multi-target range and velocity detection in automotive fmcw radar," in *Proc. IEEE Int. Conference on Intelligent Transportation Systems, ITSC'09*, pp. 1–5, 2009.

[15] M. Reiher and B. Yang, "On the occurrence of ghost targets in linear fmcw radar: A worst case study," in *Proc. IEEE Int. Radar Symposium*, pp. 1–4, 2008.

[16] G. M. Brooker, "Mutual interference of millimeter-wave radar systems," *IEEE trans. on Electromagnetic Compatibility*, vol.49, no.1, pp.170–181, 2007.

[17] R. Schmidt, "Multiple emitter location and signal parameter estimation,"

IEEE trans. on Antennas and Propagation, vol.34, no.3, pp.276–280, 1986.

[18] R. Roy and T. Kailath, “Esprit-estimation of signal parameters via rotational invariance techniques,” *IEEE trans. on Acoustics, Speech and Signal Processing*, vol. 37, no. 7, pp. 984–995, 1989.

[19] A.G. Jaffer, “Maximum likelihood direction finding of stochastic sources: A separable solution, “ *in Proc. ICASSP 88*, vol.5, pp.2893,2896, 1988.

[20] M. Reiher, and B. Yang, “On the occurrence of ghost targets in linear FMCW radar: A worst case study,” in *Proc. IEEE Int. Radar Symposium*, pp.1-4, 2008.

[21] E. Conte, and M. Longo, “Characterisation of radar clutter as a spherically invariant random process,” *in IEE Proc. F (Communications, Radar and Signal Processing)*, vol.134, no.2, pp.191-197, 1984.

[22] J. E. Lee, et al. “Enhanced iron-tunnel recognition for automotive radars,” *IEEE trans. on Vehicular Technology*, 2015.

[23] M. Goppelt, H. Bl¨ocher, and W. Menzel, “Automotive radar–investigation of mutual interference mechanisms,” *Advances in Radio Science*, vol. 8, pp. 55–60, 2010.

[24] H. Krim, and M. Viberg, “Two decades of array signal processing research: the parametric approach,” *IEEE signal Processing Magazine*, vol.13, no.4, pp.65-94, 1996.

[25] R. Okuda, Y. Kajiwara, and K. Terashima, “"A survey of technical trend of adas and autonomous driving,”" in *Proc. IEEE VLSI Technology, Systems and Application (VLSI-TSA), Proceedings of Technical Program-2014 International Symposium on*, pp.1-4, 2014

[26] H. Akaike, “A new look at the statistical model identification,” *IEEE trans.*

on Automatic Control, vol.19, no.6, pp716-723, 1974.

[27] M. Wax and T. Kailath, "Detection of signals by information theoretic criteria," *IEEE trans. on Acoustics, Speech and Signal Processing*, vol. 33, no. 2, pp. 387–392, 1985.

[28] I. Matsunami and A. Kajiwara: "Clutter suppression scheme for vehicle radar," in *Proc. IEEE Radio and Wireless Symposium (RWS)*, pp. 320-323, 2010.

[29] R. Kapoor, G. Tsihrintzis, and N. Nandhakumar: "Detection of obscured targets in heavy-tailed radar clutter using an ultra-wideband (UWB)," in *Proc. IEEE conf. Signals, Systems and Computers, Pacific Grove*, pp. 863-867, 1996.

[30] A. G. Stove: "Linear FMCW radar techniques," *IEE Proceedings F (Radar and Signal Processing*), vol.139, no.5, pp. 343-350, 1992.

[31] M. I. Skolnik : "Introduction to radar systems," (McGraw-Hill, 3rd edn. 2001)

[32] T. Abe, T. Kobayashi, and S. Imai: "Harmonics tracking and pitch extraction based on instantaneous frequency," in *Proc. IEEE Int. Conf. Acoustics, Speech, and Signal Processing (ICASSP)*, pp. 756-759, 1995.

[33] R. D. Kent: "Acoustic analysis of speech," (Singular Publishing Group, 2002)

[34] P. Borghesani, P. Pennacchi, R. Randall, N. Sawalhi, and R. Ricci: "Application of cepstrum pre-whitening for the diagnosis of bearing faults under variable speed conditions," *Mechanical Systems and Signal Processing*, vol.36, no.2, pp. 370-384, 2013.

[35] B. Borgert, M. Healy, and J. Tukey: "The quefrency analysis of time series

for echoes: cepstrum, pseudo-autocovariance, cross-cepstrum and saphe craking, " in *Proc. symp. on time series analysis*, pp. 209-243, 1963.

[36] R. Randall, "A history of cepstrum analysis and its application to mechanical problems," in *Proc. Int. Conf. Surveillance 7*, pp. 1-16, 2013.

[37] R. Randall, N. Sawalhi, and M. Coats: "A comparison of methods for separation of deterministic and random signals," *International Journal of Condition Monitoring*, vol.1, no.1, pp. 11-19, 2011.

[38] S. Watts, "Cell-averaging CFAR gain in spatially correlated k-distributed clutter," *IEE Proceedings-Radar, Sonar and Navigation*, vol.143, no.5, pp. 321-327, 1996.

[39] L. Mu, T. Xiangqian, S. Ming, and Y. Jun, "Research on key technologies for collision avoidance automotive radar," in *Proc. IEEE Intelligent Vehicles Symposium*, pp. 233–236, 2009.

[40] J.-H. Zhang, G.-S. Liu, H. Gu, and W.-M. Su, "A novel transmit signal based on high range-resolution concept for flar or aicc system applications," in *Proc. CIE International Conference on Radar*, 2001.

[41] H. Rohling, "Some radar topics: waveform design, range cfar and target recognition," *in Advances in Sensing with Security Applications. Springer*, pp. 293–322, 2006.

[42] A. Eriksson, P. Stoica, and T. Soderstrom, "Markov-based eigenanalysis method for frequency estimation," *IEEE trans. on Signal Processing*, vol. 42, no. 3, pp. 586–594, 1994.

[43] M. Haardt and J. A. Nossek, "Unitary esprit: How to obtain increased estimation accuracy with a reduced computational burden," *IEEE trans. on Signal Processing*, vol. 43, no. 5, pp. 1232–1242, 1995.

[44] S. Blake, “Os-cfar theory for multiple targets and nonuniform clutter,” *IEEE trans. on Aerospace and Electronic Systems*, vol. 24, no. 6, pp. 785–790, 1988.

[45] M. S. Lee and Y. H. Kim, “An efficient multi target tracking algorithm for car applications,” *IEEE trans. on Industrial Electronics*, vol. 50, no. 2, pp. 397–399, 2003.

초록

자동차 기술 분야의 안전 및 편의에 대한 수요가 증가함에 따라, 주행 보조 시스템의 많은 응용 제품들이 연구, 개발 중이다. 차량의 주행 정보를 제공하기 위해서, 라이더, 카메라, 레이더, 초음파 레이더와 같은 다양한 센서 중에서, 레이더 센서는 시계 및 기상 상황에 대해 훌륭한 성능을 보여준다. 특히, 글로벌 생태계의 긴급 제동 시스템과 같은 안전 관련 기술의 의무장착화 진행과 맞물려 차량 레이더 센서의 시장을 폭발적으로 증가할 것으로 예상된다. 최근에는, 작은 크기를 가지면서도 성능이 우수한 레이더 센서에 대한 개발이 필수적이다. 또한 기존의 단거리, 중장거리 레이더 기능을 통합하는 다중 모드 레이더의 개발이 요구된다. 따라서 고해상도 파라미터 추정, 다중 타겟 감지, 클러터 억제, 간섭 완화 등의 기법은 여전히 레이더 신호처리 분야의 도전 과제로 남아있다.

고해상도 파라미터 추정에 대해서, 타겟 차량들을 구분하기 위한 각도 추정 기법들이 연구되고 있다. 특히 복잡한 도심환경에서는 비슷한 거리 및 속도로 주행하는 차량들이 빈번히 존재한다. 이러한 근접 차량들을 구분하기 위해서는 차량용 레이더에 적합한 고해상도 각도 추정

알고리즘이 필수적이다.

한편 레이더 센서 시야 범위 내에 존재하는 다중 타겟들을 분리하는 다중 타겟 감지기법이 요구된다. 다중 타겟 감지 기법은 각각의 타겟들이 가지는 고유의 주파수 성분들을 페어링하고 결합하는 과정이다. 특정 환경에서는 잘못된 주파수 페어링을 통해서 고스트 타겟이 검출될 수 있다. 따라서 신뢰성 높은 페어링 또는 결합 기법이 요구된다.

클러터는 주변 환경으로부터 반사되는 원하지 않는 신호 성분을 말한다. 차량 주행 환경에서는 가드레일, 교통표지판, 도로 주변의 정지물체들이 될 수 있다. 클러터의 효과를 최소화하기 위해서, 기존 레이더 시스템은 클러터의 비유동적인 특성 및 저주파 특성을 가정하고 이를 필터링한다. 그러나 차량용 레이더 환경에서는 클러터들이 다양한 주파수 성분 및 에너지를 가지고 분포하므로 적용이 어렵다. 특히, 철제 구조물과 같은 특수한 환경에서는 클러터의 높은 파워로 인하여 타겟 차량이 검출되지 않는다.

상호 간섭은 차량 안전 기능 제공을 위해서 반드시 풀어야 할 문제이다. 동일한 대역, 동일한 순간에 동작하는 레이더 센서를 탑재한 차량의 수가 증가할수록, 다른 레이더 센서의 신호로부터 정확한 타겟 구분에 실패 할 확률일 점차적으로 증가한다. 따라서 이에 대한 적절한 대책이 필요하다.

본 논문에서는, 차량용 레이더 시스템을 위한 효율적인 파라미터

추정 기법을 제안한다. 제안된 기법들은 앞서 설명한 신호처리 이슈들을 각각 포함하고 있다. 먼저, 주파수 영역에서 고해상도 각도 추정 기법을 제안한다. 본 기법은 타겟 차량의 고유한 비트 주파수를 이용하여 고해상도로 각도를 추정한다. 타겟의 비트 주파수는 거리 및 속도 정보를 제공하기 때문에, 추정된 각도 정보는 자연스럽게 거리 및 속도정보와 페어링 된다. 다음으로는, 철제 터널 환경에서의 클러터 억제 기법을 제안한다. 철제 터널 환경의 클러터는 철제 구조물의 반사 신호 성분으로 타겟의 감지 성능을 매우 열화시킨다. 제안된 기법은 켑스트럼에 기반한 클러터 억제 기법으로서, 주파수 영역에서의 주기적인 클러터 특성을 이용한다. 마지막으로, 간섭 제거 기법을 제안한다. 차량용 레이더의 간섭은 대부분 주파수 영역의 잡음 전력의 증가로 나타나며, 타겟의 감지 실패로 이어진다. 따라서 우리는 간섭 환경에서의 고해상도 주파수 추정 기법을 제안하고, 성능의 개선을 제시한다.

주요어 : 차량 레이더, FMCW, 각도 추정, 간섭, 완화, 클러터, 억제, 고해상도, 신호처리

학 번 : 2009- 30928